

PH.D THESIS

UNIVERSITÀ DEGLI STUDI DI NAPOLI “FEDERICO II”

DIPARTIMENTO DI INGEGNERIA ELETTRONICA
E DELLE TECNOLOGIE DELL’INFORMAZIONE

PH.D IN
INFORMATION TECHNOLOGY AND ELECTRICAL ENGINEERING

ULTRA-FAST CHARGING STATION:
DESIGN, CONTROL & DEVELOPMENT OF
A REAL-CASE STUDY

PASQUALE FRANZESE

Ph.D School Coordinator

Ch.mo Prof. Daniele RICCIO

Supervisor

Ch.mo Prof. Diego IANNUZZI

A. A. 2020–2021

PH.D THESIS

UNIVERSITÀ DEGLI STUDI DI NAPOLI “FEDERICO II”

DIPARTIMENTO DI INGEGNERIA ELETTRONICA
E DELLE TECNOLOGIE DELL’INFORMAZIONE

PH.D IN
INFORMATION TECHNOLOGY AND ELECTRICAL ENGINEERING

ULTRA-FAST CHARGING STATION:
DESIGN, CONTROL & DEVELOPMENT OF
A REAL-CASE STUDY

PASQUALE FRANZESE

Ph.D School Coordinator

Ch.mo Prof. Daniele RICCIO

Supervisor

Ch.mo Prof. Diego IANNUZZI

A. A. 2020–2021

Abstract

The automotive industry is today one of the most important industries worldwide, not only economically, but also in terms of research and development. The full electric vehicles can be charged from an external electrical source (eg. PHEV and BEV) and are not dependent on how the energy was generated. If the energy production technologies or storage technologies change, the vehicles would not undergo any changes.

This PhD thesis focuses on the analysis and study of the electric vehicle charging in order to document the design, realization and control of a real prototype of an ultra-fast charging station built at the DIETI (Department of Information Technologies and Electrical Engineering) of University of Naples - Federico II. The proposed contents deal with the presentation of the case study and the application of the requirements engineering on it, an IEC standards overview on the electrical vehicles supply equipment (EVSE), the choice of the electrical topology of converters, the sizing of components, the description of the low-level controls and the energy flow management, the brief introduction on the real implementation and the display of the experimental performances and results.

Contents

Abstract	i
1 Introduction	1
1.1 A look at the world of EVs	1
1.1.1 Hystory of EVs	1
1.1.2 Advantages and classifications of EVs	3
1.1.3 Classification of EVSE	7
1.1.4 Current trend of EVs	11
1.2 Thesis objectives and organization	21
2 Project requirements, operative choices and standards	24
2.1 IEC standars	25
2.2 Functional requirements	42
2.2.1 Renewable's penetration	42
2.2.2 Multiple Slots	47
2.2.3 Output values	48
2.2.4 Input values	51
2.2.5 Reliability and safety	55

3	Power converters for UFCS: comparison, sizing and control	58
3.1	Electrical topologies comparison	59
3.2	AC/DC converters	63
3.3	DC/DC converters	67
3.4	Sizing and control of chosen converters	73
4	Energy Storage Systems for UFCS: comparison, modeling and sizing	79
4.1	Definitions	79
4.2	Technology comparison	83
4.2.1	Mechanical storage systems	84
4.2.2	Thermal storage systems	86
4.2.3	Chemical storage systems	87
4.2.4	Electrical storage systems	90
4.2.5	Electrochemical storage systems	92
4.2.6	Hybrid storage systems	103
4.3	Modelling of Li-ion battery	104
4.3.1	White box models	105
4.3.2	Black box models	107
4.3.3	Grey box models	109
4.3.4	Estimation parameters	114
4.4	Sizing of the BESS	116
4.4.1	Sizing validation	120
5	Energy & Power Management of UFCS	127
5.1	Scheduling strategies	128

5.2	Optimal charging power planning	131
5.2.1	A simplified closed form strategy	131
5.2.2	An advanced strategy	142
6	Real case study: UFCS prototype of DIETI	158
6.1	Experimental setup	160
6.2	Experimental results	166
6.2.1	Acceptance testing	166
6.2.2	Vehicles charging profiles	170
7	Conclusions	174

Introduction

At the beginning, an overview of electric vehicles is shown: a hint is made to the history of their technological development and the advantages they have gained over time compared to internal combustion vehicles are highlighted. The chapter continues by illustrating how the car market has responded to the electrification of mobility, through reviews and reports from international organizations, with a particular focus on the spread of charging infrastructures. Finally, the research objectives and thesis organization are explained.

1.1 A look at the world of EVs

1.1.1 Hystory of EVs

In 1801, Richard Trevithick built a steam-powered carriage. Almost 30 years passed when, between 1832 and 1839, the first two battery powered electric vehicles (EV) were built by the industrialist Robert Anderson in Scotland and by Professor Sibrandus Stratingh in Holland. The first petrol-powered internal combustion vehicle (ICV) was built in 1885, so the EV is about 50 years older

than ICV.

By the 1920s the American electric car market declined in popularity for the following reasons: America had a better system of roads that connected cities, bringing with it the need for longer-range vehicles; the discovery of Texas crude oil reduced the price of gasoline so that it was affordable to the average consumer; the invention of the electric starter by Charles Kettering in 1912 eliminated the need for the hand crank; the initiation of mass production of internal combustion engine vehicles by Henry Ford made these vehicles widely available and affordable.

Electric vehicles had all but disappeared by 1935; they would reenter the market around the '60s and '70s when the problems of exhaust emissions from internal combustion engines and of shortage of crude oil were about to be addressed. In the '90s, new federal and state regulations create a renewed interest in electric vehicles. The result: Automakers begin modifying popular vehicle models into electric vehicles, enabling them to achieve speed and performance much closer to that of gasoline-powered vehicles. The development of EVs has its own characteristics in different historical stages. The momentum or the driving force for the inventions, the technical features, applications, charging infrastructure, and business model were not all the same in different historical periods.

At the beginning of the 21st century, electric vehicles have become more popular due to the advance of electrical machines, drives and the availability of rechargeable batteries. Lead-acid batteries had been the primary choice for energy storage for more than a century, but their heavy weight in relation to their low-energy storage capacity did not fit the needs of EVs for running at higher speeds and over longer distances. Lithium-ion technology has proven to

be a game changing solution, offering higher energy density. In 2006, TESLA MOTORS[®], a Silicon Valley startup, announces it will produce a luxury electric sport cars with a range of 200+ miles. Other automakers take note, accelerating work on their own electric vehicles.

Today, we need high energy density, high power density, high efficiency, long life, reliable and reasonable cost of modern EV batteries and modern EV motors that can suit the driving requirements of vehicles in urban as well as rural areas.

1.1.2 Advantages and classifications of EVs

Since the market is ready to adopt the diffusion of EVs, it is high time we discussed the advantages of electrification.

The main advantages of EVs over ICVs are in terms of [1]:

- Moment of Torque: EVs deliver maximum torque at zero speed, just when a higher torque value is required. The high torque at low speed of the EVs contributes to their stop and go performance.
- Electric Regeneration: Through regenerative braking, the EVs can recover kinetic energy during braking, potentially reducing energy consumption.
- Conversion efficiency: the electrical engines (EEs) convert about 95% of the energy supplied into mechanical energy for traction, the petrol internal combustion engines (ICEs) normally convert no more than 30% of the supplied energy, those to diesel up to 40%.
- Power per unit of mass or volume: with the same output power, the EEs

have smaller dimensions than traditional ICEs. In addition, the cooling systems in the EVs are less complex and the emission control system is not necessary. All the volume and weight that is recovered by eliminating unnecessary components is taken up with the battery pack.

- Noiselessness: The ICEs work by combustion or controlled explosion of fuel and air mixtures, therefore they are intrinsically noisy. Their noise can be substantially attenuated, but at the cost of a reduction in energy efficiency. The EEs hardly make any acoustic noise.
- Low pollution levels: almost all the pollution produced by ICE vehicles consists of the emissions produced by combustion. The EEs have no direct emissions, but the electricity used for recharging, production and disposal are still a source of pollution and production of greenhouse gas.
- Flexibility with regard to production:

the EVs that can be charged from an external electrical source (eg. PHEV and BEV) are not dependent on how the energy was generated. If energy production technologies or storage technologies change, the vehicles would not undergo any changes.

The most common electric vehicles are those that integrate electric traction with the traditional one with ICE; therefore, vehicles can be classified according to the level and mode of hybridization [2].

- Series Hybrid (series HEV)

In a series hybrid system, the ICE drives an electric generator (usually a

three-phase alternator followed by a rectifier) which in turn powers an electrochemical battery and the traction EE, the vehicle's only engine. When high traction powers are required, the engine is powered by both the generator and the battery. Series hybrids can be equipped with high power density storage systems such as ultracapacitors or Kinetic Energy Recovery System (KERS), used during acceleration peaks or during regenerative braking phases, to improve the efficiency of the system conversion. A complex transmission system is not required for series hybrids since electric motors are often keyed directly onto the wheel axle with a direct drive system. Some vehicles include the use of an EE on each drive wheel, simplifying traction control (absence of transmission, differential, reducers). The EE used are of the asynchronous and PM brushless type. An electric vehicle with Fuel Cells is classified as a series hybrid vehicle: the ICE is replaced by the Fuel Cells.

– Parallel Hybrid (parallel HEV)

In a parallel hybrid system, traction is provided by both the ICE and the EE mechanically connected in parallel to the transmission. The batteries are present and recharged in any case by the ICE; many solutions integrate the electric generator and the engine in the same machine, replacing both the starter motor and the alternator. The two different propulsions are used in different moments of driving, based on the maximum speed, the required power levels and the energy available in the electrochemical battery. The battery can be recharged during regenerative braking, but also when the power required by the vehicle is less than the power supplied

by the combustion engine.

– Combined Hybrid (combined HEV)

Combined hybrid systems integrate both series and parallel hybrid characteristics. There is a double connection between the engine and drive shaft, the power to the wheels can be provided by both the electric motor and the combustion motor, as in parallel hybrid vehicles. The main difference is that in combined systems the power required by the vehicle is decoupled from that supplied by the ICE. The power distributed HEV includes a wide range of performance levels. For example, for lower engine speeds, this system works like a series hybrid, while at high speeds, when the series hybrid is less efficient, the ICE takes over. This system is more expensive than a pure parallel system, as it requires an additional generator, a mechanical split power system and more computing power to control the dual system.

– Plug-in Hybrid (PHEV)

A PHEV integrates the characteristics of a conventional hybrid electric vehicle and a fully electric vehicle, also equipped with the ability to charge the batteries by connecting them to an external electrical source. PHEVs have a much wider all-electric range than conventional HEVs ensuring greater autonomy as the combustion engine works as a backup when the batteries are low. PHEVs can be either series HEV, parallel HEV, or combined HEV, the only addition is the ability to charge the batteries externally through a connector when the vehicle is stationary. The charge of these cars is typically only slow or quick since charging through the

connector is only one of the alternatives (the other is refueling).

– Battery full electric (BEV) or Pure electric (PEV)

The PEVs have an architecture simpler than those previously proposed: the transmission systems may also be absent if a Direct Drive electric motor solution is contemplated, the only engine is the EE (or more electric motors on the different drive wheels) and the only energy source is the battery pack. The battery is also charged through regenerative braking, but above all through a charging infrastructure. Since the battery is the only energy tank to move the EV, its capacity is much higher than that of the batteries used for HEVs. PEVs are the cars most subject to disadvantages on autonomy and charging time, in fact almost all these cars have the possibility of fast or Ultra-Fast recharges (cars with battery packs with a capacity greater than 60 kWh are equipped with a connector for Ultra-Fast charging as standard). Since the focus of this thesis is the design of an Ultra-Fast station, only PEV vehicles (henceforth referred to as EVs only) will be taken into consideration.

1.1.3 Classification of EVSE

Electric vehicle supply equipment (EVSE) plays a decisive role in the development of electric vehicles.

Today, European reference standards for charging systems, connectors and facilities refer to the [S1] and [S2]. The standard [S1] allows EVSE to be classified according to several factors.

- According to the type of power supply of the EVSE compared to the

interface power grid: AC or DC connection.

- According to the electric connection method: plug to plug, permanent connected EV cable to the EVSE plug, permanent connected EVSE cable to the EV plug.
- Depending on the type of power supply of the EV compared to the EVSE: AC charge, DC charge, AC & DC charge.
- According to environmental conditions: outside use, internal use.
- According to the location they are intended for: equipment for locations with restricted access or equipment for locations with non-restricted access.
- According to the protection against short circuits, the type of location (public or private environment), the types and speed level of charge.

The charging time and operating life of the vehicle's battery are also connected to the characteristics of the charge, which must ensure sustainable use of the battery. To evaluate a good charging structure, according to different contexts and uses, the following are taken into account: efficiency, reliability, power density, costs, volumes and weights.

The main parameter for a charger is its power, it affects the charging time, the costs of the structure and the operating costs, the technologies used on the station and on the vehicle, the requirements of the network and the impacts on it.

The CEI standard [S1] classifies different types of charging according to the power level and charging time, defining 4 categories [3]:

- Mode 1 – Slow or low power charging: it is a passive direct connection between the vehicle and the power line, at 250V single phase or 480V three-phase, including ground and with a maximum current of 16A. This type of connection does not have communication contacts. For electrical protection, the charging system must provide the ground for the vehicle and include a protection system in case of grounding malfunction. In some countries, including the United States, *Mode 1* is prohibited as grounding is not present in all domestic consumers. The main application is domestic or for long-term parking, the power levels are less than 3.7kW. Charging times are of the order of 12-16 hours.
- Mode 2 – Fast or medium-power charging: it is a semi-active direct connection between the vehicle and the power line, at 250V single phase or 480V three-phase, including ground and with a maximum current of 32A. There is an active direct connection between the power line and the vehicle charging system, with a passive component control system. The charging system provides grounding and a protection system in case of its malfunction, protection against overcurrent and excessive temperature and a shutdown system depending on the power required for charging. The main application is in public or private infrastructure, power levels are between 3.7kW to 22kW. Charging times are of the order of 5-10 hours.
- Mode 3 – Fast AC charging: it is an active connection between the vehicle and the charging system, at 250V single phase or 480V three-phase, including ground and a control system. It must also have a

connection cable with some extra conductors suitable for a maximum current of 250A. The charge voltage is not active by default but requires activation through the control system. The communication cable between the vehicle electronics and the charging station allows integration into smart grids. The charging times are of the order of 2-5 hour. It is present only in public infrastructure where power levels can be more than 22kW.

- Mode 4 – DC Ultrafast charging: it is an active connection between the vehicle and the 600V charging system in DC, including grounding and a control system, with a maximum current of 400A. A 1000V charging system is planned in the coming years, to reduce the charging current on the vehicle. Changes in the insulation levels of the electric vehicle and the traction supply system are preparatory to this proposed voltage level. Charging times are about 1 hour for a 0-100% of state of charge (*SoC*) and below 20 min for a 5-70% of *SoC*.

The need to recharge the vehicle battery within a limited time frame comparable to traditional ICE vehicles requires the high-power Connection of Mode 4, the only one capable of meeting this specification. Once the power, voltage and number of phases have been defined; the charging modes of an electrochemical battery are the follows [4]:

- Constant voltage: the voltage is kept constant on the battery, this implies very high currents when the battery is low and decreasing currents as the charging state increases. There are examples of design with this mode in the slower chargers, but also for lead-acid battery chargers and power backup systems in power supplies.

- Constant current: the current is kept constant up to charging status values not exceeding 70%-80% according to the battery technology used, to prevent the voltage from exceeding the maximum permissible charging values, and in order to completely convert the electricity supplied into electrochemical energy avoiding overheating of the battery pack.
- Impulsive reload: In this mode, the charge current waveform consists of a sequence of pulses of varying duration and amplitude. The charge speed (based on the average current) can be precisely controlled by varying the width of the pulses. During the charging process, the current pulses are followed by short rest periods that allow chemical actions in the battery to stabilize by equalizing the reaction through most electrodes. This allows the chemical reaction to transform electrical energy into electrochemical energy in a better way.
- Alternating impulsive reload: This method should be used in conjunction with the impulsive charging method. During the charging rest period, discharge pulses of very short duration (2 to 3 times the amplitude of the charge current) are applied in order to depolarize the cell. These discharge pulses remove the gas bubbles developed on the electrodes during charging, which improves the stabilization process and the entire charging process.

1.1.4 Current trend of EVs

The success of the commercialization of electric vehicles depends on the adequate management of four factors: initial cost, functionality, energy consumption and

exhaust emissions. So far only the last two have been achieved and satisfied. Many authors, including [5–9], have been involved in making direct and indirect emissions comparisons between ICV, HEV PEV. In particular, [8] presents an interesting prospect of emissions comparing electric and traditional vehicles and also the different market segments.

The emissions due to the production of EVs are in any case higher than those of the ICVs, the reason is the development of technology that makes the production plants not yet optimized for mass production. When production will get up to speed, the flexibility required to the production plants to chase technological developments will be less and the transition to electricity will become more widespread, emissions, as well as costs, will tend to drop.

Operational emissions, those associated with the use of the vehicles, must be carefully compared. In fact, EVs recharged from a fossil fuel source have an emissions impact comparable to an ICV. Instead, if the production of electricity comes from renewable sources, or at most from natural gas, then the electricity emissions become considerably lower. Furthermore, if production plants are converted to the sole use of energy from renewable sources, a big step towards reducing emissions will already be made.

A synthesis between production, operational and disposal emissions is present in [6] and it is evident that EVs are overall greener than ICV.

In [7] considerations are made on the costs occurred for the production and maintenance of an EV. The design of an EV is not a replacing of IC engine powertrains with electric powertrains, but additional work and components are required. The EV body can be designed to accommodate batteries, which represent the most likely energy storage device for EVs, without increasing the

overall vehicle cost. The batteries will make up a significant fraction of the vehicle mass ($\sim 20\text{-}40\%$) and cost. EVs are expected to have very low energy costs because of their efficient use of electricity from batteries. However, such vehicles are likely to require one or more replacement battery packs during their lifetime; these replacement packs would add substantially to the EV's annual operating costs.

Low production volumes and labor-intensive manufacturing processes make the costs of its components high. When EVs come to be produced in sufficient volume, significant cost reductions will be possible. The functionality of EVs mentioned above is a delicate issue and focuses almost entirely on electric charging. Unlike what happens with fluid fuels (gasoline, gas oil and natural gas), the electricity that flows from the charging station to the vehicle batteries cannot be transferred very quickly. To fill in the tank of an ICV car, it takes a few minutes and an autonomy from 300 to 600 km. The electric charging is divided into 4 categories based on time and charging power: slow, quick, fast and Ultra-Fast. Slow charging is designed for long-term vehicle parking (home, office, ...), quick and fast charging are designed for short-term parking where the key is to optimize the time spent outside the vehicle (restaurant, supermarket, gym, ...), Ultra-Fast recharging, on the other hand, is intended as a service dual to that of the charging of a traditional car with a thermal engine at the distributor.

Different charging services require different infrastructures both in terms of the power taken from the network, the size and type of components, but also the number of charging slots, the methods of payment and use and the location of the stations. The question about the type, quantity, and location of charging

stations is key for the coordinated build-up of the charging network in the coming years.

Tab. 1.1 [10] provides an overview of charging types by power and an estimate of how many kilometres of travel distance the charger will provide in 10 minutes. Charging time remains a clear drawback for PEVs compared to conventionally fuelled cars. The table also shows how much power can be delivered by each charging type. Using the Renault Zoe Z.E. 40 as an example, a full charge

Table 1.1: Currently available charging points [10]

Type	Power output	km per 10 min of charge	Typical locations
AC Mode 2 Home	up to 11kW	1-2	Home
AC Mode 2 Commercial	up to 19.4kW	3.2	Private, Workplace and Public
AC Mode 3 Fast Charging	22kW or 44kW	21	Public, Private
DC Fast charging (standard)	20-50kW	64	Public, Private
DC high power fast charging	100-400kW	90	Public

would take 13.5 hours at a $3kW$ charging point; 6 hours at a $7kW$ charging point; and 2 hours at a $22kW$ charging point. At a $50kW$ DC fast charger, the vehicle could get an 80% charge in 1 hour. To fully recharge the Volkswagen Golf with $300km$ range would take 10 hours at a $3.6kW$ charging point, while a $50kW$ DC fast charger provides an 80% charge in 45 minutes.

EVs sales data At the end of 2020, 10 million were the electric cars on the world's roads [11]. EV registrations increased by 41% in 2020, despite the

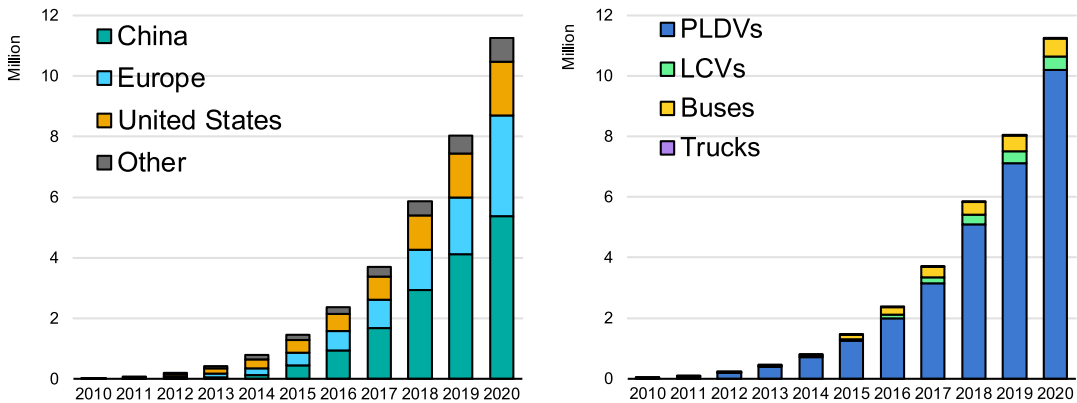


Figure 1.1: EVs' market condition of last decade

pandemic-related worldwide downturn in car sales in which global car sales dropped by 16%. In the first-quarter of 2021, global electric car sales rose by around 140% compared to the same period in 2020, driven by sales in China of around 500k vehicles and in Europe of around 450k. US sales more than doubled relative to the first quarter of 2020, even though from a much lower base.

In the Fig. 1.1 [11], a summary of the given data are reported. The acronyms PLDVs and LCVs are passenger light-duty vehicles and light-commercial vehicles respectively. Electric vehicles include battery electric and plug-in hybrid electric vehicles. Overall Europe, Germany registered 395k new electric cars and France registered 185k. The United Kingdom more than doubled registrations to reach 176k. Electric cars in Norway reached a record high sales share of 75%, up about one-third from 2019. Sales shares of electric cars exceeded 50% in Iceland, 30% in Sweden and reached 25% in the Netherlands.

EVs sales incentives Individual EU Member States formulate targets and incentives the deployment of charging infrastructure in accordance with [S3]. There are no explicit targets at EU level, but rather a multitude of supporting measures. As a result, most charging stations currently exist only in urban areas in Western European countries. An EU-wide network of fast chargers along the main motorways across the continent does currently not exist. The resilience of EV sales in the face of the pandemic is mainly related to:

- Supportive regulatory frameworks: even before the pandemic, many countries were strengthening key policies such as CO_2 emissions standards and zero-emission vehicle (ZEV) mandates. By the end of 2020, more than 20 countries had announced bans on the sales of conventional cars or mandated all new sales to be ZEVs.
- Additional incentives to safeguard EV sales: Some European countries increased their purchase incentives, but the majority of them decreased the incentives in total spending on electric cars over the past five years, suggesting that EVs are becoming increasingly attractive to consumers. The number of EV models expanded and battery cost continued to fall.

According to the EU's 2016 low-emission mobility strategy, the ultimate policy objective is to make EV charging as easy as filling a conventional vehicle tank, so that EVs can travel without obstacle across the EU [S3]. Tax breaks are the most common measure to incentivise EVs in EU Member States. These include exemption or reduction of registration tax, road tax, and company car tax [12].

EVSE diffusion While EVs market is affected by the consumer perception of cost/effectiveness return, the public incentives, technological change, government policy, city planning, and power utilities all play a role in the diffusion of EV charging infrastructure. The location, distribution, and types of electric vehicle supply equipment (EVSE) depend on EV stocks, travel patterns, transport modes and urbanisation trends.

The EU does not have an overall strategic roadmap for electro-mobility and an integrated policy on vehicles, infrastructures, grids, batteries, economic incentives, raw materials, and digital services; the recharging infrastructure development is scattered and mainly coordinated at regional level.

Travel across the EU is still complicated by the absence of minimum requirements for harmonised payment systems and user information.

The estimated number of private chargers in 2020 is 9.5 million, of which 7 million are at residences and the remainder at workplaces [11]. This represents 40GW of installed capacity at residences and over 15GW of installed capacity at workplaces. Private chargers for electric vehicles rise to 105 million by 2030 in the Stated Policies Scenario, with 80 million chargers at residences and 25 million at workplaces. This accounts for 670GW in total installed charging capacity and provides 235TWh of electricity in 2030. Studies indicate that current charging of privately used cars occur mainly at private homes or at workplaces and in the future also during shopping at semi-private charging stations.

Moreover, a recent analysis has shown that charging will probably shift towards public options, and away from the home, as more people without access to home charging start to buy EVs [13].

For commercial fleet vehicles, charging occurs mainly at the premises of their company. Hence, the requirement for public charging stations focuses mainly on long distance trips, and therefore along the highway network.

Publicly accessible chargers reached 1.3 million units in 2020, of which 30% are fast chargers. Installation of publicly accessible chargers was up 45%, a slower pace than the 85% in 2019, likely because work was interrupted in key markets due to the pandemic. China leads the world in availability of both slow and fast publicly accessible chargers.

For the installation of slow chargers, Europe is second to China with around 250k slow chargers, with installations increasing one-third in 2020. The Netherlands leads in Europe with more than 63k slow chargers. Sweden, Finland and Iceland doubled their stock of slow chargers in 2020.

Publicly accessible Ultra-Fast charging stations (UFCS) located in city centres next to shopping malls, workplaces or leisure facilities, are most suitable to be positioned along highways in order to enable long-distance trips by PEV.

In Europe, fast chargers are being rolled out at a higher rate than slow ones. There are now more than 38k public fast chargers, up 55% in 2020, including nearly 7.5k in Germany, 6.2k in the United Kingdom, 4k in France and 2k in the Netherlands. As they are increasingly deployed, they will enable longer trips and encourage late adopters without access to private charging to purchase an electric vehicle.

Only a single platform provides already 315 UFCSs along the German highway network and on the European average, we see already almost 25 UFCSs per 100 km on the highway [14]. Hence, the reality already created a situation, where we have (theoretically) more than enough FCS, which however does not

necessarily provide enough charging points per location.

Apart from government incentives, the industry is also increasingly taking action in order to realise a comprehensive charging infrastructure in Europe. One example is IONITY[®], a strategic partnership between BMW[®], DAIMLER[®], FORD[®] and VOLKSWAGEN[®] with AUDI[®] and PORSCHE[®]. Their goal is to build a network of reliable, high power charging stations (up to 350kW) along major routes across Europe.

EVSE accessibility The electro-mobility charging system involves multiple actors that need to communicate with each other. As well as charging point operators (responsible for installing and maintaining charging points) and mobility service providers (providing consumers with a range of mobility product or services), they include EV users, vehicle manufacturers and grid operators. The AFID stipulates that the charging point operators must be allowed to provide EV charging services to customers on a contractual basis, including on behalf of other service providers to allow drivers to charge using a single identification or payment method, and stations to communicate equally with all EVs. It involves at least the following: a contractual agreement among all the entities concerned, either direct (bilateral) or indirect (via a roaming hub), the charging points to be equipped with an internet connection, a card reader or a remote activation function, and interoperable communication protocols. However, currently, physical connections and information exchange among these actors go through a variety of communication protocols. There are no harmonised roaming systems with minimum requirements that would allow EV users to use all different charging networks of the EU under a single contrac-

tual agreement. Consequently, depending on their charging point operators and the mobility service providers they use, EV drivers may require multiple subscriptions and use different payment methods.

For a successful market take-up of plug-in electric vehicles, Ultra-Fast charging stations along the highway network play a significant role [15].

How many stations do we need? To highlight the question about the relationship between charging infrastructure and PEV adoption and use, two different indicators, the number of PEVs per charging point in relation to market uptake and the number of PEVs per million inhabitants in relation to market uptake, are considered. The Alternative Fuels Infrastructure Directive (AFID) recommends that EU Member States ensure a ratio of a maximum of 10 PEVs per charging point. The expectation is that markets where this ratio is not met will experience a slower PEV adoption. [7] argue that the ratio of charging points per million inhabitants may be more useful, as this indicator is independent of both the number of vehicles already in the market and the geographical size of the countries to be compared. European countries for the most part failed to meet the recommended electric vehicle supply equipment (EVSE) per EV 2020 targets. In the European Union, the average public EVSE per EV ratio was 0.09 at the end of 2020. The Netherlands and Italy are above the target at 0.22 and 0.13 respectively, with almost all being slow chargers, though fast chargers are 3% of the installations in the Netherlands and 9% in Italy.

1.2 Thesis objectives and organization

This PhD thesis focuses on the analysis and study of the electric vehicle charging in order to document the design and construction of a real prototype of an ultra-fast charging station built at the DIETI (Department of Information Technologies and Electrical Engineering) of University of Naples - Federico II. The thesis is composed by 7 chapters which lead the reader into the disclosure of the preliminary, final and executive planning, the control of the infrastructure and its energy/power management. A brief overview of the main topics of each chapter is presented as follows:

- *Chapter 2.* The requirements based on the desired performances, physical and economic constraints are exposed. Among the requirements, the compliance of IEC standards in terms of safety, reliability, regulation sequences, and harmonisation of communication are covered.
- *Chapter 3.* A literature review is used to make a broad comparison between converters mainly used in UFCS. A conversion system with a common DC bus is chosen, so the converter further discussed are the AC/DC rectifier and DC/DC transformer. The modeling and sizing of the chosen topologies are dealt as baseline for the development and the control phases.
- *Chapter 4.* The energy and power constraints highlighted in *Chapter 2* forced the presence of an ESS. The static ESS for UFCS application is selected between several typologies; the preference is well-documented. Furthermore, the chapter goes on with the modeling of a Li-ion BESS with

regard to electrical, chemical and thermal behaviour. A portion of [16] is used to introduce the design and sizing of the BESS and its validation.

- *Chapter 5.* A hint towards the modulation (low-level control) of the converters fills the first part of this chapter. In addition to the control of converters, through [17], the energy flow management and the case study of multiple slots charging stations (priority strategy and queuing) are shown.
- *Chapter 6.* After the preliminary and final planning, a long period of implementation, testing, and validations of the UFCS prototype occurs. The presented experimental results refer to the efficiency of the station in different operating point (also when it is a supplier for the grid) and to the performance in the EV charging. Real EVs are used to check the EVSE compliance with the requirements. Finally, the requirements placing of EV/EVSE charge/discharge emulator is conducted.
- *Chapter 7.* The last chapter summarizes the work described in this Ph.D. thesis, and derives the main conclusions, emphasising the advantages of the design method proposed, and introducing the main ideas for future developments.

This thesis contains material from the scientific publications listed in the following.

- P. Franzese and D. Iannuzzi, “Ultrafast charging station forelectrical vehicles: Dynamic modelling, design and controlstrategy,” *Mathematics and Computers in Simulation*, vol. 184, pp.225–243, 2021, ELECTRI-

MACS 2019 ENGINEERING - Modelling and computational simulation for analysis and optimisation in electrical power engineering. [Online].

Available: www.sciencedirect.com/science/article/pii/S037847542030149X

- P. Franzese, D. Iannuzzi, F. Mottola, D. Proto, and M. Pagano, "Charging strategies for ultra-fast stations with multiple plug-in electric vehicle parking slots," in *2020 AEIT International Annual Conference (AEIT)*, 2020, pp. 1–6
- P. Franzese, A. Cervone and D. Iannuzzi, "Power Control Strategy of a Delta-Connected Photovoltaic Cascaded H-Bridge Converter for Low Voltage Distribution Networks in Energy Community," *2021 IEEE 6th International Forum on Research and Technology for Society and Industry (RTSI)*, 2021, pp. 346-351, doi: 10.1109/RTSI50628.2021.9597305.
- P. Franzese, A. Di Pasquale, D. Iannuzzi and M. Pagano, "Electric Ultra Fast Charging Stations: a Real Case Study," *2021 AEIT International Annual Conference (AEIT)*, 2021, pp. 1-6, doi: 10.23919/AEIT53387.2021.9626929.

Project requirements, operative choices and standards

Requirements engineering can be decomposed into the activities of requirements elicitation, specification, and validation. One way to reduce requirements errors is by improving requirements elicitation, an activity often overlooked or only partially addressed by current requirements engineering techniques [18].

In the first section, the IEC standards on Ultra-Fast are presented. These requirements are essential for a properly design, they are general and not use case dependent. The IEC standards are, in large part, functional and concern safety, standardization of the charge phases and charge connectors and communication between EV and EVSE.

In the second section, the design is bound by the functional and non-functional requirements chosen ad hoc for the EVSE project under consideration. Some requirements concern the EV market situation at the moment, others are due to arbitrary choices to provide some useful features for the station. These features regard on one hand research purposes, on the other, a forecast for EVSE

market's requirements. No requirements on volume, weight or arrangement of components are considered.

2.1 IEC standars

The main target for electric vehicle conductive charging systems is *IEC 61851*. In particular, part 1 provides general requirements on EVSE, sections 23 and 24 provide requirements for *Mode 4* charging on DC EVSE connected with the grid at 1000V in AC 50 – 60Hz with rated current not exceeding 250A, in accordance with [S4], and with connection to the vehicle at no more than 1500V in DC with nominal current not exceeding 400A.

Requirements for EVSE design The preferred values of the rated operational DC voltages of *Mode 4* are: 480V, 600V, 750V, 1000V. The preferential rated DC currents are: 70A, 80A, 125A, 200A, 250A and 400A. The standard does not prescribe any particular electrical topology for EVSE *Mode 4*, but it provides instructions on the design specifications, the checks necessary for safe operation and other functional requirements. The necessary design specifications concern:

- Devices and components used: Electric devices and components of EVSE shall comply with their relevant standards. The standard also assigns some requirements regarding reliability, life styles, utilization category, inrush current, overvoltage category, insulation resistance, touch current, IP degrees.
- Protective device and conductor: in the EVSE *Mode 4*, the fault protec-

tion is based on electric separation. Emergency switching or disconnect equipment shall be used either to disconnect the supply network from EVSE or to disconnect the socket-outlet or the cable assembly from the supply network. The protective earthing conductor and the protective conductor shall be of sufficient rating in accordance with requirements of [S5] and [S6]. If the EVSE presents more than one connecting point used simultaneously and they are connected to a common input terminal of the EVSE, each point must have an individual protection incorporated in the EVSE. The standard also defines the breaking capacity of the devices, how to carry out measurements of leakage current and contact current, electromagnetic compatibility tests. The station with plug for DC charging of the EVs must be equipped with a residual current device (RCD), which, in turn, can be equipped with an overcurrent protection device. The ground of the DC charging station must be connected to the terminal of the external protective conductor.

- EVSE to EV cable: the voltage and current ratings of the cable assembly shall be compatible with the rating of the EVSE. A cable assembly must be a flexible tube, it may include one or more conduit cables or wires. The maximum cable length shall be $5m$. The cable insulation shall be wear-resistant and maintain flexibility over the full temperature range required by the classification of the EVSE. Cables used with accessories according to [S7] for *Mode 4* shall have a minimum withstand I^2t value of $80000A^2s$.
- Other specification reference: The [S8] standard regulates the safety re-

quirements about power transformers, power supplies, reactors and similar products. The [S6] concerns protection systems against electric shock; of interest for the EVSE are parts 4 and 5 which deal with protection for low voltage installations. [S9] concerns insulation coordination systems for equipment within low-voltage systems. [S10] concerns low-voltage switchgear and controlgear; for their assembly, reference is made to [S5]. The standard applies to equipment designed to be used at an altitude up to 2000*m*. The [S11] contains High-voltage test techniques for low-voltage equipment; [S12] prescribes the requirements for plugs, socket-outlets and couplers for industrial purposes; and [S7] deals with plugs for conductive charging of electric vehicles. [S13] regulates the safety requirements about electromechanical elementary relays; [S14] and [S15] respectively prescribe the safety of electronic and programmable boards and of control and communication systems. [S16] regulates the safety in connection to an external electric power supply.

The [S4] standard is the standard concerning the environmental tests to be carried out for the commissioning of electrotechnical systems.

For installation in a plant located in an environment open and accessible to the public, there are other rules to be respected. These standards do not concern the electrical design and installation, so they are out of this discussion.

Charging connectors The first step in researching the requirements of EVSE is to identify which configuration is worth using to interface with the EV. Different configurations imply a different sequence of recharge and a different implementation of the protection systems. The connection between the vehicle

and the station must be made through the cable and the connector, therefore, the choice of the connector is the starting point of this analysis.

The [S7] specifies the requirements for plugs, fixed sockets, movable connectors, fixed connectors and power cables described in [S1]. [S7] deals with mechanical, electrical and performance requirements for plugs, fixed sockets, mobile vehicle connectors and fixed vehicle connectors to interface such dedicated charging equipment with the electric vehicle. The [S1] distinguishes connections into cases, types and systems; these subdivision is not aimed at increasing the complexity, but at harmonizing and grouping the different products existing before the formulation of the standard.

Indeed, based on whether the cable is connected or integral with the EVSE or with the EV, there are 3 cases [S1] (Fig. 2.1):

- case A: connection of an EV to the supply network with a plug and a cable permanently attached to the EV;
- case B: connection of an EV to a supply network with a cable assembly detachable at both ends;
- case C: connection of an EV to a supply network utilizing a cable, permanently attached to the EV charging station, and the vehicle connector.

All *Mode 4* charging configurations are case C connections.

The standard [S7]-1 prescribes 3 types of AC standard connectors:

- Type 1 – Yazaki: single-phase coupling at 250V and 32A nominal
 - based on the specifications of *SAE J1772/2009*.

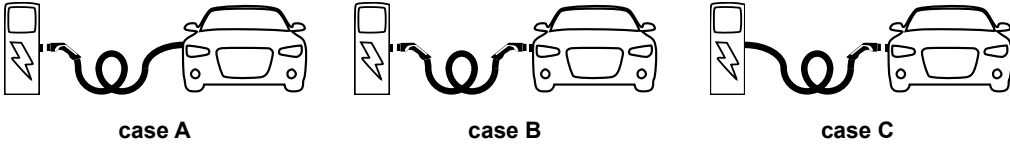


Figure 2.1: Classification of EV/EVSE connections according to fixed or mobile plugs and cable

The original *SAE J1772/2009* standard establishes power voltages of 120V at 12A or 16A and 240V at 32A or 80A.

- Type 2 – Mennekes: single-phase coupling at 250V and 13A or 20A or 32A or 63A or 70A nominal and three-phase coupling at 380V or 480V and 13A or 20A or 32A or 63A nominal.
- based on the specifications of the *VDE-AR-E 2623-2-2* and the [S12] standard with the addition of signal contacts.
- Type 3 – SCAME: single-phase coupling at 250V and 16A or 32A and three-phase at 380V or 480V and 32A or 63A nominal. – based on the proposal of EV Plug Alliance.

The Scame connector is a fixed socket, so particularly suitable for connecting the cable with the charger, while the other types can be used to connect the cable with the electric vehicle.

The standard [S7]-3 extends [S7]-1 and describes the specific designs of connectors and sockets for charging electric vehicles in DC in *Mode 4*.

- Config AA – CHAdeMO: implements System A according to [S17] and uses CANbus communication according to [S18] between the station and the vehicle; the nominal output voltage is limited to 600V and 200A in

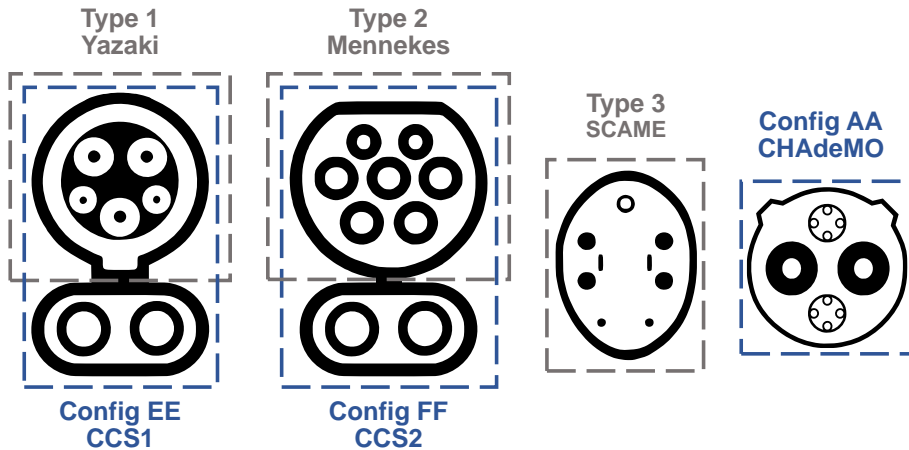


Figure 2.2: AC (grey label) & DC (blue label) EV charging connectors

DC;

– based on *JEVS G105-1993* specifications.

It is mainly used on Japanese electric vehicles.

– Config BB: implements System B according to [S17] and uses a second CANbus communication [S18] between the station and the vehicle, as reported in [S7]-3; the nominal output voltage is limited to 750V and 250A in DC;

– based on the specifications of *GB/T 20234.3*.

It is mainly used on Chinese electric vehicles.

– Config EE – CCS1: implements System C according to [S17] and uses PLC communication according to [S18] for digital communication between the station and the vehicle; the nominal output voltage is limited to 600V and 200A in DC

– based on the specifications of *SAE J1772*.

It is mainly used in the USA.

– Config FF – CCS2: implements System C according to [S17] and uses PLC communication according to [S18] for digital communication between the station and the vehicle, the nominal output voltage is limited to 1000V and 200A in DC;

– is the evolution of CCS1.

It is a global standard mainly used in the EU, USA, India.

Table 2.1: DC couplers and maximum system output voltage for combined charging system C

Configurations	Maximum DC voltage
Configuration CC according to IEC 62196-3-1	500V
Configuration DD according to IEC 62196-3-1	500V
Configuration EE according to IEC 62196-3	500V
Configuration FF according to IEC 62196-3	1000V

The rated DC output voltage of the combined charging system C is limited to the maximum system output voltage, as shown in Tab. 2.1 of [S17].

A plug not mentioned is the Tesla connector. It is used just from Tesla vehicles and Tesla stations, thus, it would draw interest only if this design was conducted on behalf of TESLA MOTORS®.

The *CCS2*, named *System C - Config FF* by the norm, is the choice for the prototype because it is the most used in Europe by several car makers. The name CCS means combined charging system because it provides both AC and DC charge including additional DC power contacts. The basic portion of the combined vehicle inlet can be used with a basic connector for AC charging only

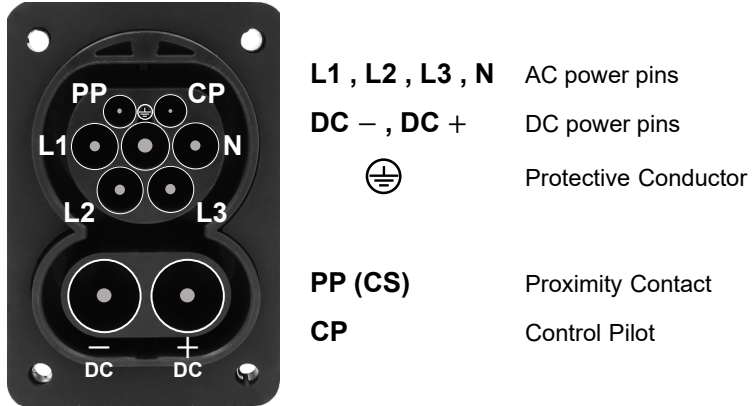


Figure 2.3: *CCS2* pins scheme

or with a combined connector having separate contacts for AC or DC charging. AC and DC power transfer shall not occur through the combined interface at the same time.

The specific pins scheme of *CCS2* is shown in Fig. 2.3. The proximity contact (PP) is used to monitor that the connection is done correctly, the control pilot pin (CP) is the main channel (but not the only one) for communication and control between EV and EVSE. The rated signal or command voltage is 5V and the current is 2A.

The next requirements will be general for all the connectors; when in the text the prerequisites will regard specifically the System C (*Config FF - CCS2*) it will be explicitly declared.

Communication levels The communication between the EVSE and the EV can be established through basic communication and high level communication. The communication channels implementation is shown in Fig. 2.4.

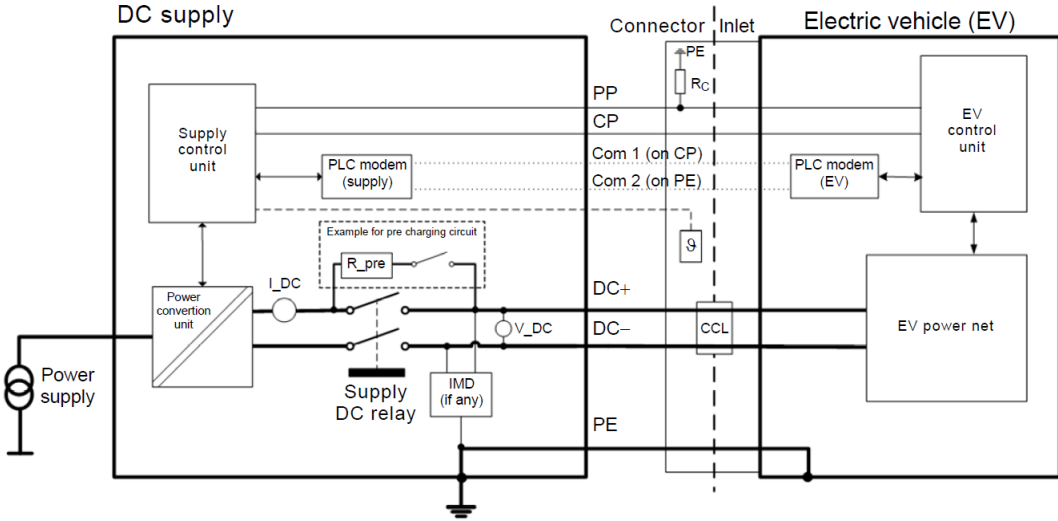


Figure 2.4: System schematics of *CCS2*

- Base communication: Key steps in the charge control process, such as charging start and normal / emergency stop, must be handled via basic communication with the exchange of signals through the CP.
- High-level communication: In addition to basic communication, the EVSE must be equipped with digital communication means for the exchange of the DC charge control parameters through high-level communication. Different standard protocols use different communication means: a) the control area network (CAN) on the dedicated digital communication circuit or b) the power line communication (PLC) on the control pilot circuit. The *CCS2* uses the PLC.
- Human-Machine Interface: In this scenario the user needs to interact with the charge. He must be able to start and stop the charge by through an interface both on EVSE and EV.

Charging features The control of the EVSE must follow both static and dynamic regulation specifications:

- Vehicle Charge Control Function: The EVs are equipped with on-board storage systems with different technologies, topologies and electrical dimensions, therefore, the charging process must be completely managed by a battery management system (BMS) of the EV. The BMS of the EV manages and controls the charge through a vehicle charge control function (VCCF). The EVSE must supply the current or the voltage to the EV in accordance with the request by EV in the modalities of controlled voltage charge (CVC) or controlled current charge (CCC). The vehicle can change the maximum voltage limit during the charging process. In any case, the maximum nominal values are the minimum between those that can be supplied by EVSE and those requested by EV.
- CCC mode: The tolerance between the EVSE output current compared with the prescribed values sent by EV must be $\pm 2.5A$ for prescriptions below $50A$, and $\pm 5\%$ of the prescribed value for $50A$ or more. The current must be adjusted by EVSE to the value required by EV with a slew rate of at least $20A/s$ for increasing current and $100A/s$ for decreasing current in normal conditions. For the emergency stop and for the fulfillment of the general safety requirements, even much higher reduction rates are required.

The ripple of the EVSE current in CCC mode must not exceed the peak-to-peak values of $1.5A$ at a frequency below $10Hz$, $6A$ at a frequency below $5kHz$ and $9A$ at a frequency below $150kHz$. The measurement

must be conducted at the maximum rated power and current or, in the worst case, when the output voltage and output current theoretically correspond to the maximum ripple of the current. The ripple of the current is not included in the tolerances defined for the gain and slew rate of the controlled system.

- CVC mode: The tolerance between the output voltages from EVSE compared with the prescribed value sent by EV must not be greater than 5% in the precharge phases and 2% in CVC operation. The maximum voltage variation in normal operation must not exceed $\pm 20V/ms$, in case of load loss must not exceed $\pm 250V/ms$. The maximum ripple of the voltage in normal operation must not exceed $\pm 5V$.
- Recharge status: Tab. 2.2 defines the charging statuses, which show the physical situation of the system between EVSE and EV. The EVSE and the EV can exchange state of charge with each other through signal communication and digital communication.
- Synchronized control: EVSE and EV must synchronize the control processes with each other. For synchronization, the signals, via the pilot conductor circuit, the parameters, via the digital communication circuit and the measured values such as the voltage and current level of the charging circuit must be used. EVSE and EV must preserve specified time constraints and control timing to ensure fine control of the charge and smooth operation. The charge control process at the system action level is shown in Tab. 2.3 of [S17]. Parameters, formats and other communication requirements of digital communications are specified in [S18].

Connection sequence The checks to be carried out for safe recharging are listed below, more or less ordered as they should be performed in time. If the EVSE can supply more than one vehicle simultaneously, it shall ensure that the CP pins performs the above functions independently at each connecting point.

- Continuous continuity checking of the protective conductor: both in isolated and non-isolated systems, the continuity of the protective conductor between EVSE and EV must be checked. The emergency stop must occur only if the voltage between $DC+$ and PE or between $DC-$ and PE is greater than $60V$ in case of loss of electrical continuity for a time greater than $5s$ or of incapacity to verify the continuity.
- Retention/release of the coupling device: the mobile plug used for DC charging must be locked on a fixed socket; when the connectors are not locked together, the voltage between $DC+$ and $DC-$, between $DC + / -$ and PE must not exceed $60V$. A mechanism must be provided for retaining/disengaging the vehicle coupling device. This mechanism may consist of a mechanical, electrical interlock or a combination of interlock and mechanical lock. The interlocking device must be present on EV and/or EVSE according to the type of connection (on the EV for case C); the interlocking occurred is one of the preliminary messages exchanged between EV and EVSE. A means must be provided for safe disconnection in the case of malfunction of the locking system. Even in conditions of mechanically defective clamping, the release detection must lead to the disconnection of the connectors.

Table 2.2: Charging status of DC EV charging station

Status		Vehicle connected	Vehicle contactor	Charging possible	Description
DC-A	Not connected	No	Open	No	Vehicle unconnected
DC-B1	Initialization	Yes	Open	No	Vehicle connected not ready to accept energy, communication not established, connector unlocked, vehicle contactor open
DC-B2		Yes	Open	No	Vehicle connected not ready to accept energy, communication established, connector unlocked, vehicle contactor open
DC-B3		Yes	Open	No	Vehicle connected not ready to accept energy, communication established, connector locked, vehicle contactor open, other supplemental processes not completed
DC-C	Energy transfer	Yes	Close	Yes	Vehicle connected ready to accept energy, indoor charging area ventilation not required, communication established, connector locked, vehicle contactor close, other supplemental processes completed
DC-D		Yes	Close	Yes	Vehicle connected ready to accept energy, indoor charging area ventilation required, communication established, connector locked, vehicle contactor close, other supplemental processes completed
DC-B'1	Shutdown	Yes	Close	Yes	Vehicle connected, charging finished, communication maintained, connector locked, vehicle contactor close
DC-B'2		Yes	Open	No	Vehicle connected, charging finished, communication maintained, connector locked, vehicle contactor open, other supplemental processes completed
DC-B'3		Yes	Open	No	Vehicle connected, charging finished, communication maintained, connector unlocked, vehicle contactor open
DC-B'4		Yes	Open	No	Vehicle connected, charging finished, communication finished, connector unlocked, vehicle contactor open

Table 2.3: Charging control process of DC EV charging station at system action level

Charge control phase (process)		Status	Action
Initialization	Handshaking	DC-A	Vehicle unconnected
		DC-B1	Connector plugged in
		DC-B1	Wake up of VCCF
		DC-B1	Communication data initialization
	DC-B1→DC-B2	Communication established, parameters exchanged, and compatibility checked	
	Charge preparation	DC-B2→DC-B3	Connector locked
		DC-B3	Insulation test for d.c. power line
DC-B3		Pre-charge (depending on the system architecture)	
Energy transfer	DC-C or DC-D	Vehicle side contactors closed	
	DC-C or DC-D	Charging by current demand (for CCC)	
	DC-C or DC-D	Charging by voltage demand (for CVC)	
	DC-C or DC-D→DC-B'1	Current suppression	
	DC-C or DC-D	Renegotiate parameter limits (option)	
Shutdown	DC-B'1	Zero current confirmed	
	DC-B'1→DC-B'2	Welding detection (by vehicle, option)	
	DC-B'2	Vehicle side contactors open	
	DC-B'2	DC. power line voltage verification	
	DC-B'3	Connector unlocked	
	DC-B'4	End of charge at communication level	
	DC-A	Connector unplugged	

- Requirements for adaptor: vehicle adaptors shall not be used to connect a vehicle connector to a vehicle inlet. Adaptors between the EV socket-outlet and the EV plug shall only be used if specifically designated and approved by the vehicle manufacturer or by the EVSE manufacturer and in accordance with national requirements.
- Properly connection verification: proper connection is assumed when the continuity of the PP and the CP circuit is detected. For DC charging, established digital communication between EV and EVSE validates the

DC energy transfer. The DC supply to the vehicle shall not be connected until such complete validation from the vehicle is achieved.

- Checking the integrity of the power supply circuit: if a ground fault, short circuit or overcurrent is detected in the output circuit of the EVSE, the power circuit must be disconnected from its supply, but the control circuit power supply must not be interrupted unless the power circuit interruption is due to a loss of the AC power supply.
- Compatibility assessment: the compatibility between the EV and the EVSE must be verified by exchanging information during the initialization phase.
- Short circuit test: The EVSE must have a means to verify the short circuit between $DC+$ and $DC-$ of the cable and the EV plug with the EV connected to the EVSE and before the EV contactor is closed.
- Overvoltage protection: the EVSE must interrupt the charging current supply and disconnect the power circuit to remove the overvoltage source. An overvoltage condition can occur if the voltage between $DC + / -$ and PE is greater than 110% of the DC output voltage for more than 5s. Overvoltage occurs even if, due to the minimum output voltage from EVSE, the voltage between the $DC + / -$ and the PE is not included between $\sqrt{2}(U_n + 1200)V$ and $\sqrt{2}(2U_n + 1000)V$ or if a voltage pulse exceeds the nominal value of 2500 V. The EVSE must interrupt the supply of the charging current and disconnect the power circuit to remove the source of overvoltage.

- Insulation test: the EVSE must confirm the insulation resistance between its DC output circuit and the protective conductor to the vehicle chassis, including the charging station casing, before the closing of the EV contactors is allowed. During the test, any relay in the EVSE DC output circuit must be closed and the insulation resistance must be greater than $(100\Omega/V)U_n$, where U_n is the nominal DC output voltage towards EV. If the prescribed value is not respected, the EVSE must send the signal to the vehicle that the charging is not allowed.
- Emergency power off: in the event of a fault in the EVSE control circuit, such as a short circuit, ground fault, CPU fault or overtemperature, the EVSE must cut off the charging current supply and disconnect the control circuit power supply. The interruption of the charging current or voltage occurs at an accelerated and controlled speed or at a sudden and uncontrolled speed. In the case of controlled power supply, the vehicle is duly notified of the fault so that it can adapt its charging circuit accordingly. In addition, the conductor, in which the earth fault or overcurrent is present, must be disconnected from its power supply. One second after the EV has been disconnected from the power supply, the voltage between the accessible conductive parts or between any accessible conductive parts and the protective conductor must be less than or equal to $60V$ and the available accumulated energy must be less than $20J$.
In case of failure of the mechanical or electrical block of the mobile connector, the station must not supply the DC power lines of the connected connector. If the failure is detected during the charging, the station must

reduce the output current in DC less than $5A$ within $2s$. Therefore, the switches placed on $DC+$ and $DC-$ must open, to avoid welding of the EV contactor.

- Energization of the power supply to the EV: the EV socket-outlet or the vehicle connector shall not be energized unless the control pilot function between EVSE and EV has been established correctly with signal states that allow the energization.
- Maximum allowable current: the value of the EV maximum current permitted shall be transmitted at the beginning of the recharge phase by the EV to the EVSE. The maximum charge current is the minimum value between the maximum current that the EV permits and the maximum current that the EVSE provides ($400A$ for *Mode 4*). The actual values of current and voltage may change during the charging phase, they follow the recharge request from the EV and adapt to power limitations, e.g. for load management. The EVSE may interrupt the energy supply if the current or voltage drawn by the EV exceeds the transmitted value.
- De-energization of the power supply to the EV: if the control pilot signal is interrupted, the power supply to the EV shall be interrupted; if the control pilot signal status no longer allows energization, the power supply to the EV shall be interrupted but the control pilot signaling may remain in operation.
- Disconnection of plug connected to EV or EVSE: if the EVSE is connected to the cable with a plug (*case A* or *B*), the connection pins are

still accessible after unplugging. Therefore, the voltage between any combination of accessible contacts of the standard plug shall be less than or equal to $60V$ or the stored charge available shall be less than $50\mu C$. For *case C* the EVSE shall not provide automatic or remote reclosing of protective devices.

2.2 Functional requirements

The standards provide an excellent basis for choosing the requirements of a UFCS; however, these constraints grant a lot of freedom in design. Therefore, the characteristics of the station must be carefully chosen based on the operations, the impact on the network and the budget.

The topics addressed below concern the number of slots to charge more than one vehicle at same time, the input and output voltage and current values, the integration with renewable sources and with storage systems. Furthermore, also a non-functional requirement such as reliability is appointed.

2.2.1 Renewable's penetration

In the next future, when the diffusion of UFCSs will be affective, the charging stations will be load with smart microgrids. Smart microgrid is an effective form of distributed generation (DGs) integration on distributed network, it must be able to measure, predict and manage flows of power from sources and loads. UFCS, basically, is an energy-greedy load which, if not managed correctly, can cause distribution grid issues.

Depending on the time and the location, when the EVs are plugged in, these

extra electrical loads have an impact on the distribution grid which is analyzed in terms of power losses and voltage deviations. From the distribution system operator point of view, the power losses during charging are an economic concern and must be minimized and transformer and feeder overloads must be avoided. Uncoordinated charging of EVs may lead not only power losses, but also power quality losses, voltage collapse, frequency instability, harmonics injection and many other problems; they are essential to the distribution grid operator as well as to grid customers.

In [19], PHEV charging impacts on the distribution grid are analyzed considering a residential feeder of 10 kV into some of its aspects such as load profile, power loss, voltage quality, and several penetration level scenarios. Furthermore, [20] provides details of an analytical framework to evaluate the impact of PHEV loading on distribution system operations as part of a large, multi-utility collaborative study.

In [21], the potential impacts of charging operations are analyzed with emphasis on three areas: load profile and peak demand; change in voltage levels and violation of statutory limits; voltage imbalance (for single-phase operation). Moreover, [22] proposes a comprehensive approach for evaluating the adverse impact of different levels of PHEV penetration on the loss of distribution transformers' life. The proposed method is applied to a sample distribution transformer supplying residential customers. In [19], the impact of charging of the EVs on the distribution network and a resolution with an optimal design of a smart grid has been analyzed.

Hence, the penetration of large numbers of EVs will demand a better coordination of the power flow between the grid, the EVSEs and the EVs [23]; this can

be achieved by designing smart charging stations.

All these remarks must be taken into consideration in the design of an infrastructure that don't want to be a laboratory prototype yet, but also a scalable system low impactful on the distribution grid and ready to be diffused on the market.

Recent studies have shown that significant deployment of distributed generation creates reverse power flow in distribution networks and that bi-directional power flow can have effects on the quality of power supply and voltage levels. Distributed generation may also lead to increased fault currents, malfunction of the network protection system and phase imbalance (specific to single-phase applications). If we can coordinate the charging and discharging, many ancillary services can be easily handled, and this can become an efficient tool to run the grid in stable region and the most suitable solution for the spread of UFCSs. The most used operation performed by a smart microgrid is the equalization of the power flow with strategies of peak shaving [22, 24–30], load shifting [31–37] and load levelling [38–40].

These techniques of equalization and all the devices to generate and store energy can be applied in the smart control of EVSEs both locally and globally.

The global levelling means straightly interfacing the station to the entire distribution grid and handling power load; with this solution the grid is the single supplier for the EV charger. In [19], a wide coordinated network of charging structures is proposed to minimize the power losses and to maximize the main grid load factor. In this paper, the uncoordinated and coordinated charging of the batteries of the PHEVs are discussed and deterministic household profiles are used, assuming that there is a perfect knowledge of the future data. In [41],

a novel planning model that allows co-optimizing the investment and operating costs of conventional generation assets and demand flexibility, in the form of smart charging/discharging electric vehicles (EV), is proposed. In [42], various indirectly controlled charging schemes have been proposed to control energy prices, in order to indirectly influence the charging operations.

Smart charging schemes can directly control a rich set of charging parameters to achieve various performance objectives, such as minimizing power loss, maximizing operator's profit, ensuring fairness, and so on. In [43], a scheduling method allows EV charging at the lowest cost while complying with technical constraints required by distribution system operator and transmission system operator. In this paper, the advantages of the coordinated charging method are quantified in a real case study in the city of Quito, Ecuador. In [44], the impact of uncoordinated, coordinated, and smart charging of plug-in hybrid electric vehicles (PHEVs) on the optimal operation of microgrids (MGs), incorporating the dynamic line rating (DLR) security constraint, is investigated. In [19], a Smart charging method is explored which can optimize the chargeable power in each period by the short-term load forecast while meeting the charging requirements, and achieve smoother load profile, less power loss and better voltage quality.

The global levelling is not often a solution sufficiently acceptable for the UFC because the stations connected to the MV grid can be supplied directly with the whole required power, the same thing is not feasible in station connected to the LV grid. Therefore, adding DGs and ESSs as proper parts of the station is becoming increasingly popular; the local levelling is the management of these smart microgrid integrated with the charging stations.

The solution adopted for the prototype in this dissertation is definitely the direct integration of RESs and ESSs into the station and the utilization of the local levelling. There are several different ways to configure and control a system consisting of PEV chargers, renewable distributed generation, energy storage and the electric grid and it is unclear what architectural combination and control methodology makes the most practical sense in terms of cost and performance.

The system might be a self-sufficient system with substantial renewable DG and storage, but no grid interface. If renewable DG, storage, and grid are all present, their relative ratings can be quite different depending on how power flow is managed. For example, the system may or may not prefer to draw power from storage and/or renewable DG before drawing power from the grid; and it may impose different limits on the power that can be drawn from or delivered to the grid. Different designs can also be developed using alternate technologies for renewable DG (e.g., solar photovoltaic versus wind turbine) and storage (e.g., electrochemical battery versus flywheel). In [45], a conceptual framework and a methodology for designing optimal architectures of grid interfaced PEV chargers that also integrate renewable DG and storage is presented. They chose to compare alternative designs in terms of system lifecycle cost, which includes initial capital costs and operating costs (consisting of energy and maintenance costs). By including energy and maintenance costs in system lifecycle cost, [45] incorporates the impact of system efficiency and reliability on the results of our comparative analysis. In that paper a system with a single charger, a single renewable distributed generator, and a single storage unit is analyzed, but the framework presented is applicable to systems with multiple chargers, sources

and storage units.

In the prototype both a photovoltaic generation system and an energy storage system must be integrated. PV panels must be able to provide energy to the station, when it is running and charging vehicles, but also to provide energy to the building where the station is placed; this because the station will be used mainly for experimental tests. ESS must store the energy from PV panels and support the grid in power during EV's charging phase. Certainly, the continuity of charging must be preserved as possible. This information is utilized to size the subsystems of the microgrid and to place them in the suitable point of circuit.

2.2.2 Multiple Slots

One of the objectives of the realization of the UFCS prototype is to study the management of energy flows in the case of multiple charging vehicles at same time. In fact, this requirement results into the design of a station that has at least two slots. The main issues to be treated are the queueing and the management of energy flows from and to the shared resources as the ESS.

A multiple slots station is different from multiple single slot stations; the main difference is the use of shared resources. The number of components that allows the station to interface with the vehicles depends on the number of vehicles, thus, it is the same for both solutions. Having n single slot stations means multiplying by n all the components to connect the station to the grid, thus, increasing the costs. For this reason, a multiple slots station is a more flexible and cheaper solution.

In *Mode 1* and *Mode 2* charging, the solution of a multiple slots station also

offers the possibility of a simpler vehicle-to-grid (V2G) implementation.

The multiple slots station has an extra standard constraint, it regards the explicit galvanic isolation of each slot from the others. This constraint is already satisfied by the single slot stations because the isolation from the grid also allows the isolation among the charging slots. For the above mentioned issues, the UFCS prototype is a double slots station.

2.2.3 Output values

The standards suggest specific choices of the range of values of EVs voltage and current. The current at the output of the station get up to $400A$, rather, the maximum value of voltage is set to $1kV$ due to the isolation and protection issues. While the maximum current is a defined value, the operative maximum and minimum values of voltage are not normalized.

According to the author, in 2021 no certified source provides a complete list of all electric cars available on the market, the sources [46–48] are unofficial lists, but still reliable, they are available online and constantly updated. In particular, [47] is a directory made available by Idaho National Laboratory, a complex of national laboratories, part of the U.S. Department of Energy, which contains a huge set of documentation and tests performed on hundreds of electric cars. The most relevant information concerns the charging/discharging voltage, current and power curves, performed in different operating cases, the charging times and some aggregate data on the management of the battery pack temperature by the vehicles.

These sources allow to concretely fix the nominal voltage of an EV's battery in a range between $300 - 800V$; the maximum and minimum values can be

evaluated by the modeling of the battery.

The energy storage on EVs is an electrolytic battery; typically, the most used technology is a stack of Li-ion cells. In an electrolytic cell, the direction of the current flow depends on the difference between two electrodes, the cathode and the anode. At the cathode, electrons are transferred from outside the electrolyte causing the discharge of some positive ion (cation), or the generation of a negative ion; it is also called reduction. The opposite occurs at the anode, in which the phenomenon is the oxidation. It should be noted that anode and cathode indicate the direction of the current flow and not the polarity. In a rechargeable battery, the electrodes switch function between charge and discharge. Major details on battery technologies are given in Chapter 4. The next step is to know which are the main modeling approaches in order to estimate the voltage.

A good choice is to use a reduced-order equivalent electric circuit model (EECM), that combine voltage sources, resistors and capacitors to characterize the physical behaviour of the battery. The simplest model is a zero-order V-I based EECM:

$$OCV = (\alpha_1 + \alpha_2 SoC) \cdot V_n \quad (2.1)$$

$$V = OCV + R_{int} \cdot i \quad (2.2)$$

where OCV is the open circuit voltage, that is the voltage on the battery terminals when no current flows, SoC is the state of charge, that is the ratio between the total storable energy in the battery and the energy actually stored, V_n is the nominal value of OCV , R_{int} is the internal resistance that refers

to the joule power losses and α_1 and α_2 are parameters dependent on the technology of battery.

This model approximates the relation between the *OCV* and *SoC* with a linear time-invariant (LTI) equation, it neglects the dependency of *OCV* on temperature, and it doesn't describe the dynamic effects, polarization effects and aging effects of the battery. The accuracy of this model is typically low, only suitable under constant current and constant temperature conditions; these conditions may be realistic for a cell, but not for a battery. Nevertheless, this model is widely utilized in literature in broad sizing.

In Chapter 4 the selection criterion of α_1 , α_2 , k and R_{int} is better explained, the used values here are $\alpha_1 \approx 0.8$, $\alpha_2 \approx 0.3$. The equivalent resistance is strongly dependent on temperature, aging, technology, and topology of battery; its value is less than few hundreds of $m\Omega$.

In addition, the maximum value of the voltage is not that at the maximum values of the *SoC* and the current. Even assuming that the maximum value of the current is provided up to $SoC = 0.8$, a vehicle with the nominal voltage of $800V$ has a maximum voltage of $830V$ during the charging phase. The minimum voltage can be evaluated in the same way, a vehicle with the nominal voltage of $300V$ has $240V$ of minimum voltage at $SoC = 0.1$ during the charging phase.

Therefore, an UFCS must be able to provide the voltage and the current in a range of $240 - 830V$ and $0 - 400A$, respectively. Due to this huge working area, a right design is mandatory to assure similar values of efficiency in the whole range.

2.2.4 Input values

The previously calculated output voltage and current values of the station suggest that the output power on a single charging slot must be able to reach approximately $320kW$; thus, the input power value is the same, less the losses. The standards do not refer to the input voltage and current values of the station, in literature and on the market the proposed infrastructures are installed both on LV and MV grid.

While the standards on the interface between the charging station and the electric vehicle are international standards, so that, given the design directives, it should be the same for all car makers, the guidelines on voltage and current values of the interface between the station and the network are thickly dependent on the characteristics of the network; these characteristics are not globally harmonized.

The international standard [S4] defines a set of standard voltages of LV and MV for both AC and DC electricity supply systems. The standard aims to consolidate AC and traction voltages within the industry and defines the following bands:

- band 1 - A.C. systems 100 V to 1000 V;
- band 2 - A.C and D.C traction systems;
- band 3 - A.C. systems above 1 kV to 35 kV;
- band 4 - A.C. systems above 35 kV to 230 kV;
- band 5 - A.C. systems above 245 kV;

In [S19], a standard on requirements for grid connection of generators is established; [S20] deals with demand connections; [S21] legislates the requirements for grid connection of HV direct current systems and direct current-connected power park modules. The European standard [S22] specifies the technical requirements for the protection functions and the operational capabilities of micro-generating plants, designed for operating in parallel with public LV distribution networks.

In particular, [S19] subdivides connection points into 4 distinct classes, based on the size and voltage:

- Type A : power equal to or greater than 800 W and less than or equal to 11.08 kW;
- Type B : power greater than 11.08 kW and less than or equal to 6 MW;
- Type C : power greater than 6 MW and less than 10 MW;
- Type D : power greater than or equal to 10 MW or connection point voltage greater than or equal to 110 kV;

It is then up to the European countries to individually define the details on voltage and frequency levels and the classification of the networks in HV, MV, LV.

The prototype to which this thesis refers is made in Italy; therefore, the normative reference that regulate the technique for the connection of active and passive users is [S23]. It derives from the European regulations and it regulates the LV distribution network, and [S24], which regulates the MV and HV distribution network.

The connections to the LV distribution network are characterized by a nominal voltage value between the phases lower than or equal to $1kV$ in alternating current. Unless otherwise stated, it is $230V$ for single-phase supplies and $400V$ for three-phase supplies; the rated frequency is $50Hz$. The connections to the MV distribution network are characterized by an effective value of the rated voltage between the phases greater than $1kV$ and less than or equal to $35kV$ in AC. In the case of nominal voltage between the phases above $35kV$ and up to $150kV$, the connection is in HV.

UFCSs supplied by a MV grid are the most widespread and already in place, but their use implies that the installation point has an MV electrical substation. An electrical substation is a part of the electrical system that includes terminations of transmission or distribution lines, equipment, and electrical panels and which can also include transformers. The electrical substation also generally includes all the devices necessary for control and protection. Depending on the function performed, it can be defined as a transformer, conversion, transmission, or distribution substation.

The typical required steps to install a MV connection to the grid via MV PoD are:

- Request for power increase to the energy provider;
- Supply and install the MV cabinet, including the entire set of instrumentation, equipment of the local energy distributor and other civil works. Often the MV cabinet is already installed, and this step is not required;
- Unless the MV PoD is not installed yet, supply, installation and civil works of the MV cabinet, including the entire set of instrumentation and

equipment of the local energy distributor;

- Supply and install a new LV PoD and modify the MV main electric panel to feed the new UFCS;
- Supply and install the MV/LV transformer, MV and LV cables and civil works to connect together the main electric panel, the transformer and the new LV PoD;
- Wait until the energy provider check the entire process.

On the other hand, the installation of an infrastructure directly connected to the LV grid needs only a request of power increase to the energy provider (the power is limited in the LV range) and the modification of the already existing LV PoD, if necessary.

The MV connection provides benefits in terms of the cost of energy and less power losses, but it also involves many fixed and management costs of MV electrical substation. Even though the costs change a lot depending on the countries, the MV connection has definitely higher initial and maintenance costs than the LV connection. In Italy, the regulatory body of mandatory tariffs and methods of connection to the electricity distribution network is ARERA (Autorità di Regolazione per Energia Reti e Ambiente).

The cost assessment shows that if the connection to the MV is available at the installation point and the main management and maintenance costs are already incurred for other loads, a UFCS connected to MV is undoubtedly the best choice. The issue is that, in major European countries, MV connections are not widespread in every highway and in the urban and rural areas are less than

in the industrial ones.

The LV connection is more expensive in operating costs, but less expensive in installation and maintenance costs. The LV-coupled infrastructures are also typically easy integrated with renewables. In Sec.2.2.1, the renewable's penetration is addressed; that discussion results in the constraint on the presence of a PV system and an ESS. In this scenario, some of the needed charging power may be provided by the local smartgrid to the station and the grid power could be less than $100kW$ and the LV connection may be not a priori rejected. The constraint chosen for the realization of the prototype is utilizing a three-phase LV connection ($400V$ and $< 100kW$).

2.2.5 Reliability and safety

Reliability often plays the key role in the cost-effectiveness of systems. It is closely related to availability, which is typically described as the ability of a component or a system to function at a specified moment or interval of time [49]. Availability, testability, maintainability and maintenance are often defined as a part of reliability engineering.

A reliability assessment is a complex learning and knowledge-based system unique to one's products and processes. This process affects the whole design cycle, from the assignment of requirements up to the production and testing phase, therefore, the reliability assessment concerns the system from general to specific.

Each level of reliability assessment can be analyzed with different tools, the most solid and application-independent strategies are Reliability Block Scheme and Failure Mode and Effect Analysis (FMEA) or Root Cause Analysis (RCA).

Reliability Block Scheme is a technique to identify how the reliability of the components impacts the reliability of the system in different operative conditions. Reliability function is defined as the probability of success at time t , which is denoted $R(t)$. This probability is estimated from detailed (physics of failure) analysis, previous data sets or through reliability testing and reliability modelling. It allows to represent "probability of failure" as a symbol in an equation, but it is difficult to predict its true magnitude in practice. It is interesting to note that reliability block scheme doesn't necessarily coincide with physical block scheme and there are different reliability block schemes for the same system changing reliability function.

FMEA is a qualitative and systematic tool to find the possible causes of failures and to anticipate what might go wrong with a product or process. FMEA provides a structured approach for evaluating, tracking and updating design/process developments. There are currently two types of FMEA: Design FMEA (DFMEA) and Process FMEA (PFMEA). An FMEA uses three criteria to assess a problem: the severity of the effect on the customer; how frequently the problem is likely to occur; how easily the problem can be detected.

Root cause analysis (RCA) is a method of problem solving used for identifying the root causes of faults or problems. RCA can be decomposed into four steps: Identify and describe the problem clearly; Establish a timeline from the normal situation up to the time the problem occurred; Distinguish between the root cause and other causal factors; Establish a causal graph between the root cause and the problem.

In general, both a working but not safe system and a safe but not working system can be realized. A good practice in safety matters is to include the

constraints about safety on the design of the system, so they become necessary conditions to a proper functioning. Instead, a safe system is unable to endanger people or objects, if it is properly used, but the safety is only one of the requirements for the normal operation of the system.

The requirements on reliability and safety are part of not functional requirements, because they don't affect directly the purpose of the system. Despite this classification, a report on the reliability is always required when a prototype is designed.

In this discussion, no requirements regarding reliability and safety are directly assigned in addition to those already envisaged by the standards. In Chapter 6, the experimental validation, the performance evaluation and a discussion on reliability and safety of the prototype are presented.

Power converters for UFCS: comparison, sizing and control

In Chapter 2 the general constraints, due to the standards, the limits of the installation area and the design choice, are declared. Those constraints are used in this chapter to define the EVSE conversion chain and the electrical topology of the converters.

To summarize, the prototype discussed in this thesis is a microgrid whose main components are 3 sources, which are the grid, the ESS and the PV system, and 2 loads, the two charging slots. It is connected in input to the three-phase AC LV grid and in output to two dispensers, interfaced in DC with the charging EVs. The two dispensers can work at very different voltages and currents depending on the type of vehicles connected and their respective *SoC*. Galvanic isolation must be guaranteed not only between the dispensers and the network, but also between the two slots. Furthermore, a PV system and an ESS must be interfaced with the station.

3.1 Electrical topologies comparison

In literature, smart grids are typically divided according to the type of connection point into: AC common bus, DC common bus, and Hybrid common bus. An excellent overview of this classification is presented in [50].

For the AC-connected systems, the AC common bus supplies each charger at the station, and each charger features a separate AC/DC stage. This approach significantly increment the number of conversion stages among sources and loads, increasing the system complexity and cost while decreasing the system efficiency. The advantages of using the AC bus include the availability and maturity of the rectifier and inverter technology, availability of the AC switchgear and protective devices, and well-established standards and practices for the AC power distribution systems. For the DC-connected systems, the main front-end AC/DC converter is used to create a DC bus, providing a more energy efficient way of interfacing ESSs and RESs. The main front-end features a low-frequency transformer followed by an LV rectifier stage or an solid-state transformer (SST) that provides the rectification, voltage step-down, and isolation function in a single unit. Each charger is interfaced between the DC bus and a DC/DC converter, removing the individual AC/DC converters. With a reduced number of conversion stages, the system efficiency is improved compared to the AC-connected systems.

One potential advantage of the DC common bus approach is that there is a single interconnection with the utility through the main front-end. This provides an opportunity to exploit the load diversification resulting in varying the EV battery capacities and *SoCs*, significantly derating the AC/DC converter

and the grid connection, thus reducing the system installation cost. Other advantages of the DC systems include the absence of the reactive power in DC systems, which simplifies control [51]. The single inverter interconnection with the grid also simplifies islanding from and connection to the main grid. Another potential advantage of the DC distribution systems is the opportunity to use partial power converters to interface between the DC bus and the vehicle [52]. These partial power converters only process a portion of the power delivered to the vehicle, reducing the converter ratings and thus the cost and improving the conversion efficiency. For example, in [53, 54], different partial power DC/DC converters are proposed to interface with a common DC bus of an UFCS. Despite its advantages, a DC-connected system presents unique challenges such as DC protection and DC metering. While there are available protective devices for LV DC systems including fuses, circuit breakers, solid-state circuit breakers, and protective relays [55], there are no established standards for protection coordination in the DC common bus stations. The protection coordination for the DC-connected systems is a complex function of the grounding configuration, fault type, system topology, component specification, size, and so on [56]. This issue becomes even more complicated if the chargers are bidirectional. Because a DC-connected system has limited inertia, it is sensitive to disturbance and might become unstable without fast fault clearance. As a result, the speed of fault detection and isolation is critical to system restoration. Studies on existing DC power distribution systems, such as LV DC microgrids, provide guidelines for the protection coordination of DC common bus stations. In [57], a protection strategy is presented for a LV DC microgrid considering the coordination between different protective devices. In [58], a protection scheme

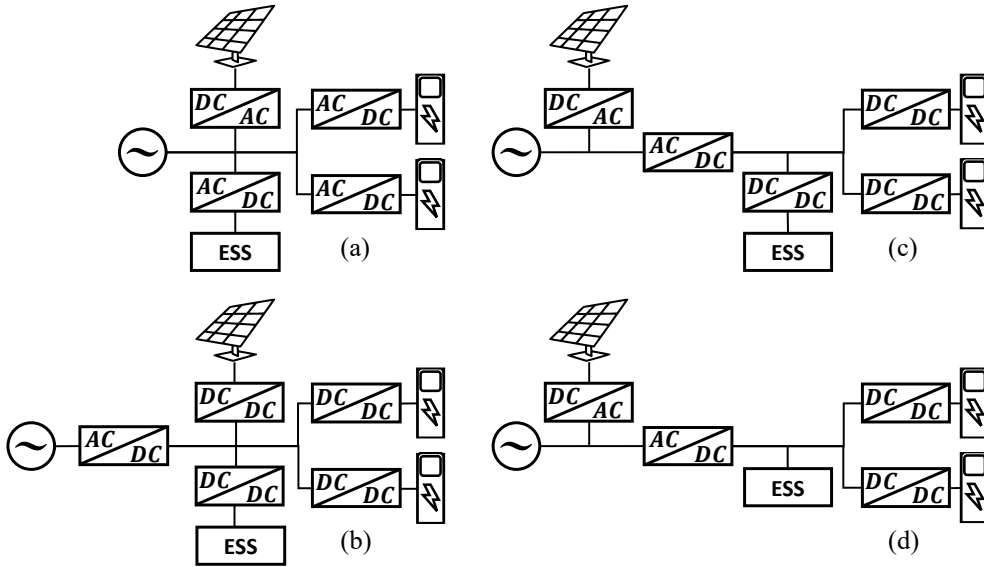


Figure 3.1: Comparison of different topologies of the UFCS meeting the project requirements. (a) AC common bus; (b) DC common bus; (c) Hybrid common bus with free common bus voltage; (d) Hybrid common bus with the common bus voltage equal to the ESS voltage

is proposed for DC systems with a loop type bus. The proposed scheme is able to detect and isolate the fault and provide power uninterruptedly. In the DC-connected systems, DC meters need to be installed to measure the energy generation and consumption of the RESs, ESS and EV chargers.

The Hybrid common bus is a combination of the two other connection schemes. It doesn't combine the advantages of both AC-connected and DC-connected systems, but the number of conversion stages can be reduced a lot because more flexible configurations can be implemented.

To meet the project requirements, both types of connection can be implemented. The different options of electrical topology are shown in Fig.3.1. Fig.3.1a is an AC common bus based system. Sources and loads are connected to the grid

through AC/DC converters, they are sized on the basis of voltage and power values. This solution is very suitable for the PV system, because it is able to supply loads in the direction of EVSE or in that of the grid. The charging slots are connected to the grid through their isolated unidirectional AC/DC converters. The converter of the ESS must be bidirectional.

Fig.3.1b is a DC common bus based system. The grid is connected to the DC common bus through an AC/DC converter, the other sources and loads are connected through DC/DC converters. The total number of converters are more than those presented in Fig.3.1a. Therefore, the energy from the PV system must cross two conversion stages to reach the grid, decreasing the efficiency. The solution in Fig.3.1c, solve the problem of the inefficient connection between the grid and the PV system.

The major drawback of the solutions of Fig.3.1a, Fig.3.1b and Fig.3.1c is the fact that the energy from the ESS must cross two conversion stages to reach the vehicles. Fig.3.1d allows one conversion stage between the PV system and the grid, and the ESS and the vehicles. In this configuration the only bidirectional converter is the AC/DC front end. In addition, the two degrees of freedom of the voltage values of the DC common bus and the ESS can be reduced to one, simplifying the design.

All the presented solutions in Fig.3.1 are valuable, thus, the choice among them depends only on the most frequent directions of power flows and on the expected conversion efficiencies. The prototype is realized in accordance with the electrical topology of the system Fig.3.1d. In the following section the main topologies of both AC/DC and DC/DC converters are compared.

3.2 AC/DC converters

Grid-tied AC/DC converters provide an interface between the grid and a regulated DC bus. A key performance requirement for these converters is high power quality on the AC and DC sides, achieved by input current shaping and output-voltage regulation [59,60]. In Fig.3.2, the AC/DC converters suitable for UFCSs are identified; their features are summarized in Tab.3.1. They are further categorized as bidirectional and unidirectional converters.

Bidirectional AC/DC Converters The most widely used grid-tied AC/DC converter is the three-phase active PWM converter with an LCL filter. It is also called Active Front End (AFE) and it is shown in Fig.3.2a. This boost-type converter has an output voltage higher than the input phase-to-phase voltage. The six-switch PWM converter generates low-harmonic input currents, it provides bidirectional power flow, and enables arbitrary power factor regulation. Due to the simple structure, the well-established control schemes, and the availability of low-cost IGBT devices with sufficient current and voltage ratings, this topology is widely adopted in the state-of-the-art DC fast chargers [61]. In [61], two AFE converter architectures for recharging infrastructure applications are presented and, based on both low-frequency (LF) and high-frequency (HF), isolation requirements are discussed.

Another boost-type converter implementation is the neutral-point-clamped (NPC) converter shown in Fig.3.2b. This three level converter enables the utilization of devices with lower voltage rating that can provide lower switching losses at an acceptable cost. Moreover, the resulting three-level voltage

waveform reduces the input current harmonics and dv/dt . In [62], a $30kW$ EV charger prototype with an NPC front end achieves low THD input current with the leakage inductance of input transformer serving as the ac-side filter. The [63] explores the fundamental limitations of the neutral-point voltage balancing problem for different loading conditions of three-level voltage source inverters. The low-frequency ripple of the neutral point caused by certain loading conditions is reported and quantified. Another advantage of using an NPC converter as the AC/DC front end is that it explicitly creates a bipolar DC bus [63]. This property is explored in [64,65] to implement an EV charging station with a bipolar DC bus, allowing the DC/DC converters to connect to half of the DC bus voltage. The availability of a bipolar DC bus also provides opportunities for the partial-power converter implementation for the DC/DC stage.

The charging station based on the neutral-point-clamped (NPC) converter can bring many merits, but it has unbalanced power problems in the bipolar DC bus. To solve this issue, [65] propose a comprehensive DC power balance management (PBM) in conjunction with high-power three-level DC/DC converter based fast charger.

The other proposed structures in literature are more complex even if they may be more efficient or with reduced volume and costs. For example, in [66], the full conversion stage is composed of a 6 leg-inverter with three ports (for grid, a charging slot and an ESS) and a high frequency link transformer as interface. In [67], an integrated solid-state transformer (I-SST) with high-frequency (HF) isolation for electric vehicle (EV) fast-charging applications is proposed. A direct multipulse AC/DC rectifier is shown to eliminate low-order harmonics in the

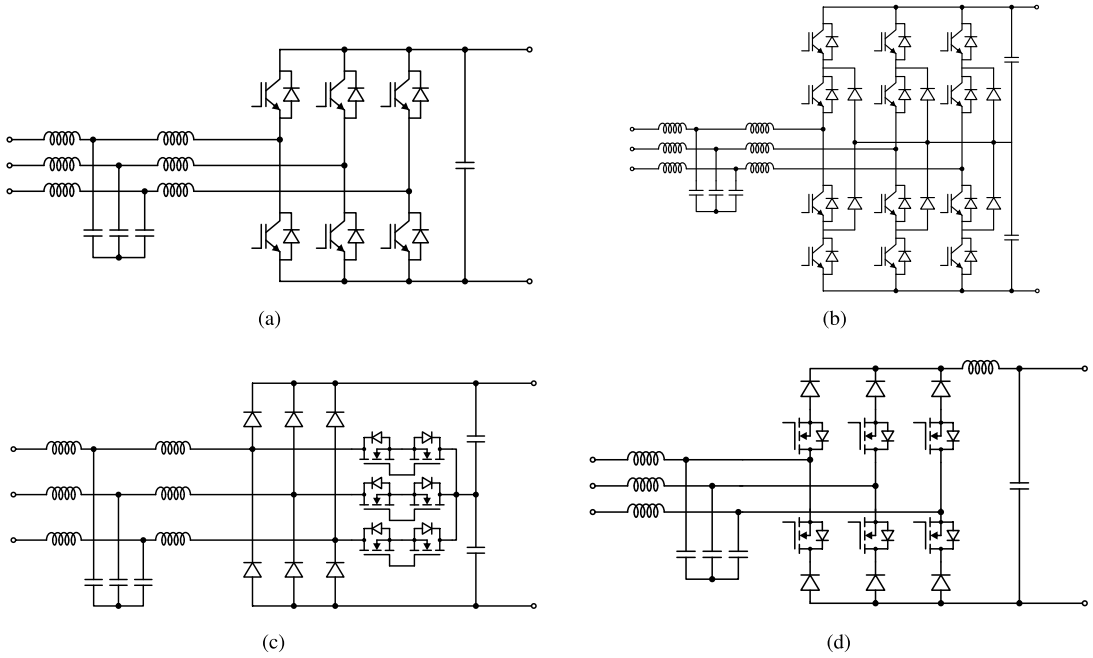


Figure 3.2: Electrical topologies of the most used AC/DC converters in DC charging stations. (a) PWM or AFE converter; (b) NPC converter; (c) Vienna converter; (d) Buck-type converter.

input current over a wide range of output DC voltage variation. The proposed approach has the following advantages: no DC link, hence no bulky electrolytic capacitors, galvanic isolation is via a three-phase HF transformer, high-power density, and simple control scheme for regulating output voltage. In [68], a 7-level grid-tied CHB converter based fast charging station is developed.

Converter	Switches/Diodes	Bidirectional	THD	PF Range	Control Complexity
PWM Converter	6 / 0	Yes	Low	Wide	Low
NPC Converter	12 / 6	Yes	Very Low	Wide	Moderate
Vienna Converter	6 / 6	No	Very Low	Limited	Moderate
Buck-type Converter	6 / 6	No	Low	Limited	Low

Table 3.1: Comparison of AC/DC converters of 3.2, taken by [50]

Unidirectional AC/DC Converters If only unidirectional power flow is required, the T-type Vienna rectifier, shown in Fig.3.2c, is a three-level solution with a reduced number of active switches. While it preserves all the advantages of three-level converters, it also shares the common issues of three-level converters including the need for DC-link capacitor voltage balancing. One major limitation for the Vienna rectifier is the unidirectional power flow and the limited reactive power control. Due to the restricted modulation vector, the range of the achievable reactive power is narrow and depends on the output voltage. The [69] presents a $25kW$ EV charger prototype with a single-switch Vienna rectifier and four parallel three-level DC/DC. In [70], a $20kW$ SiC-based Vienna rectifier switching at $140kHz$ is 98.6% efficient and features compact passive components. In [71], an EV charger is proposed that uses a Vienna rectifier and two isolated DC/DC converters with each DC/DC converter interfaced to half of the DC bus voltage. By using the DC/DC converters to inject the sixth-order harmonic in the DC bus voltage, only one phase of the Vienna rectifier is PWM at a time, improving the system efficiency. If the output voltage is lower than the input phase-to-phase voltage, a buck-type unidirectional AC/DC converter shown in Fig.3.2d can be used. This converter has some advantages over the boost-type topologies, such as inherent short-circuit protection, simple inrush current control, and lower output voltage. An additional advantage is that the input current can be controlled in an open loop. The power flow can be reversed only if the output voltage is reversed. Thus, the converter is only unidirectional with a fixed output-voltage polarity. The achievable phase difference between the input voltage and the input current fundamental depends on the required output voltage. In order to achieve a

higher phase difference, the converter needs to operate with a reduced output voltage range. The conduction losses are generally higher for the boost-type converter because more devices are connected in series [72], but the switching losses can be lower. The buck-type converter can still operate at very high efficiency, as reported in [73], where 98.8% efficiency was achieved. In [74], the buck-type rectifier is modified to allow two input phases connecting to each phase leg. With two phase legs conducting the current, in contrast to one phase leg for the buck-type rectifier shown in Fig.3.2d; the device conduction loss is reduced while maintaining low THD of the input current. Adding a fourth diode bridge leg connected to the midpoint of the diode bridge and the star-point of the input capacitors leads to reduced voltage stress on the switches [75]. This allows the use of switches with lower voltage rating and better performance, potentially achieving higher system efficiency.

3.3 DC/DC converters

A DC/DC converter after the AC/DC front end provides an interface to the RES, ESS, or EV slots. Since the EV's battery must not be grounded at all times, galvanic isolation is required to maintain the isolation between the grid and the charging slots so that the battery protection remains unaffected by the charging system. This can be achieved by using an isolated DC/DC converter. Isolated DC/DC converter topologies suitable for EV chargers are presented in Fig.3.3; their features are summarized in 3.2. A more comprehensive review of the isolated DC/DC converters is provided in [76, 77].

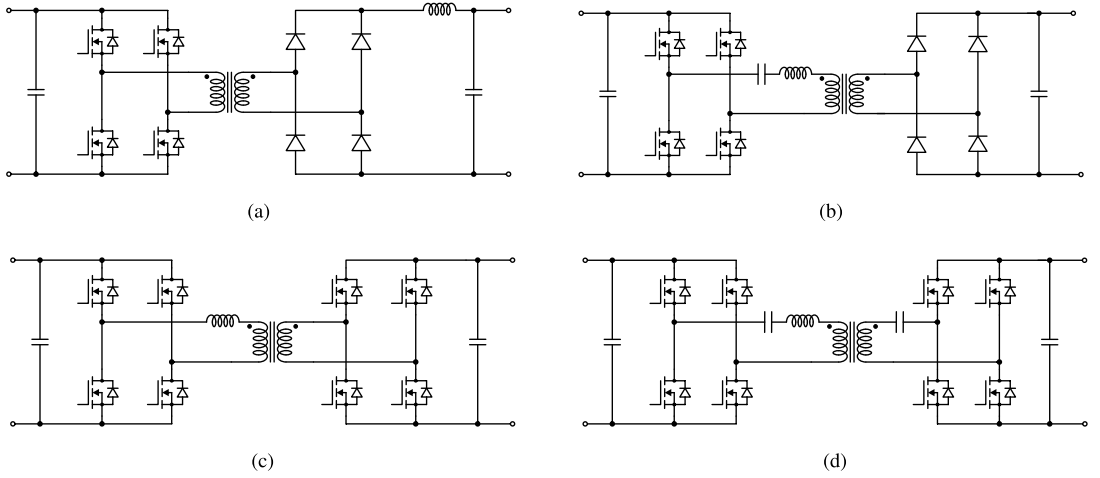


Figure 3.3: Electrical topologies of the most used DC/DC converters in DC charging stations. (a) Single Active bridge (SAB) converter; (b) LLC converter; (c) Dual Active bridge (DAB) converter; (d) CLLC converter.

Converter	Switches/Diodes	Bidirectional	Major Advantages and Disadvantages
SAB converter	4 / 4	No	Simple Control; wide output range. High switching losses in primary switches and output diodes; duty-cycle loss; hard to realize ZVS under light-load.
LLC converter	4 / 4	No	Low reactive current; ZVS on primary side and ZCS on secondary side. Limited controllability; hard to maintain high efficiency and ZVS under wide operating range
DAB converter	8 / 0	Yes	Wide achievable output range. Inherent reactive current; trade-off between reactive power and ZVS condition
CLLC converter	8 / 0	Yes	Low reactive current; wide ZVS range. Limited controllability under wide output range

Table 3.2: Comparison of DC/DC converters of 3.3, taken by [50]

Unidirectional Isolated DC/DC Converters If only unidirectional power flow is required, a possible implementation is the single active bridge (SAB) converter, shown in Fig.3.3a. When the converter operates in phase-shift PWM control, its active switches operate at ZVS turn-on [78]. The main disadvantages of this topology are the turn-off losses in the active switches, high losses in the output diodes, and large ringing across the output diodes due to the LCL resonance of the transformer leakage inductance and the parasitic capacitance of the reverse-biased diodes and the output inductor. To reduce the voltage overshoot and the ringing, active [78] or passive [79] snubber circuits can be applied at the cost of reducing the system efficiency. In [80,81], a current-fed SAB converter is proposed by moving the output inductor to the primary side of the transformer and connecting the diode bridge to an output capacitor directly. This approach minimizes the voltage overshoot and the ringing, but the ZVS range becomes highly load-dependent. Similar auxiliary circuits are used in [82] to achieve ZVS for the SAB converter from the no-load to full-load condition of an EV charger.

Another unidirectional isolated DC/DC converter for UFC is the LLC resonant converter, shown in Fig. Fig.3.3b. The converter output voltage is regulated by changing the switching frequency to adjust the impedance ratio of the resonant tank to equivalent load. The LLC converter uses the magnetizing current to achieve ZVS, resulting in low turn-off losses and low transformer losses [83]. The LLC converter can achieve very high efficiency if the input-to-output voltage ratio is closer to one [84]. However, it suffers from limited light-load power regulation capability and the ZVS condition may not hold for a wide operating range, thus negatively affecting the efficiency. Multiple

approaches are proposed to improve the performance for a wide output-voltage range and at light load conditions. Various control methods are proposed including PWM, phase shift, and other hybrid modulation schemes to narrow the range of operating frequency while broadening the output range [85, 86]. In [87], a variable DC voltage is regulated by the AC/DC converter to match the EV battery voltage, allowing the LLC converter to always operate around the resonant frequency with maximum efficiency. Although this method is simple and effective with no extra hardware, a wide output-voltage range is not guaranteed, since the DC voltage variation is limited by the grid-voltage and switch-voltage rating. Hardware modifications include employing multiple transformers [88] and multiple rectifiers on the transformer secondary side [89]. In [90], an extra capacitor paralleled with a four-quadrant switch is inserted in the LLC resonant tank. By modulating the four-quadrant switch, the inserted capacitance and, therefore, the resonant frequency adapt to the load, improving the efficiency at light-load condition. Despite their effectiveness, these methods require additional hardware and result in higher system cost and larger system volume. In addition, a smooth transition between multiple configurations during operation is difficult to achieve. Another issue for the LLC converter is that the resonant capacitor has to withstand high-voltage stress at high power, which complicates component selection. To enhance the power rating and alleviate the stress on switching devices and resonant components, a multilevel LLC converter [91], a three-phase LLC converter [92], and an LLC converter with paralleled modules [93] can be used.

Bidirectional Isolated DC/DC Converters If bidirectional power flow is required, a dual active bridge (DAB) converter (shown in Fig.3.3c) can be used for EV charging applications due to its high power density, high efficiency, buck and boost capability, low device stress, small filter components, and low sensitivity to component variation [94]. When introduced in 1991 [95], the DAB converter was not widely adopted due to the high power losses and relatively low switching frequency of the power semiconductor devices at that time. More recently, the DAB converter started gaining attention, due to the capabilities of the new SiC- and GaN-based power semiconductor devices and the advances in the nanocrystalline and amorphous soft magnetic materials, which enabled the converter efficiency and power density improvements [96]. In the DAB converter, the power flow is controlled by adjusting the phase shift between the primary and the secondary voltage, with transformer leakage inductance serving as the power-transfer element. Owing to its simple structure and ZVS operation, the DAB converter has been extensively used in isolated bidirectional DC/DC conversion applications [97,98]. For EV battery charging, the converter is required to operate with a wide range of voltage gain and power due to the EV charging profile, under which reactive power can increase dramatically and ZVS condition no longer holds [99]. This causes a dilemma in the design of leakage inductance, in which high leakage benefits a wide ZVS range but worsens the reactive power and results in lower efficiency, and vice versa [100]. To improve the performance under a wide operating range, various modulation schemes have been proposed. The [101] propose dual-phase-shift (DPS) modulation to minimize the current stress of the switching devices, where the primary and secondary duty cycles are introduced as an additional

degree of freedom. In [102], the DPS is adopted to achieve ZVS under full load range. In [103,104], the concept of DPS is further extended to triple-phase shift (TPS) to enable more degrees of freedom and achieve multiple design objectives such as broader ZVS range, lower current stress, and improved efficiency. In addition, hybrid modulation incorporates operating frequency and pulse density to regulate the transferred power without sacrificing ZVS while controlling the reactive power flow [105,106]. Recent work in [107] applies TPS to enhance light-load efficiency while switching to DPS to reduce the circulating current under the medium- and heavy-load conditions. However, all proposed control strategies have inherent performance trade offs and require complex modulation schemes that may be difficult to implement and may not be as robust to parameter variation. One more concern regards the high-frequency charging ripple resulting from the reactive power that is inherent to the DAB converter operation [94]. Another variant of the bidirectional DC/DC converter is the CLLC converter shown in Fig.3.3d [108,109]. Due to its symmetrical circuit, the CLLC converter provides the same voltage gain characteristic in both power flow directions, which reduces the control complexity and facilitates power regulation. Moreover, the CLLC converter distributes two resonant capacitors on both sides of the transformer, which helps reduce the resonant capacitor voltage stress compared with the LLC converter [110]. The leakage inductance required for the CLLC resonant tank is much smaller than that required for the DAB converter. As a result, the reactive power circulating in the converter is also smaller. Furthermore, the sinusoidal resonant current of the CLLC converter exerts smaller stress on the high-frequency transformer than the DAB converter [111]. However, due to its similarities with the LLC

converter, the CLLC converter exhibits similar design tradeoffs as the LLC converter such as the ZVS condition and efficiency degradation for a wide voltage and power operating range. The controllability of the CLLC converter is another challenge, as the voltage gain curve against frequency tends to be steady in specific frequency ranges [108]. To solve the above issues, [112] add an auxiliary transformer to help realize full-load-range ZVS while improving power regulation. A detailed parameter design methodology is provided in [113] to realize robust power regulation with a wide operating range. The [114] present a design procedure that handles wide voltage gain requirements, and integrated magnetic components, used to improve power density. In many cases, there is a desire to minimize the number of active devices in a topology. One way to achieve this is to use the half-bridge equivalents of the converters shown in Fig.3.3 including the widely used half-bridge LLC converter [115, 116] and the dual half-bridge (DHB) converter [117–119]. The half-bridge converters use only four active switches, which reduces the cost. Comparing with the full-bridge version, the voltage applied is half of the DC link voltage. This feature is beneficial to the high-frequency transformer design when used in MV applications. However, the current stress on the active devices is doubled, and the degrees of freedom available for converter control are reduced.

3.4 Sizing and control of chosen converters

The converters chosen in the prototype are presented in Fig.3.4. The AFE is the most suitable solution to guarantee the bidirectionality, low complexity in control and an easy way to implement the power factor correction. It is

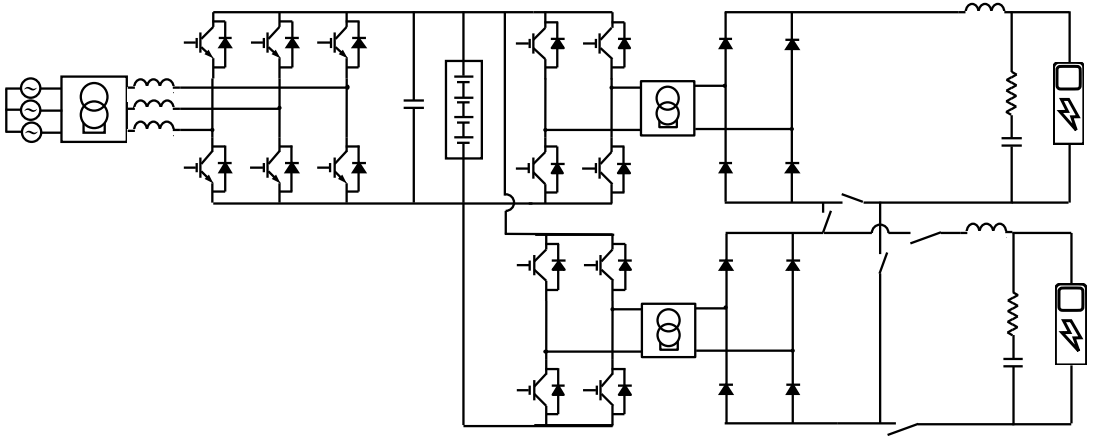


Figure 3.4: Electric scheme of DIETI UFCS prototype

connected to the LV grid through an isolation transformer. The SAB is the easiest presented unidirectional solution in the number of components and control. The constraints on the output current ripple and the dynamic response of the system can be met with a right sizing of the output filters.

The switches on the output side of the SAB converters in Fig.3.4 allow them to work individually, in single configuration, or in input-series-output-parallel (ISOP) configuration. The modular design gives redundancy to the system and allowing to meet the constraints for both normal-size vehicles (400V target voltage and 160kW maximum power) and big-size vehicles (800V target voltage and 320kW maximum power). Therefore, the EVSE in Fig.3.4 can charge two normal-size vehicles at same time or one big-size vehicle using both two converters.

According to the requirements in 2.2.4 and 2.2.3, the sizing specification are:

- the AFE is connected to the three phase LV grid. The input phase-to-ground voltage is $230V_{rms}$ at $50Hz$ and the target power value is around

50kW.

- the SAB is connected to the DC charging slot. The output values range from 200V to 450V and 160kW for a normal-size vehicle; in ISOP configuration the values of voltage and power become twice.

The AFE is a step-up converter, thus, the output voltage value must be higher than the peak of input phase-to-ground voltage. It means the output voltage must be more than 330V to guarantee the modulation index ranging from 0 to 1. Instead, the DAB is a step-down converter, its input voltage must be higher than the output value; it means more than 450V. According to these assumptions, the voltage and the discharging power of the ESS, the last degrees of freedom to discuss, are uniquely assigned: $V_{\text{ESS}} > 450V$ and $P_{\text{ESS,dis}} > P_{\text{EV}} - P_{\text{grid}} = 270kW$.

In this section, also the control of the converters of electrical scheme of Fig.3.4 is discussed. The system control of the UFCS is based on a hierarchized architecture of different local controller which implement inner closed loop control. In the designed charging station the main subsystems which must be controlled are the AC/DC AFE converter and the DC/DC SAB converter. Other subsystems such as the ESS, the data acquisition systems, the cooling system and the human/machine interface (HMI) are also controlled. But in this case the control is practically traditional, and it is little dependent on the specific use of these components in the charging infrastructure, therefore it is not addressed in this thesis. The control of the two converters has been briefly illustrated, since it does not differ from the common control strategies of these subsystems.

The main target of AFE control is to supply the maximum power provided by the grid, P_{grid} , to charge the EV and the ESS. Since the input voltage and current are fixed, also the output power is constant, less the losses. The output voltage is that given by the ESS which changes over time according to its state of charge; consequently the current changes to keep P_{grid} constant.

The model equations of the converter are reported in 3.1, while the 3.2 is the direct-quadrature-zero transformation.

$$\begin{cases} v_k = L \cdot \frac{di_k}{dt} - V_{\text{DC}} \cdot s_k - v_{\text{NO}} \\ C \cdot \frac{dV_{\text{DC}}}{dt} = \sum_{k=1}^3 i_k \cdot s_k - I_{\text{DC}} \end{cases} \quad (3.1)$$

$$\begin{cases} L \cdot \frac{di_d}{dt} = v_d + \omega L i_q - v_{rd} \\ L \cdot \frac{di_q}{dt} = v_q - \omega L i_d - v_{rq} \\ C \cdot \frac{dV_{\text{DC}}}{dt} = \frac{3}{2} \cdot (s_d i_d + s_q i_q) - I_{\text{DC}} \end{cases} \quad (3.2)$$

The decoupled current method has been used for active and reactive power control on the AC side. The control block, depicted in Fig.3.5, allows the constant voltage (CV) and constant current (CC) modes to work, or a combination of both in constant power (CP) mode. The component i_d of space vector of current is controlled by the voltage or the current loop through a PI controller; the reference value of i_q is fixed to zero, in order to guarantee the power factor correction. The d,q duty-cycle components are calculated taking into account the compensation of crossed voltage components.

The control strategy on the SAB converter is a common PWM, Fig.3.6. As in the case of AFE converter, this converter must also have the ability to

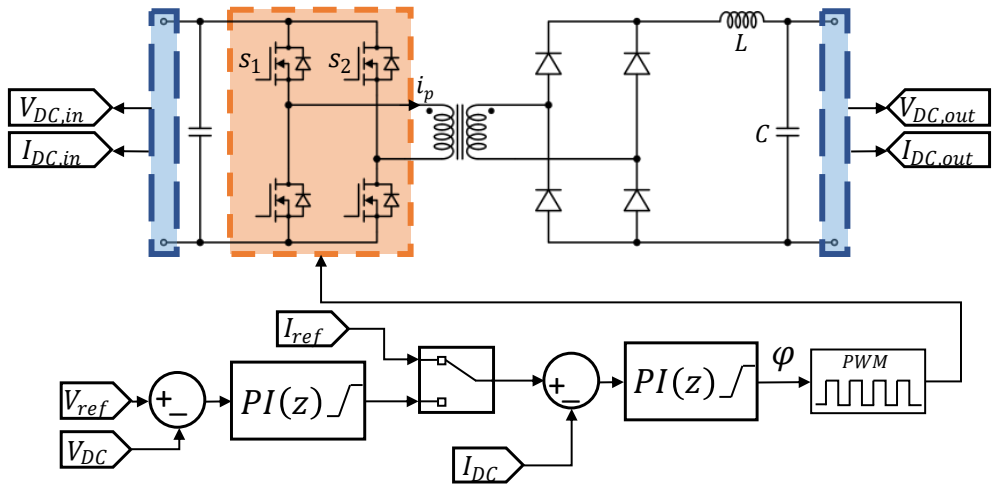


Figure 3.6: SAB control scheme: CV or CC control

switching period, to reduce the current ripple on the ESS. When the station works in ISOP configuration, the power demand is informally distributed to the two converters; this configuration doesn't affect badly on the control.

Energy Storage Systems for UFCS: comparison, modeling and sizing

4.1 Definitions

An ESS is a system able to absorb energy and store it for a period of time before releasing it to supply energy or power services. Through this process, when they are coupled with other energy infrastructure components, the storage technologies can bridge temporal and location gaps between energy supply and demand. The ESS has an important effect on overall electric systems; it provides continuous and flexible power supply to maintain and to enhance power because of congestion and interruption of transmission line for excessive demand.

First of all, a definition of cell and battery must be done. The cell is the elementary part of an ESS; the way to connect more cells together depends

on their technology. The battery is a stack of cells connected in series or parallel, it is interfaced with electrical systems with an anode and a cathode. The term battery is more general and it is used also to refer to a cell. Concerning the main characteristics of ESS, we can highlight the following:

- Capacity. The capacity of an ESS represents the maximum amount of energy that can be extracted from the ESS when it is stored after a full charge. The utilization of the capacity may vary between different technologies in terms of charge/discharge power, thermal conditions, self-discharge, *DoD*, and response time. Regardless of how the energy is stored into the ESS, the capacity can be expressed as Q in *Ah* or as E in *Wh*, although the latter is more used by electric vehicles.
- State of Charge (*SoC*). The *SoC* refers to the battery level with regard to its 100% capacity. It is expressed in percentage or in per unit.

$$SoC = \frac{\text{Remaining Capacity}}{\text{Rated Capacity}} \quad (4.1)$$

$$\Delta SoC = SoC(t) - SoC(t_0) = \frac{1}{Q} \int_{t_0}^t i(\tau) d\tau \quad (4.2)$$

- Depth of Discharge (*DoD*). The *DoD* is used to indicate the percentage of the total battery capacity that has been discharged to preserve the state of health of the ESS.

$$DoD = 1 - SoC \quad (4.3)$$

For deep-cycle systems, they can be discharged to 80% or higher.

- Cut-off Voltage. The cut-off voltage is the minimum allowable voltage (V_{\min}) when the battery is in the “empty” state. Its value is hard to determine and it is often assigned by the manufacturer.
- C-rate. C (nominal C-rate) is used to represent a charge or discharge rate equal to the capacity of a battery in one hour. For a $1.6Ah$ battery, $1C$ is equal to charge or discharge the battery at $1.6A$. Correspondingly, $0.1C$ is equivalent to $0.16A$, and $2C$ for charging or discharging the storage at $3.2A$.
- Energy density or specific energy. Obtaining the highest energy density possible is another important aspect in the development of batteries, or, in other words, with equal size and weight a battery is able to store a higher energy quantity. The energy density of batteries is measured as the energy that a battery is able to supply per unit volume (Wh/L). Some authors distinguish energy density from specific energy, the latter is expressed in energy per unit mass (Wh/kg).
- Power density and specific power. The power that a battery can supply per unit of weight (W/kg).
- Charge/discharge cycles. A charging/discharging cycle is completed when the ESS has reached the maximum/minimum SoC . To define the maximum and minimum values of SoC is not a trivial operation, the specific definition depends on the ESS technology.
- Cycle Life. The cycle life is the number of charge/discharge cycles the battery can handle at a specific DoD (normally 80%) before it fails to

meet specific performance criteria. The goal is to obtain systems that can endure a greater number of loading and unloading cycles.

- Lifespan. The lifespan is the expected calendar life of the ESS, it depends on the cycle life and on the preservation of the system.
- State of Health (SOH). *SoH* can be defined as the ratio between the maximum charge capacities of an aged battery and a brand-new battery [120].

SoH is an important parameter for indicating the degree of performance degradation of a battery and for estimating the battery remaining lifetime.

$$SoH = \frac{\textit{Aged Energy Capacity}}{\textit{Rated Energy Capacity}} \quad (4.4)$$

- Charging power loss. During the charging process, some energy is dissipated in the form of heat (namely, thermal loss). The generated heat per unit of time might be seen as the power loss in resistance in an electric circuit, so the equivalent internal resistance will have a greater impact in high power charges [121].

Typically, the power losses in the charging phase are different from those in the discharging phase.

- Discharging power loss. The discharging phase is more energy consuming than the charging phase. Moreover, more energy will be lost during quick discharging processes when compared to slow ones. Therefore, it is highly important that ESS can support quick discharging and higher temperatures.

- Self-discharging. Although an ESS is not working, its *SoC* decrease over time. How fast self-discharge in a battery occurs is dependent on the type of battery, initial *SoC*, ambient temperature and other factors.
- Memory effect. It is also known as battery effect, lazy battery effect, or battery memory. It describes the situation in which batteries gradually lose their maximum energy capacity if they are repeatedly recharged after being only partially discharged. The battery appears to "remember" the smaller capacity.

An ESS comprises mainly the energy storage, the *Control and Power Conditioning System (C-PCS)*, and the rest of equipment (protection, cooling, etc). Depending on the type and technology of the ESS, the C-PCS components used are different; in the *Battery Energy Storage Systems (BESS)*, the C-PCS is also called *Battery Management System (BMS)*.

A classification of the different types and technologies of ESS is shown below, the storage categories are then compared; from this comparison, the electrochemical BESS with lithium ions are the most suitable for the UFCS application. A detailed analysis of the physical effects and mathematical modeling is disclosed. Subsequently, the voltage, power and energy sizing is carried out respecting the project specifications. Finally, some simulations of UFCS operation are shown to validate the dimensioning of the BESS.

4.2 Technology comparison

The classification of ESS systems is determined according to the way in which the energy is stored. ESSs are classified into mechanical, electrochemical,

chemical, electrical, thermal, and hybrid [122]. These systems are classified into various types according to their formations and composition materials [122,123]. Flywheel, secondary electrochemical batteries, FCs, UCs, superconducting magnetic coils, and hybrid ESSs are commonly used in power electronics applications, in particular for EVs [122–131]. The [132] proposes an excellent statement of classification of ESS reported in Fig. 4.1.

4.2.1 Mechanical storage systems

Mechanical storage systems (MSSs) are commonly used to produce electricity throughout the world. Three MSSs are pumped hydro storage (PHS), compressed air energy storage (CAES), and flywheel energy storage (FES).

The most popular MSS is *PHS*, which is used in pumped hydroelectric power plants. Reserved water of high head is used and pumped to a power turbine with a generator to produce electricity. This storage system contributes approximately 99% of the world electric storage capacity, which is around 3% of the capacity of global electricity generation [133].

CAES is applicable for large capacity electricity production. In CAES, compressed air is mixed with natural gas, expanded, and further converted into modified gas to feed a gas turbine shafted with a generator to produce electricity [134]. The isothermal, adiabatic, and diabatic storage systems are considered to implement CAES [131].

The *FES* systems are suitable for applications for EVs and power systems because of the advances in power electronics and material engineering [135].

The FES comprises a rotating cylindrical body in a chamber, coupled bearings,

Energy Storage Systems for UFCS: comparison, modeling and sizing

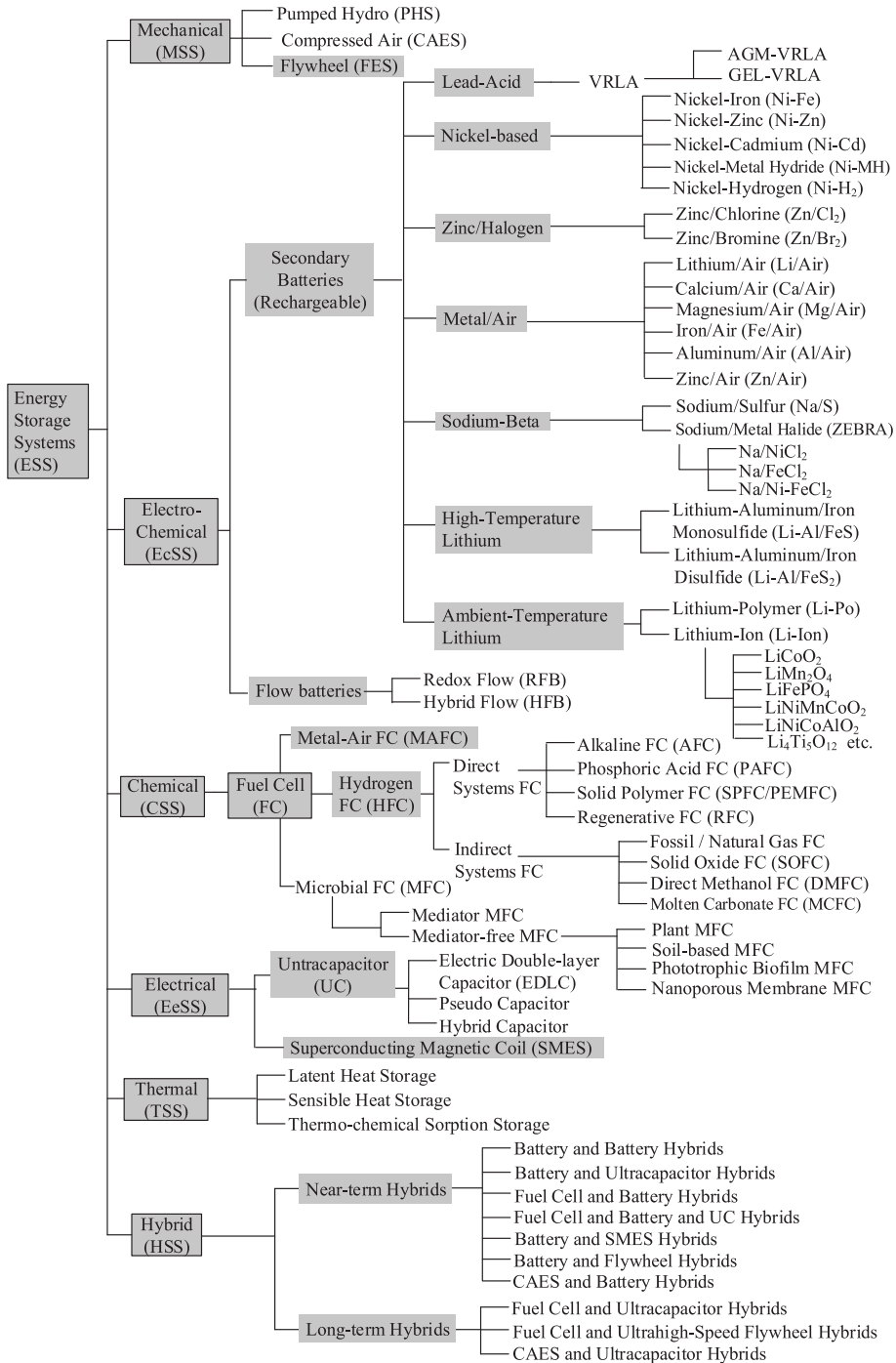


Figure 4.1: Caption

and energy transmission device, i.e., generator/motor together mounted on a common shaft [122, 126, 135, 136]. The rotational kinetic energy maintained by the constantly rotating flywheel is converted into electrical energy by means of a transmission device. The main advantages of the FES systems are high energy and power density, theoretically infinite charge and discharge cycles, low cost, long life, and no *DoD* effect [131, 135, 136].

Although the technological progress in terms of materials, designs, geometry to build the advanced ultra-high-speed flywheel (UHSF) and frictionless bearings, FES has high self-discharging features because of windage and bearing friction losses.

MSSs are the most robust and durable storage solution, the thermal management is simpler than other storage solutions and the maintenance is easy and, most of the time, inexpensive. But this type of storage is not in line with the specifications of an ESS for UFCS due to the self-discharge, which does not allow the storage system to be kept empty for hours or days, and the low energy density, which results into solutions too heavy and bulky to provide the right amounts of energy for the entire charging period of an EV.

4.2.2 Thermal storage systems

The Thermal storage systems (TSSs) store energy in the form of heat into an isolated repository from solar or electric heater for later use in electricity generation plants or different heating purposes CAES [122, 131].

Thermal energy storage is achieved in various ways, such as latent heat storage, sensible heat storage, and thermo-chemical sorption storage systems [122, 137, 138].

Latent heat storage systems have high energy density and efficient heat transfer capability at constant temperature [122,138]. *Sensible heat storage systems* are common, and widespread technologies which storage mediums that are solid (e.g., ground, cast iron or concrete) or liquid (e.g., water or thermo-oil) [122]. The *phase change materials (PCM)*, as molten salt, are used as storage medium to allow heat exchange during the phase change of the storage medium [122]. The *thermo-chemical sorption storage systems* are complex and expensive to design, given adsorption and absorption processes of heat in the materials. However, the energy density of such systems is three times higher than that of a sensible storage system with water [122].

Like MSSs, TSSs are also ecological and robust solutions for energy storage and are used in photovoltaic applications. They suffer of self-discharge less than MSSs, but require more maintenance and slightly more complex control systems. Generators of electricity are widely used, starting from thermal energy, but, for trivial thermodynamic considerations, transforming electricity from the grid into thermal energy and then transforming it again into electricity is no more an efficient solution. This type of ESS is not suitable for UFCS application because there are solutions with higher energy densities and efficiencies.

4.2.3 Chemical storage systems

Chemical storage systems (CSSs) store and release energy through chemical reactions of chemical compounds composed in the system, thereby forming other compounds [139].

The *Fuel cells (FCs)* are chemical storage systems that convert chemical energy of fuel to electrical energy continuously [123,140]. The main difference between

a FC and a battery is the way they supply energy source. In a FC, the fuel and oxidant are supplied externally to generate electricity, and these parts are integrated in the battery (except metal-air batteries) [140].

FCs are composed of liquid or gaseous fuel as anode and oxygen, air, and chlorine as the oxidant in the cathode side. *Hydrogen-based FCs (HFCs)* are especially popular and available in the market. HFCs use a combination of hydrogen and oxygen to produce electricity. This combination could be regenerative and reversible from electricity and water [123].

Depending on fueling, HFCs are categorized into direct and indirect system FCs [140]. In direct system FCs, fuel (e.g., hydrogen and methanol) reacts directly, whereas in indirect system FCs, fuel (e.g., fossil fuels and natural gas) is first converted to reform rich hydrogen gas and then supplied into the cell for the reaction [141].

Simplifying the operation of a FC, a power electrolyzer separates water into hydrogen and oxygen to be fed again to the cell, thereby producing electricity and water, and recycling them repeatedly as long as electricity is needed [140]. The overall chemical reaction in fuel cells is given in 4.5:



Thus, a FC produces electrical energy starting from chemical energy, and thanks to this capability it is an energy accumulator. In fact, a FC can be both powered by electricity, which carries out electrolysis and produces hydrogen to be crammed into a tank, but it can also be powered directly by hydrogen from outside. The capacity of the FC depends on how much hydrogen can

be stored in the tank. The advantage of FCs is their capability to generate electricity as long as the active materials are supplied to it, offering 40 – 85% fuel efficiency [123, 142].

FCs are classified into several types based on fuel and oxidant combinations, electrolyte type, operating temperature, and applications; these types include alkaline FC (AFC), phosphoric acid FC (PAFC), solid polymer fuel cell-proton exchange membrane FC (SPFC-PEMFC), regenerative FC (RFC), solid oxide FC (SOFC), direct methanol FC (DMFC), molten carbonate FC (MCFC) [123, 140, 143, 144], metal-air FC (MAFC) and microbial FC (MFC) [145, 146]. AFC, PAFC, PEMFC, and RFC are used directly as hydrogen fuel at the anode. *MFCs* are biological FC systems that produce electrical energy from chemical energy through catalytic reactions of microorganisms [147]. They are very ecological, but mediators are toxic and costly.

In mediator-free MFCs, electrochemically active bacteria, such as *Shewanella putrefaciens* and *Aeromonas hydrophila*, help transfer electrons [147, 148]. These types of MFCs are now applicable for wastewater treatment and for producing electricity directly from plants, such as rice and tomato [149].

MFCs are mainly employed for low-power applications, such as wireless sensor networks, wastewater treatment, hydrogen generation, biosensors, medical applications, and education kits [147–149].

The maintenance and disposal of a FC are more expensive operations than those of a MSS, but they are equally ecological solutions and largely quieter and smaller than MSS. This type of technology meets the interest of many applications and it may be chosen for charging station solutions with storage, especially where it is possible to produce hydrogen on site. However, they

do not represent the general solution suitable for a UFCS because the energy density is not high enough respect to the cost of production and transportation of the hydrogen.

In fact, producing large quantities of hydrogen on site involves a whole series of precautions to be implemented for safety reasons and this solution does not meet the constraints of all geographical contexts in which a UFCS may be usefully installed. Alternatively, the fuel needed by the FC could be produced in complete safety in ad hoc infrastructures and then distributed, but the network infrastructure to transport hydrogen would be expensive and not flexible enough for a wide diffusion of UFCSs.

4.2.4 Electrical storage systems

The Electrical Storage Systems (EeSSs) store electrical energy directly as electricity in the form of electric field by separating charges or magnetic field by flux. EeSSs are ultra-capacitors and superconducting electromagnets.

A *Ultracapacitor (UC)* is similar to a normal capacitor in terms of structure and function. However, an UC have a high energy capacity with the value of kF [131, 143], its specific power can achieve the value of $1000 \sim 2000 W/kg$ with 95% energy efficiency [123, 143, 144, 150–153].

Among all ESSs, UCs have the longest lifetime of almost 40 years. UCs are adopted in EV applications because of its high-power storage due to its features; it does not require maintenance, and it exhibits temperature insensitivity and a long operation time [123, 143, 153].

The energy stored in the capacitor is directly proportional to its capacitance and squarely proportional to the voltage across electrodes, and the capacity

increases with the increase of the surface area of the electrode and the permittivity of dielectric materials, and with the decrease of the distance between electrodes. For their fast charging and discharging profile, the UCs are used as energy storage during electric braking and as energy source during rapid acceleration needed for hilling in EVs [150–154].

Lead carbon capacitors are good examples of asymmetric Electric Double Layer Capacitor (EDLC) [155]. Carbon nanotube UC technology have the highest power density among the UCs. *Pseudo capacitors* and *hybrid capacitors* exhibit ameliorated performances in energy storage applications because of their higher power and energy densities [156].

Recently, *Li-ion capacitors (LIC)* have been developed; they have higher terminal voltage and energy density than other UCs [157–159]. *LICs* of $80Wh/kg$ are now commercially available in the market for EV applications as substitutes for Li-ion batteries [157, 159].

Superconducting magnetic ESSs (SMES) store electrical energy in the form of magnetic field in a superconducting electromagnetic coil, which is made of niobium-titanium alloys at liquid helium (or super liquid helium) temperature, i.e., $2 - 4K$ [145, 153, 160, 161]. The energy stored by SMES is directly dependent on the self-inductance of the coil and square of the current that flows through [145]. However, SMES needs a refrigeration system to maintain the low temperature and a power converter for DC/AC supply [144, 162, 163]. High-temperature superconducting materials are being developed with a cheaper coolant, such as liquid nitrogen. Generally, SMES is utilized in UPSs, power quality applications, and grid systems [162].

SMES systems have a high energy storage efficiency of approximately 97%, full

energy discharge capability, a long life cycle of $100k$, and quick response of milliseconds [140, 145, 163, 164]. Their initial cost is high, although the cost is lower than that of EDLC [145, 164].

UC as storage for a UFCS can be an excellent solution in terms of efficiency, dimensions and costs for the same energy and power that can be supplied by ESS. In the design of the prototype of UFCS, EeSS is not taken into consideration for two reason:

- The station prototype might be not used frequently, so the typical high level of self discharge of EeSS could compromise the readiness of the station (a previous recharge of EeSS at each use is needed).
- There is a more marked interest in EcSS, rather than EeSS, given that the battery technology is widespread in several sectors and more in development. If the research interest had been less, the solution of EeSS would have been evaluated in higher detail.

4.2.5 Electrochemical storage systems

The most widespread conventional rechargeable batteries are electrochemical storage systems (EcSSs) [165].

In EcSSs, energy is transformed from electrical to chemical energy and vice versa through a reversible process with energy efficiency, low physical changes [165] and no harmful emission and little maintenance [144].

The *Flow Batteries (FBs)* are rechargeable EcSSs, in which the chemical energy is stored in electroactive species dissolved in liquid electrolyte in tanks. The liquid is pumped via electrochemical cell to convert chemical energy into

electric energy; the total size of the tank defines the total energy of the battery.

The Redox batteries (RFBs) are the most used type of FB.

The RFBs have advantages in terms of high life cycle stability (the life expectancy is of 15–20 years), high efficiency (60~70%), quick response time, flexibility in power, low maintenance, which make RFBs attractive in any autonomous and standalone grid systems [162, 166–170].

They are safe because they typically do not contain flammable electrolytes, which can be stored away from the power stack anyway. The two main disadvantages are low energy density (it needs large tanks of electrolyte to store useful amounts of energy), and low charge and discharge rates (compared to other industrial electrode processes). Another drawback is the increased capital and running costs associated with the operation of a chemical plant involving pump systems, and flow control with external storage.

The FBs are also promising for applications which require long duration storages due to its non-self-discharge capability. The main challenges associated with the future development of flow-battery technology are concerned with providing increased power density.

Nowadays, FBs are being designed for large-scale power storage for community energy storage and utility-scale application for enhancing power quality, UPSs, peak shaving, increasing security of supply, and integration with renewable energy systems [145, 171].

The *secondary rechargeable Batteries (SBs)* dominate the market for portable energy storage devices for EVs and other electric and electronic applications. These batteries store electricity in the form of chemical energy and produce electricity through an electrochemical reaction process [122].

Generally, SBs consist of two electrodes, namely anode and cathode, electrolyte, a separator and a case. They have good characteristics, such as high specific energy, high power density, flat discharge profile, low resistance, negligible memory effect, and wide range of temperature performance [172]. However, most batteries contain toxic materials.

Among the EcSSs, SBs are more suitable for applications where high charge/discharge power is the fundamental requirement. Furthermore, the recharging operation of the FBs is more complex and less reliable than that of the SBs; this reason is sufficient to prefer SBs to FBs in applications where discharges and charges are frequent. In the following the SBs are explored in more details than other types of ESS, as it is the technology implemented as storage of the UFCS prototype.

Secondary Rechargeable Batteries The most used SBs include lead-acid (LA), nickel-based ($Ni - Fe$, $Ni - Zn$, $Ni - Cd$, $Ni - MH$, $Ni - H_2$), zinc-halogen-based ($Zn - Cl_2$, $Zn - Br_2$), metal-air-based ($Fe - Air$, $Al - Air$, $Zn - Air$), sodium-beta ($Na - S$, $Na - NiCl_2$), high-temperature lithium ($Li - Al - FeS$, $Li - Al - FeS_2$), and ambient temperature lithium [lithium-polymer (Li-poly), lithium-ion (Li-ion)] batteries [122, 123, 140].

Lead-acid batteries ($Pb - PbO_2$ or *LA*) have been used commercially as energy sources since 1860 [140] and they are the oldest kind of rechargeable battery. LA batteries are used in every internal combustion vehicle (ICV) as a starter and typically applied for emergency power supply, renewable energy storage, and grid storage because of their ruggedness, safe operation, temperature tolerance,

and low cost [122, 126]. These battery operates for 6–15 years with a maximum of 2000 life cycles at 80% *DoD* and provides 70–90% efficiency [122, 123]. Among SBs, the LA battery is the oldest and most mature technology, used for the majority power system applications.

Starting-lighting-ignition (SLI) batteries and UPS batteries are LA batteries with a small rating and voltages of 6, 8, and 12V [139, 142]. Although this kind of battery is very common it has very low specific energy and energy density ratios. Recently, valve-regulated LA (VRLA) has become a popular battery for powering EVs because of its high specific power, low initial cost, and quick charge capability, and no maintenance requirement [123]. Present research investigates minimization of the size and weight of materials of advanced VRLA battery, maintaining high energy density [173, 174]. Common VRLA batteries include adsorbed glass material (AGM) and GEL batteries.

Nickel-based batteries ($Ni-x$) utilize nickel hydroxide as positive electrode and different negative electrode materials. Depending on negative electrode materials, nickel-based batteries are classified into $Ni-Fe$, $Ni-Cd$, $Ni-Zn$, $Ni-MH$, and $Ni-H_2$ [122, 123, 140, 143, 175]. Generally, in nickel-based batteries, the active materials comprise nickel oxyhydroxide as positive electrode, potassium hydroxide solution as electrolyte, and any metal $Fe/Cd/Zn$, MH , or H_2 material as negative electrode [123].

Nickel-iron and zinc batteries have low specific power, high cost, low life cycle, and high maintenance requirement, but provide until 75% of energy efficiency [123]. However, $Ni-Cd$ has a high memory effect and price, which is more than 10 times the price of LA battery [123, 154, 156, 175–178]. In [156, 176–178], recycling issues and toxic effects are considered, although this type employs the

most advanced technology among all nickel-based batteries. They have a greater energy density [179] but present high memory effect, low lifespan, and cadmium is a very expensive and polluting element. For these reasons, nickel-cadmium batteries are currently being substituted by nickel-metal-hydride (*NiMH*) batteries.

By contrast, *Ni - MH* has low memory effect, negligible environmental effect, and a large operating temperature range [122, 126, 140, 175]. The environmental friendliness and its maintenance-free nature ensure that *Ni - MH* is more applicable than *Ni - Cd* for powering EVs [123], although it generates heat during operation and needs a complex algorithm and a costly charger [143, 180]. However, this battery type is expensive, has self-discharge that is proportional to H_2 pressure, has low volumetric energy density, and is specially produced for space power [140, 175]. Although NiCd and LA can supply excellent pulsed power, they are large, contain toxic heavy metals and suffers from severe self-discharge.

Zinc-halogen batteries, including *Zn - Cl₂* and *Zn - Br₂*, have high specific energy, fast charging capability, and low material cost, but also low specific power and large size for electrolyte circulation and temperature control [123, 140, 181, 182]. The *Zn - Br₂* batteries use a zinc-bromine solution stored in two tanks, and in which bromide turns into bromine in the positive electrode. This technology was used by a prototype, called “T-Star”, in 1993 [183].

Metal-air electrochemical batteries consist of electrodes of metal as anode and oxygen from inexhaustible air supply as cathode [140, 146, 177, 184–187]. In metal air batteries, *Li*, *Ca*, *Mg*, *Fe*, *Al*, and *Zn* are used as anode

metal [146, 184–187].

Among these elements, Lithium-air ($Li - Air$) battery is most suitable for EV applications because of its high theoretical specific energy is 100 times that of other batteries [122, 185, 188–191]. The metal-air batteries have low costs and high energy densities (ideal for many primary battery applications) but are very difficult to recharge [177]. Calcium-air ($Ca - Air$) batteries have high energy density, but they suffer from capacity fading, apart from being comparatively expensive [184]. Aluminum-air ($Al - air$) batteries are solely mechanically rechargeable and maintained by replacing the aluminum anode after every discharge, or in case the electrically rechargeable is not feasible, by using aqueous electrolytes [140]. Aluminum-oxygen ($Al - O_2$) batteries produce electricity from the reaction of oxygen with aluminum. They are mostly available in other forms given that $Al - O_2$ combination produces almost double the energy per kilogram of oxygen as hydrogen-FC [140, 146, 184–187]. Zinc-air ($Zn - Air$) battery is technically viable. This battery has several properties of FCs and conventional cells and is electrically and mechanically rechargeable. Overall, metal-air batteries are satisfactory for rechargeable storage application because of their low material cost and high specific energy [174, 192]. *Magnesium-ion* ($Mg - Ion$) batteries change the use of lithium over magnesium, succeeding in storing more than double the charge and increasing in stability. It is expected that this type of battery can have a $6.2kWh/L$ energy density [193], which would imply 8.5 times more than the best lithium batteries, which are currently able to apply up to $0.735kWh/L$. Organizations, such as the Advanced Research Projects Agency-Energy (ARPA-E), Toyota, or NASA, are investigating this type of battery [194, 195].

Sodium-beta batteries are the only batteries that use solid electrolyte. These batteries use beta-alumina ($\beta'' - Al_2O_3$) as electrolyte, which exhibits good Na^+ conductivity and electric isolation at high temperatures. Depending on cathode materials, sodium-beta batteries are classified into sodium-sulfur ($Na - S$) and sodium-metal halide [122, 123, 140, 196]. $Na - S$ batteries, although being much smaller and lighter than $Ni - Cd$ suffer from high internal resistance and Na corrosion, and need to be heated at approximately $300^\circ C$ to maintain the molten state of electrodes [139, 154].

Sodium-metal halide batteries are well known as Zero Emission Battery Research Activity (ZEBRA) [143, 197]. ZEBRA batteries have the most attractive temperature, they benefit also from high energy density, less corrosion, intrinsic safety, and better tolerance to overcharging and overdischarging than $Na - S$ because of the semisolid cathode long life cycle [140, 196], and lower cost [123, 143].

Lithium SBs are promising batteries for EV energy storage applications because of their high energy density, high specific energy and power, and light weight [143, 196]. Moreover, lithium batteries have no memory effect and no harmful effects unlike mercury or lead [143]. They are designed for high temperature and ambient temperature applications, but they need protection for safe operation and cell balancing system to ensure consistent battery performance at the same voltage and charge level [122, 131, 143, 154, 198, 199].

Lithium-sulfur batteries operate at a temperature range, have the highest energy capacity and the lowest weight among all other lithium batteries, but have a comparatively low life cycle [143].

Lithium-metal batteries are able to store double of the power than a traditional lithium battery [200]. SolidEnergy Systems, a MIT startup, have already

started to deploy this type of batteries in drones, and it is expected that they can be included in EVs [201]. This technology is still raw.

The most suitable for room temperature lithium batteries are mainly Li-poly and Li-ion batteries; the main difference is that the former uses lithium metal as one reactor, whereas no metallic lithium is used in the cell of the latter [123]. *Li-poly batteries* are useful for a variety of packaging shapes, and they exhibit toughness and dependability. However, they have poor conductivity and power density and high specific energy [143].

Li-ion batteries are popular for energy storage and portable electric and electronics products because of their small size, light weight, and potential [131, 154, 162, 196, 202]. Li-ion has the greatest potential for future development and optimization [177]. In 1991, Sony commercially produced Li-ion batteries, but this type of battery was already proposed by Bell Labs in the 1960s [175, 203, 204].

These batteries employ, as electrolyte, a lithium salt that provides the necessary ions for the reversible electrochemical reaction that takes place between the cathode and anode. Li-ion batteries have the advantages of the lightness of their components, their high loading capacity, their internal resistance, as well as their high loading and unloading cycles. In addition to small size and low weight, the Li-ion batteries offer the highest energy density and storage efficiency close to 100% and present a reduced memory effect. However, some of the major drawbacks of Li-ion technology are its high cost (due to manufacturing complexity arising from the special circuitry to protect the battery) and the detrimental effect that deep discharging has on its lifetime. Therefore, Lithium-ion batteries must operate within a safe and reliable operation area, which is

restricted by the temperature and voltage windows. Exceeding the restrictions of these windows will cause a quick mitigation of the battery performance and even result in a security hazard (e.g., catch fire or even explode), as from 150°C the electrolytes start to destroy themselves [205].

In Tab. 4.1 and Tab. 4.2, taken from [132], the properties of the various EcSSs technologies discussed above are summarized. Depending on positive electrode, Li-ion batteries are classified into lithium cobalt oxide (LiCoO_2), lithium manganese oxide (LiMn_2O_4), lithium iron phosphate (LiFePO_4), lithium nickel-manganese-cobalt oxide (LiNiMnCoO_2), lithium nickel-cobalt-aluminum-oxide (LiNiCoAlO_2), and lithium-titanate (Li_2TiO_3) batteries [123, 202].

The LiCoO_2 batteries were the first types of batteries developed. Given that cobalt oxide was more expensive than others, nickel and manganese oxide batteries were introduced, with the latter being more cost effective [206]. LiFePO_4 batteries are considered the highest power density batteries with high discharge current and the lowest cost among all *Li – Ion* batteries [143, 202]. LiFePO_4 batteries are stable in thermal and chemical operations [143] and present a great durability. Although this type of battery is starting to be tested in EVs [206], they still can be found in an early stage of research and development. $\text{Li}_4\text{Ti}_5\text{O}_{12}$ batteries are presently used in EV applications because of their faster charging behavior compared with other lithium batteries [143].

Simple but precise explanations on the chemical reactions that take place in lithium batteries are give in [207]. In Fig.4.2, a comparative scheme on specific energy, specific power, safety, performance, life span and cost is presented.

Graphene batteries are made up in pure carbon, which has a high thermal conductivity, and it is extremely light. One of the major assets of graphene-

Battery Type	Energy ^a (W h/kg)	Energy Density ^a (W h/L)	Specific Power ^b (W/ k€)	Life Cycle (no. of cycles)	Cost (US \$/kWh)	Properties
Lead acid	30–50	60–100	200–400	2000–4500	120–150	M-Low cost, mature technology, high specific power; D- Low specific energy, short service life, High maintenance requirements
Ni-Fe	30–55	60–110	25–110	1200–4000	150–200	M-Very rugged, can withstand physical and electrical abuse, long life; D-Low specific energy, Low power and energy density; high self-discharge; hydrogen evolution; high cost and high maintenance cost
Ni-Zn	60–65	120–130	150–300	100–300	100–200	M-High specific energy, no degradation for deep charge/discharge, high peak power; D- High cost, life shorten by fast growth of dendrites
Ni-Cd	40–50	80–100	150–350	2000–3000	300–350	M-High specific energy, no degradation for deep charge/discharge; D- High cost cadmium toxicity, recycling issues
Ni-MH	50–70	100–140	150–300	500–3000	150–200	M-High specific energy, large temperature ranges, safety, long service life; D- High cost, high self-discharge, memory effect
Ni-H₂	60–70	100–120	150–350	6000–40000	300–400	M- High good capacity rate. extreme long life cycle and tolerance to overcharge or over-discharge without damage, D- Expensive, Self-discharge proportional to H2 pressure, Low volumetric energy density;
Zn-Cl₂	65	90	60	200	-	M-High energy density ; D-Low specific power; requirement of plumbing operation and maintenance;
Zn-Br₂	65–75	60–70	90–110	300	150	M- High specific energy; fast charging capability and low material cost; D-Low specific power; high reactivity of bromine; large size for electrolyte circulation and temperature control;
Fe-Air	60–75	100	60	300–600	-	M- High specific energy; good life; lower life-cycle costs; no deformation of active materials or shapes for prolong electrical cycling; low materials cost; D-Low specific energy; low voltage, low efficiency;
Al-Air	190	190	16	- ^c	-	M-High specific energy; high terminal voltage and high amp-hour capacity; high columbic efficiency; operates over a large current density range; low materials cost; D-Loss due to consumption of water during discharge; necessary of aluminum anode replacement after every discharge;

Table 4.1: Electrochemical storage systems overview

Battery Type	Energy ^a (W h/kg)	Energy Density ^a (W h/L)	Specific Power ^b (W/kg)	Life Cycle (no. of cycles)	Cost (US \$/kWh)	Properties
Zn-Air	230	269	105	- ^c	90–120	M-High specific energy; technically feasible; the rate of reaction can be controlled by varying the flow of air; better life cycle; low materials cost; D-Difficult in design; necessary of Zinc anode replacement; short circuit problem;
Na-S	100	150	120	2500–4500	250–500	M-High energy and power density % Relatively high efficiency, Long cycle life; D-Relatively expensive, High temperature produces unique safety issues
Na-NiCl ₂	86	149	150	2500–3000	160–300	M-High energy density, less corrosive, intrinsically safer, good tolerance to overcharge and over-discharge than Na-S, high cycle life, lowest cost than any other batteries. D-Low specific power, need of thermal management, self-discharge problem.
LiAl-FeS	130	220	240	> 1000	110	M-High power and energy densities tolerant to freeze-thaw abuse, over-discharge and overcharge; low weight; D-Requires thermal management system; consumes some stored energy for temperature maintaining; low life cycle.
LiAl-FeS ₂	180	350	400	> 1000	-	M-High power and energy densities tolerant to freeze-thaw abuse, over-discharge and overcharge; low weight; D-Requires thermal management system; consumes some stored energy for temperature maintaining; low life cycle.
Li-Polymer	155	200	315	> 1200	> 125	M-High energy density and specific energy, slim type; high voltage operation; high aspect-ratio form factor; no memory effect; tolerant to overcharged state without explosion; high energy efficiency; low self-discharge; long life cycle; D- High cost, low conductivity and power density;
Li-Ion	120–140	240–280	200–300	1500–4500	150–1300	M-High energy density and specific energy, high voltage operation; no memory effect; lighter and smaller; high energy efficiency; low self-discharge; long life cycle; D- High cost, life shorten by deep discharges, affected by temperature, fragile; needs protection for overcharge and over-discharge;

^a At 80% depth-of-discharge.

^b At 3-h discharge rate.

^c Mechanical recharge. M- Merits. D- Demerits.

Table 4.2: Electrochemical storage systems overview

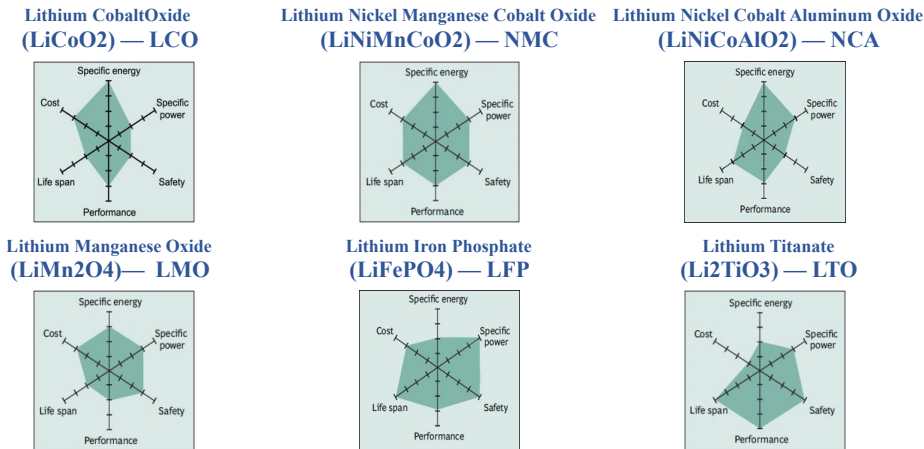


Figure 4.2: Li-ion batteries types comparison

based batteries is that they barely heat, enabling fast or ultra-fast charges without significant power losses due to heat. *Graphenano* batteries, created by a Spanish company, could be charged in only 5 min with a high-power charge. This kind of battery is in an early phase of development, although there exist prototypes of graphene batteries with a specific power of $1kWh/kg$, and it is expected to reach $6.4kWh/kg$ soon [208].

4.2.6 Hybrid storage systems

Individually, all ESSs are incapable of providing all the features, such as energy density, power density, discharge rate, life cycle, and costs [123, 138, 142, 143, 157, 209–219]. Thus, ESS is needed to optimize features for balanced energy storage and delivery by combining two or more ESSs that have complementary characteristics, thereby ensuring the optimal performance of ESSs.

Hybrid ESSs (HSSs) have been developed, and they electronically com-

bine the output power of two or more ESSs with complementary features [123, 126, 131, 134, 138, 142, 143, 209–219]. HSSs are classified into battery and battery hybrids, battery and ultracapacitor hybrids, FC and battery hybrids, battery and SMES hybrids, and battery and flywheel hybrids, CAES and battery hybrids, FC and UC hybrids, FC and ultrahigh-speed flywheel hybrids, and CAES and UC hybrids as near and long-term basis for application-dependent HSS systems [123, 126, 131, 138, 142, 143, 157, 209–219]. Zn-Air and VRLA, Zn-Air and NiMH, Zn-Air and Li-ion, FC and VRLA, FC and NiMH, and FC and Li-ion hybrids are examples of high-specific-energy and high-specific-power combinations. VRLA and UC, NiMH and UC, Li-ion and UC hybrids are low- and high-power-demand combinations. FC and UC, FC and UHSF, CAES and UC hybrids are for long-term applications; and other Li-ion and UHSF/SMES, CAES and VRLA hybrids are found in [123, 138, 157, 209–219].

4.3 Modelling of Li-ion battery

Li-ion cells represent the most widespread standard both in the automotive field and in microgrid applications; for this reason they are the choice for the BESS of the UFCS prototype.

One of the first steps of battery modeling is to decide, what is the purpose of the modeling. Every application of the model requires slightly different approaches and parameters. Numerous models for Li-ion cells and batteries are available in literature, they can be divided into three types:

- WHITE BOX: the electrochemical models, the battery microscopic and macroscopic behaviours in detail, the use of physical laws on *electrochemistry, thermodynamics, porous electrode theory* and *concentrated solution theories*.
- GREY BOX: the reduced-order and *equivalent electric circuit models*, the use of a combination of a voltage sources, resistors, capacitors and sometimes non-linear elements.
- BLACK BOX: the *data driven mathematical models* based on *neural networks* and *finite state machine*, in which no physical knowledge about the battery is required.

4.3.1 White box models

The physical models are low-level models with a high accuracy level. The electrochemical models, as firstly proposed in [220] and [221], are employed to lots of applications with the development of the battery technologies.

In general, these models describe the mass, energy, and momentum transfer of ions for each phase and component of a battery cell. They have the capability to describe the macroscopic quantities such as cell current and voltage and local distribution on a microscopic scale for cell concentration, potential, current, and temperature. They describe the structure of the materials and depict the complex electrochemical phenomena happening inside the cell, namely thermodynamics, active species kinetics and transport phenomena.

While other types of models are devoted to voltage prediction during quasi-steady state constant current discharge and charge, the electrochemical models

take into account transient phenomena. Neglecting effects of concentration dependent properties (that generally change modestly with time), the three transient processes occurring in a battery are *double-layer capacitance*, *electrolyte phase diffusion*, and *solid phase diffusion*. Due to the facile kinetics of Li-ion cells, [222] demonstrates that double-layer effects occur on the millisecond time scale and it can thus be neglected for current pulses with frequency less than 100Hz .

Unlike double-layer capacitance, electrolyte and solid phase diffusion both influence low frequency voltage response and the relative importance of various diffusion coefficient values can be judged either in the frequency domain [223,224] or through analysis of characteristic time scales [220, 225].

In [226], an overview of the physical phenomena is presented, as shown in Fig.4.3. During discharge, Li-ions diffuse to the surface of active material particles (solid phase) in the negative electrode where they undergo electrochemical reaction and transfer into a liquid or gelled electrolyte solution (electrolyte phase). The positively charged ions travel through the electrolyte solution via diffusion and ionic conduction to the positive electrode where they react and diffuse towards the inner regions of metal oxide active material particles (solid phase). The porous separator serves as an electronic insulator, forcing electrons to follow an opposite path through an external circuit or load. Electrons that are produced in the negative electrode reaction and consumed in the positive electrode reaction are blocked by the electronically insulating separator and instead must travel through an external circuit. During charge, the electron flow is inducted by the external circuit and the ions move from the positive to the negative electrode. End of discharge/charge, accompanied by sudden

voltage decay/rise, occurs when the solid phase Li concentrations at either electrode surface become saturated/depleted, or electrolyte phase Li concentration becomes depleted in either electrode.

Among the electrochemical models the most used one is the *1D model*, which captures relevant transport limitations and it is general enough to adopt a wide range of active materials and electrolyte solutions with variable properties. The 1D electrochemical model consists of four PDEs describing the conservation of Li in the solid phase [220]. The four equations are written for a spherical active material particle with reaction occurring at the surface and they are coupled by the Butler-Volmer equation describing the reaction current at the solid/electrolyte interface.

In [227], a fast computing electrochemical model has been developed in order to account for the electrothermal behavior of Li-ion batteries with multiple and/or multidispersed active materials in each electrode. In this study, the cell studied is a high power cell with lithium manganese spinel and lithium cobalt oxide at the positive and Lithium titanate at the negative with 2 particle populations. The comprehensive electrochemical models are used to characterize the behaviour of cells, to build thermal model and to study the aging effect, but they are also used to estimate the parameters' value of the reduced order models.

4.3.2 Black box models

Empirical models are also called black boxes because of the poor insight they offer into the system. They are based on empirical parameters which do not have any physical significance in some cases. The mathematical approaches used to define the transfer function from the inputs to the outputs of the black

box make these models easy to configure, and able to deliver quick responses and predictions. These models are used also to determine parameters of physical models, but they mainly help to estimate the *SoC*, the *SoH*, the aging effect and others more complex effects. However, their accuracy remains limited, especially if the model is too simple. More sophisticated models achieve better results based on stochastic models and/or fuzzy logic and can deliver battery related parameters.

A good estimation of *SoC* leads to long battery life and prevention of battery failure. However, *SoC* estimation is a complex process due to its dependency on various factors such as battery age, ambient temperature, and many unknown factors. In [228], the model-based and data-driven based *SoC* estimation are explained in terms of estimation model/algorithm, benefits, drawbacks, and estimation error. In addition, the review highlights many factors and challenges and delivers potential recommendations for the development of *SoC* estimation methods in EV applications.

The paper [229] presents a generic electrothermal model for Li-ion battery. The model is developed with the objective to simplify the parameter identification procedure, while representing adequately the thermal effects on the battery performance. In [230], a data-driven polynomial nonlinear state-space model is proposed for the operating points at the cusp of linear and nonlinear regimes of the battery's electrical operation, based on the nonparametric frequency domain characterization and quantification of the battery's behavior in terms of its linear and nonlinear behavior at different levels of the state of charge.

The article [231] proposes a mechanism-agnostic capacity fade empirical model called aging density function model (ADFM) for Li-ion batteries. The paper

[232] proposes a flexible data-driven method for online estimating the *SoH* of Li-ion batteries in both charging and discharging modes. Based on comprehensive battery aging data analytics, a novel health indicator called voltage variance during equal time interval is extracted. In [233] advanced machine-learning techniques are applied to achieve effective future capacities and RUL prediction for Li-ion batteries with reliable uncertainty management. In [234], a data-driven method to reduce the qualification time by detecting anomalies before end-of-life is developed. This method detects an anomaly in the capacity fade curve of unhealthy batteries based on their capacity fade trend. By proposing an optimization process with non-dominated sorting genetic algorithm, [235] is able to establish a more efficient *SoH* estimator with support vector regression and the short-term features from the current pulse test. NSGA-II optimizes the entire process of establishing a *SoH* estimator considering both the measurement cost of the feature and the estimation accuracy.

4.3.3 Grey box models

To summarize, the white box models best describe the fastest dynamics of a cell and the causes and effects of the current flowing, while the black box models analyze the slowest effects like aging and are mostly used for *SoC*, *SoH* and parameter estimation. The grey box models use a reduced order set of equations to study the short-term behaviours, in the range of charging/discharging time, and to manage energy flow and temperature and to estimate the *SoC* and *SoH*. The equivalent electric circuit models (EECM) and the empirical models are widely applied to *Battery Management System (BMS)*, they use electrical circuit components, such as resistors, capacitors, and voltage source to build

Model name	Equation
Shepherd model [237]	$v_b = OCV_{\max} - R_b \cdot i_b - \frac{K_1}{SoC_b}$
Unnewehr universal model [238]	$v_b = OCV_{\max} - R_b \cdot i_b - K_1 \cdot SoC_b$
Nernst model [239]	$v_b = OCV_{\max} - R_b \cdot i_b - K_2 \cdot \ln(SoC_b) + K_3 \cdot \ln(1 - SoC_b)$

Table 4.3: Main empirical models

circuit networks to describe the quasi-static electrical behaviour of batteries.

The components that cannot be missing in this type of models are:

- Open Circuit Voltage (OCV). The OCV is an ideal voltage that represents the variation of battery voltage due to SoC . It is equal to the voltage of the battery when an open circuit is at the terminals of battery. Its dependence on temperature is negligible, but it vary following the aging of the battery.
- Internal Resistance (R_{int}) is the overall equivalent resistance within the battery. It is different for charging and discharging and may vary with aging and temperature.

Empirical models. In empirical models, the OCV is represented as a mathematical function of the SoC and the current [236]. Considered a simplified electrochemical model, an empirical model represents the essential nonlinear characteristics of a battery with reduced order polynomial or mathematical expressions.

The main empirical models are shown in Tab. 4.3, where OCV_{\max} is OCV when the battery is fully charged. The accuracy of the three models in predicting the terminal voltage is compared in [236]. The Nernst model obtains the best

accuracy, and the Shepherd model performs especially well in a continuously discharging current. Generally, the three models in Tab. 4.3 can be combined for better accuracy in the following form [240]:

$$v = OCV_{\max} - R_{\text{int}} \cdot i - \frac{K_1}{SoC} - K_2 \cdot SoC + K_3 \cdot \ln(SoC) + K_4 \cdot \ln(1 - SoC) \quad (4.6)$$

Other empirical models are improvements based on these three main ones. Since the Shepherd model suffers from algebraic loop and simulation instability in real-time applications, in [241], as reported in 4.7, a modified Shepherd model is proposed for describing the dynamic behavior of the battery. In [242], as reported in 4.8, in order to improve the dynamic performance of the modified Shepherd model, the *OCV-SOC* relationship is taken into consideration and a term related to the polarization voltage is added. The Nernst model can also be improved by adding two additional constants, q_1 and q_2 , to have a stronger ability to describe the dynamic terminal voltage [243], as reported in 4.9. Classical empirical models have flaws during the relaxation time [244] because the hysteresis effect [245] of the battery voltage is not considered. Therefore, in [246], as reported in 4.10, the term $s \cdot M$ is added to the Nernst equation to represent the hysteresis effect, where M is the correction term to be identified.

Detailed expressions of the above mentioned empirical models are illustrated below.

$$v = OCV_{\max} - K \cdot \frac{Q}{Q - i \cdot T} + A \cdot e^{-B \cdot i \cdot T} \quad (4.7)$$

$$\begin{aligned}
 v &= OCV_{\max} - R_{\text{int}} \cdot i - K \cdot \frac{Q}{Q - i \cdot T} \cdot (i \cdot T + i^*) + A \cdot e^{-B \cdot i \cdot T} \\
 v &= OCV_{\max} - R_{\text{int}} \cdot i - K \cdot \frac{Q}{i \cdot T - 0.1 \cdot Q} \cdot i^* - K \cdot \frac{Q}{Q - i \cdot T} + A \cdot e^{-B \cdot i \cdot T}
 \end{aligned} \tag{4.8}$$

$$v = OCV_{\max} - R_{\text{int}} \cdot i - K_2 \cdot \ln(\text{SoC} + q_1) + K_3 \cdot \ln(1 - \text{SoC} + q_2) \tag{4.9}$$

$$\begin{aligned}
 v &= OCV_{\max} - R_{\text{int}} \cdot i - K_2 \cdot \ln(\text{SoC}_b) + K_3 \cdot \ln(1 - \text{SoC}_b) + s \cdot M \\
 s &= \begin{cases} 1, & i > \varepsilon \\ -1, & i < -\varepsilon \\ s_k - 1, & |i| \leq \varepsilon \end{cases}
 \end{aligned} \tag{4.10}$$

where Q is the battery capacity, A is the exponential zone amplitude, B is the time constant inverse of the exponential zone, K is the polarization voltage, i^* is the filtered current through the polarization resistance, R_{pol} is the polarization resistance, ε is a small threshold, and q_1 , q_2 and M are estimated parameters. Considering more effects inside the battery, the accuracy of the empirical model is improved but the computational burden is also increased.

Equivalent Electric Circuit models (EECM). Compared to empirical models, EECMs are much easier for the understanding of the electrical characteristic of the battery and they give researchers sufficient freedom to design a suitable structure for their applications. EECMs only consist of the OCV generator, R_{int}

and a series of capacitive impedences with different time constants, representing electrical dynamics of the diffusion process in electrolyte and porous electrodes and the charge transfer and double-layer effect in the electrode.

Fig. 4.4 presents an EECM with n RC networks, named the nRC model hereafter. Some authors give other names to specific EECMs, some of them are R_{int} model, *Thevenin* model, Partnership for a New Generation of Vehicles (PNGV) model, General Non-Linear (GNL) model and so on. EECMs can be modified in several ways to improve their ability to describe the terminal voltage. In order to describe the inherent electrochemical property of the battery, a physically based EECM is proposed through analyzing the Warburg element from the Electrochemical Impedance Spectroscopy (EIS) measurement [247]. The difficulty of online EIS measurement in real-time applications may decrease the accuracy of the physically based ECM. For a better interpretation of electrochemical and thermal behaviors, a multiphysical battery model with 11 parameters is proposed in [248]. The modeling accuracy is less than 2% for the electrical part and the mean error is 2.45% for the thermal part in the experimental test. For real applications, there should be a good trade-off between the complexity and accuracy before applying EECM to a specific application. The simplest model is the zero-order V-I based EECM, also called R_{int} model. This model has just the ideal generator OCV and the resistor R_{int} , it approximates the relation between the OCV and SoC with a linear time-invariant (LTI) equation, it neglects the dependency of OCV on temperature and it doesn't describe the dynamic effects, polarization effects and aging effects of the battery. The following equations describe the zero-order V-I based

EECM:

$$OCV = (\alpha_1 + \alpha_2 SoC)V_n \quad (4.11)$$

$$V = OCV + R_{int} \cdot i \quad (4.12)$$

The accuracy of this model is typically low, only suitable under constant current and constant temperature conditions; these conditions may be realistic for a cell, but not for a battery. Nevertheless, this model is widely utilized in literature in broad sizing. Due to the strong linearity of this model, the parameter identification can be conducted on a cell and then it is extended on the entire battery pack.

In the Sec. 4.4 the zero-order V-I based EECM is used to explain the sizing of a BESS for UFCS applications; in particular, the sizing of the UFCS prototype of DIETI at University of Naples - Federico II is proposed. In addition, a modified Shepherd model is used to validate the sizing and to emulate the vehicles charging.

4.3.4 Estimation parameters

Among the Li-ion cells proposed and compared in 4.2.5, the *Lithium Nickel Manganese Cobalt Oxide (Li-ion NMC)* batteries have been adopted because of their safety and energy and power density.

In this section an estimation parameters of 4.12 and 4.8 is shown for Li-ion NMC cell. The cell taken as reference is *SLPB130255255P75* (Ultra High Power 75Ah) by Kokam[®]. Fig. 4.5 shows electric cell informations from the datasheet. The maximum, minimum and nominal voltage values are standard

values, so they are common for practically all Li-ion cells. The nominal capacity is one of the most important parameters in selecting a cell, it doesn't affect only the capacity of the battery but mainly the value of current of C-Rate. For example the chosen cell can be charged at $4C$, that means $75Ah \cdot 4C = 300A$. The value of charging and discharging current may seem very high, that is before, when they are valid only for a cell and not for an entire battery. When a lot of cells are connected in series and in parallel, the operations of the BMS to balance the *SoC* and the temperature of the pack might drastically reduce the max charging/discharging rate.

Fig. 4.6 shows the charging/discharging characteristics for different C-rate values; at the bottom of the plots the operative condition of the measurements are reported. In the right plot of Fig. 4.6, it is relevant to note that there are different final relative capacities for different values of the discharging current. It seems that the maximum values of *SoC* depends on the discharging current, indeed it is the capacity which is dependant on the history of the system. This effect is well modelled by the Peukert's law [249], but it is neglected in the following. Therefore, in the estimation parameters of 4.12 the SoC_{\max} is 1 anyway and, to identify 4.8 the $1C$ curve is taken into account.

The estimation parameter of the zero-order V-I based EECM in 4.12 is trivial.

$$\begin{aligned}
 V_{\max} &= (\alpha_1 + \alpha_2 SoC_{\max}) \cdot V_n + R_{\text{int}} \cdot i_{\max} \\
 V_{\min} &= (\alpha_1 + \alpha_2 SoC_{\min}) \cdot V_n + R_{\text{int}} \cdot i_{\min}
 \end{aligned}
 \tag{4.13}$$

where $V_n = 3.7V$, $V_{\max} = 4.2V$, $V_{\min} = 2.7V$, $i_{\max} = 300A$, $i_{\min} = -600A$, $SoC_{\max} = 1$, $SoC_{\min} = 0$, $R_{\text{int}} = 0.4m\Omega$. The values of parameters of the considered cell are $\alpha_1 = 0.816$ and $\alpha_2 = 0.317$. The values of others Li-ion NMC are very similar to those, because they do not strictly depend on the nominal capacity.

The modified Shepherd model in 4.13 is the same model used in the main battery block of *Simscape* in Matlab/Simulink[®]. As suggested in the Matlab/Simulink[®] documentation, the estimation parameter of the model can be conducted following [242]. The required inputs are the nominal capacity, V_{\min} , V_{\max} , the 1C nominal discharging current, R_{int} , the capacity at nominal voltage and, the capacity and voltage in the exponential zone. The capacity and voltage in the exponential zone are the coordinates of the inflection point of the discharging characteristic. All these parameters can be determined by the datasheet of the cell.

In Fig. 4.7 the experimental 1C characteristic of *SLPB130255255P75* (Ultra High Power 75Ah) by Kokam[®] is compared with the estimated characteristic using 4.13. In [250], the estimation with the same modified Shepherd model are conducted on other types of batteries.

4.4 Sizing of the BESS

The main purpose of the BESS in the multislot UFCS interfaced to a LV grid is the energy and power balancing in order to limitate the impact on the grid of the recharging vehicles in a short time. This is possible if the load is at least partially decoupled from the grid. Therefore, the sizing is subject to a power

constraint and an energy constraint. This section is based on [16].

The discharging power of the BESS must be enough to compensate the grid and the vehicles power in the worst case to slightly oversize the storage. In the worst case scenario, all vehicles are charging simultaneously at the maximum power of slots and, the value of P_{grid} is not the maximum value, but the nominal one or less. The charging power must be almost equal to P_{grid} to minimize the charging time of the BESS.

The power constrains derives from the following equations:

$$P_{\text{BESS,dis}} = \frac{1}{\eta_{\text{BESS}}} \left(n \frac{P_{\text{EV}}}{\eta_{\text{SAB}}} - \eta_{\text{AFE}} P_{\text{grid}} \right) \quad (4.14)$$

$$P_{\text{BESS,ch}} = \eta_{\text{BESS}} \eta_{\text{AFE}} P_{\text{grid}} \quad (4.15)$$

where n is the number of charging slots, and the efficiencies may be taken as constant at a medium value declared by the converters' makers. The values of the input power by the grid and output power to the slots are presented and widely explained in Sec. 2.2.4 and Sec. 2.2.3. The choice of the rated power of the BESS is driven by the rated grid power, since the output power of $160kW$ on each slot is already assigned.

The two main decoupling and energy balancing strategies are *Load Levelling* (LL) and *Load Shifting* (LS) . In both strategies, the average value of the load power profile of the EVSE is compared with the available power supplied by the grid. The main difference between the two types of balancing strategies is in the time interval on which the energy compensation is performed. In the former case, the time interval is in the order of a fraction of an hour; in the latter, the time span might achieve 12 hours. The operating paradigm of LS is

to store energy during the night hours, when the cost per kWh is low and there is excess production, and to supply energy to the EVs during the day, strongly limiting the impact on the grid. Therefore, LS is mainly used by the energy distributors in large-scale; in that context it has an impact not on the single point of connection of the charging station but in a wider area, for example at the level of the nodal point of the medium voltage network.

The requirement for the station is to be ready to charge vehicles continuously, thus, the energy balancing required to the BESS has a very short time period. The energy constraint may be set through LL, that means the energy required by the vehicles in time period T_{EV} must be provided by the grid and the BESS. After this operation, the grid supply, in time period T_{BESS} , the energy previously subtracted to the BESS until the system is led to its initial condition. The energy constraint derives from the following energy equilibrium equation:

$$\int_{t-(T_{BESS}+T_{EV})}^t \eta_{AFE} P_{grid}(\tau) d\tau + \int_{t-(T_{BESS}+T_{EV})}^{t-T_{BESS}} \eta_{BESS} P_{BESS,dis}(\tau) d\tau = n \int_{t-(T_{BESS}+T_{EV})}^{t-T_{BESS}} \frac{P_{EV}(\tau)}{\eta_{SAB}} d\tau + \int_{t-T_{BESS}}^t \frac{P_{BESS,ch}(\tau)}{\eta_{BESS}} d\tau \quad (4.16)$$

where T_{EV} is the maximum charging time of EVs, that means the interval to completely free the station, T_{BESS} is charging time of the BESS.

The equation 4.16 is solved in the worst case too. Due to the fact that after the time interval $T_{EV} + T_{BESS}$, the system must be in its same initial condition, the energy provided by the BESS during the EV charging phase (the second integral of 4.16) must be equal to the energy provided by the grid to the BESS in its charging phase (the fourth integral of 4.16). In addition, the values of P_{grid} ,

P_{EV_k} and the efficiency are time-invariant in the worst case, so $E_{EV} = P_{EV} \cdot T_{EV}$ and $E_{BESS} = P_{BESS, ch} \cdot T_{BESS}$.

The value of E_{EV} can be determined analyzing the market and the evidences proposed in Sec. 1.1.4, it is the capacity of the ideal target vehicle of the UFCS. In the case of the DIETI prototype, the vehicles target taken into account has $E_{EV} = 40kWh$; this value might be considered a good value for the upcoming vehicles in the next 10 years.

Based on previous considerations, simplified 4.16 and replacing 4.15, the capacity of battery results in:

$$E_{BESS} = E_{EV} \frac{(nP_{EV} - P_{grid}\eta_{SAB}\eta_{AFE})^2}{P_{EV}P_{grid}\eta_{SAB}^2\eta_{AFE}\eta_{BESS}} \quad (4.17)$$

The presented constraints are used for the dimensioning of the BESS for the DIETI prototype. The storage system must therefore have the characteristics presented in table 4.4. The numerical validation phase follows the sizing phase. The goal of the simulations in this section is to form an idea of the BESS energy response within the UFCS.

Definition	Value	Unit
Rated voltage of battery pack	600	V
Rated capacity	>110	Ah
Continous rated current	Discharge	380 A
	Charge	65 A
Cycle charge/discharge per year	5k	—
Operating Temperature	0/60	°C

Table 4.4: Table of BESS requirements

4.4.1 Sizing validation

For this validation, the current, voltage and capacity values of the BESS and the voltage and current values of the converters are those established in this section and in the previous one Sec.3. The numerical simulations are carried out on the two operating configurations: charging two vehicles at the same time and charging a single vehicle at a higher voltage.

The capacity of the vehicles used for simulating simultaneous charging is the same as the normal-size target vehicle used for BESS sizing ($E_{EV} = 40kWh$). The voltage value for normal-size vehicles is the maximum voltage value on the single charging slot ($OCV_{EV} = 400V$). The maximum current and power values are those allowed by the standards and reported in Sec. 2.2.3 ($I_{EV,max} = 400A$ and $P_{EV,max} = 160kW$).

The big-size vehicle used in the simulation of the input-series-output-parallel configuration mode of the UFCS DC/DC converters, has the capacity, voltage and maximum power equal to twice the normal-size target vehicle ($E_{EV} = 80kWh$, $OCV_{EV} = 800V$ and $P_{EV,max} = 320kW$); the maximum current remains obviously at the same value ($I_{EV,max} = 400A$).

In Sec.1.1.3 the main charging strategies for the EVs batteries are discussed, focusing in particular on the constant voltage (CV) and constant current (CC) modes. In addition to these two modes, a third one is added that is constant power (CP), increasingly used in BMS algorithms. Hence, the battery charging profiles are a variation of these modes of operation based on the value of SoC . In Fig.4.8 a CC mode is used up to the value of $SoC = 0.8$ and then the battery switches in CV; in Fig.4.8b CP mode replaces CC mode. In real cases, these

strategies are only ideal, because the voltage and current values required for the charge are also influenced by other factors, such as thermal management. In this validation phase, using ideal charge/discharge profiles is more than enough for both the vehicles and the BESS.

In Fig.4.9 and Fig.4.10 the voltage, current, power and *SoC* variation of BESS and EVs and the residual energy in the BESS are shown. In these simulations the efficiencies are kept at constant values, but the battery model is that in 4.7. The Fig.4.9 refers to the charging of two vehicles with a CC/CV profile, the Fig.4.10 to the charging of two vehicles with a CP/CV profile. The Fig.s 4.9a and 4.10a show the voltage profile of the $h - th$ vehicle and the BESS. The Fig.s 4.9b and 4.10b show the current profile of the $h - th$ vehicle and the BESS. The Fig.s 4.9c and 4.10c show the *SoC* profile of the $h - th$ vehicle and the BESS. The Fig.s 4.9d and 4.10d show the power profile of the all vehicles and the BESS and, the remaining energy profile of the BESS. The simulations on the big-size vehicle are not shown because they produce the same results in terms of power, energy and *SoC*; the current and voltage values should be scaled twice.

It is worth noticing that while using the CP/CV charging profile, the maximum power reached is lower than with the CC/CV profile; the maximum current value is instead higher in CP/CV than in CC/CV. The numerical validation confirmed the success of the sizing for all the configurations and the charging profiles. In the Chapter 6, the sizing of the BESS is implemented into the choice of a real product. The configuration of the cells and other information on the dimensions and control systems of the BESS are presented.

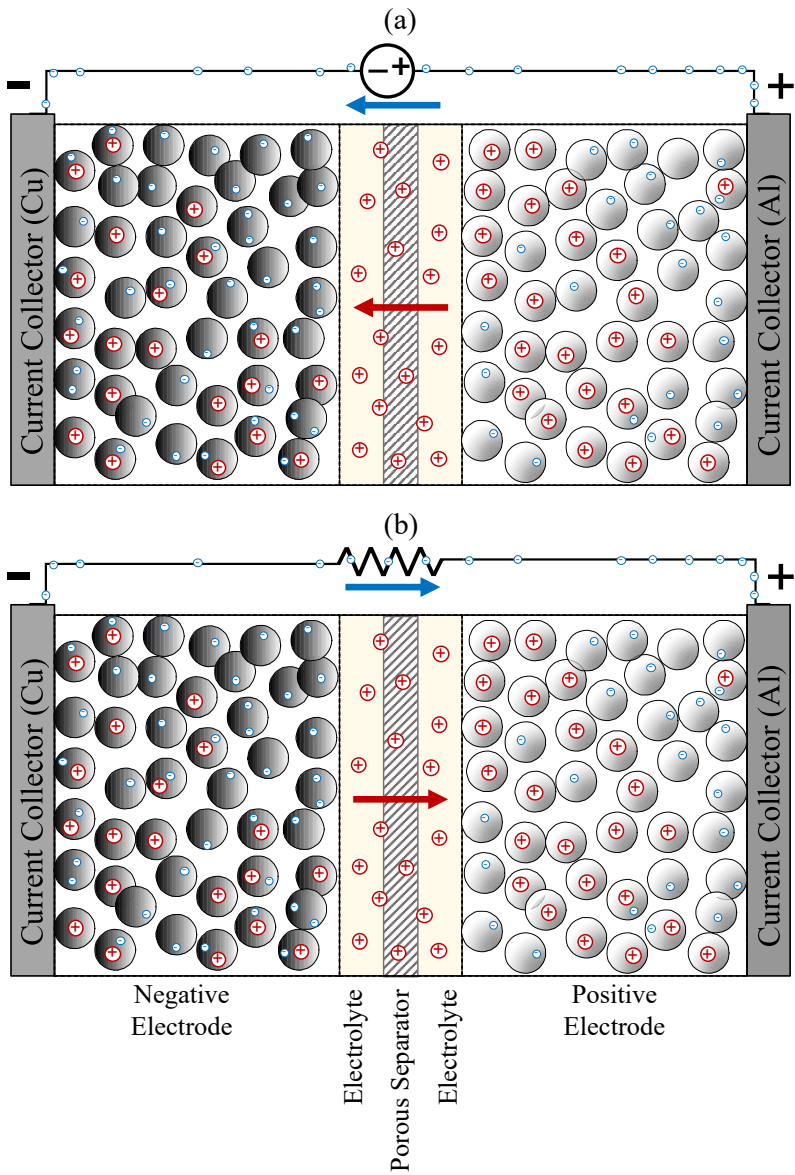


Figure 4.3: Physical structure of a Li-ion cell

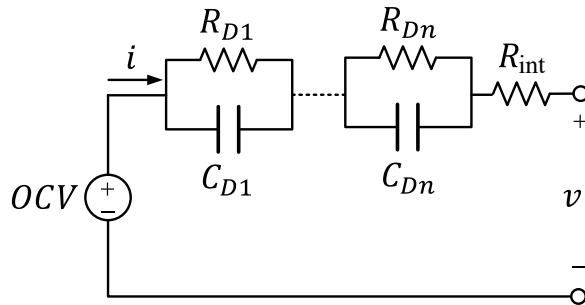


Figure 4.4: Schematic diagram of the nRC EECM

	Typical		Remarks
Nominal Capacity	75 Ah		<i>Charge@0.2C, 25±3 °C</i> <i>Discharge@0.2C, 25±3 °C</i>
Energy Density	Gravity	152 Wh/kg	
	Volume	351 Wh/L	<i>Excluded tab and seal</i>
Internal Resistance	Max. 0.4 mΩ		<i>AC @1kHz, SOC30±5%</i>
Weight	Max. 1,830 g		
Cell Dimension [Maximum]	Width ^(A)	268 mm	<i>Unfolded</i>
	Length ^(B)	265 mm	<i>Excluded tab length</i>
	Thickness ^(C)	13.7 mm	<i>0.5kgf/cm², SOC30±5%</i>
Voltage	Average	3.7 V	
	Lower Limit	2.7 V	
	Upper Limit	4.2 V	
Current [Maximum]	Charge	Cont.	300.0A (4C) @25±3 °C
		Peak	600.0A(8C) ≤10sec , ≤ SOC 50%
	Discharge	Cont.	600.0A (8C) @25±3 °C
		Peak	1,125.0A (15C) ≤10sec , ≥ SOC 50%
Cycle life to 80% of remaining capacity	1C/1C,	≥ 6,000	<i>80% DOD or 3.4-4.1V (@25±3 °C)</i>

Figure 4.5: SLPB 75.0Ah Ultra high power - Electric quantities

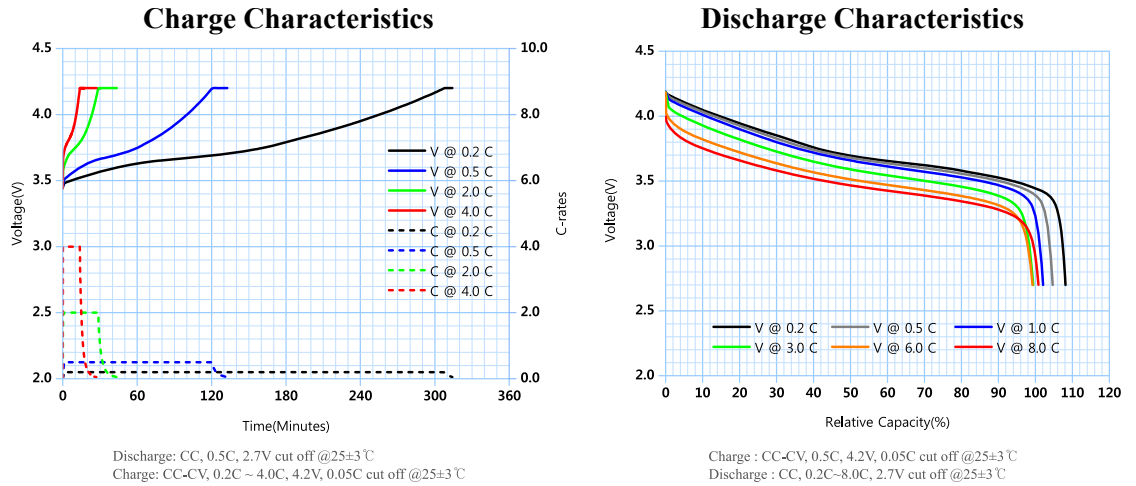


Figure 4.6: SLPB 75.0Ah Ultra high power - Charging/Discharging characteristics

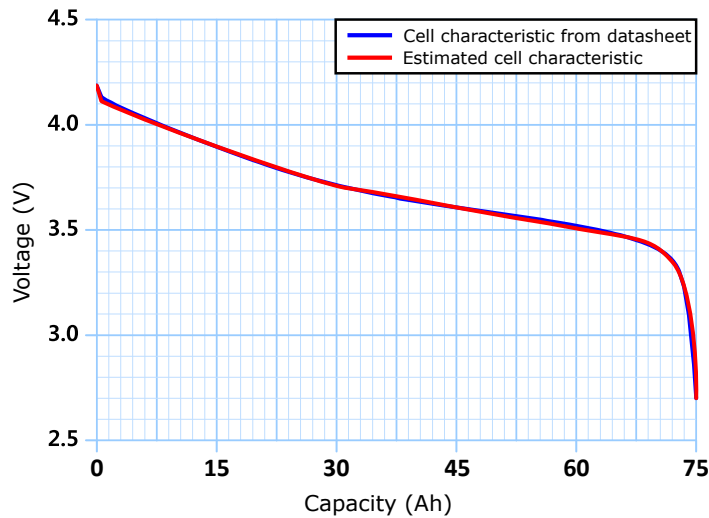


Figure 4.7: Estimation parameters of modified Shepherd model

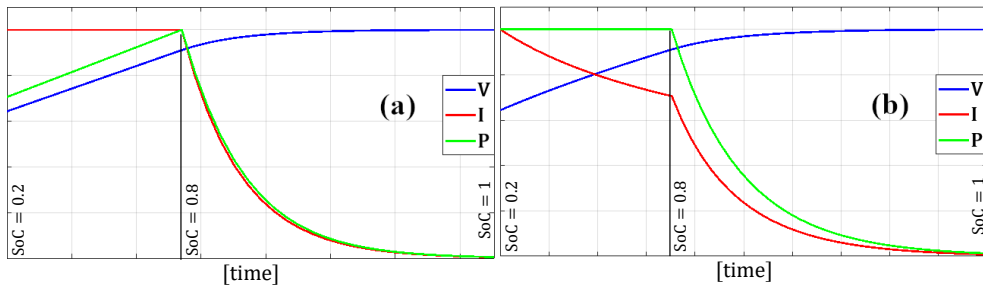


Figure 4.8: Charge management strategy: (a) current-voltage constant (CC/CV), (b) power-voltage constant (CP/CV).

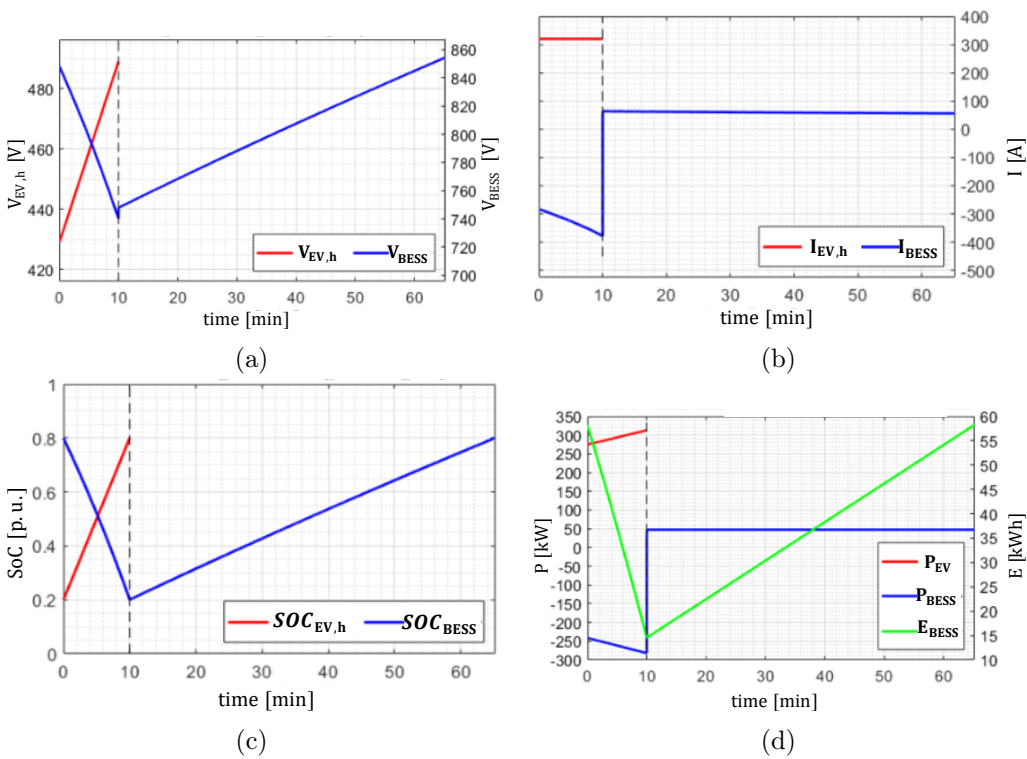


Figure 4.9: Numerical simulation of two vehicles charging in CC/CV profile: (a) voltage, (b) current and, (c) SoC of BESS and EVs and (d) power of BESS and EVs and residual energy of BESS.

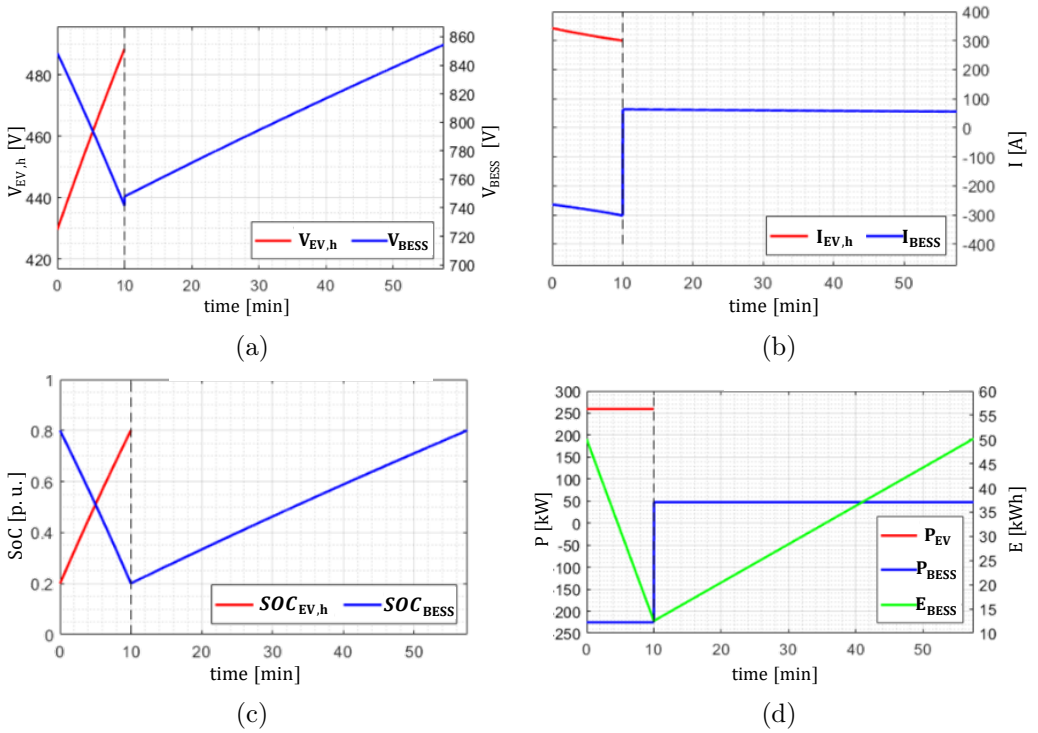


Figure 4.10: Numerical simulation of two vehicles charging in CP/CV profile: (a) voltage, (b) current and, (c) SoC of BESS and EVs and (d) power of BESS and EVs and residual energy of BESS.

Energy & Power Management of UFCS

The overall regulation of power flows can be formulated just considering the hierarchical architecture of the charging station. However, in order to both correctly assess energy consumption and predict charging power demand, the application of power scheduling methodology to UFCSs require to investigate specifically on the infrastructure technology, time-variant power constraints, available stored energy, devices' conversion efficiencies. In addition, the operation policies and the type of commercial service can influence the choices of the charging values. This section is based on [17].

The problem of management of EVs' charge in a multislot UFCS can be divided into two issues: the scheduling strategy and the EV power profile planning. The scheduling strategy concerns the arrangement of the deadline-constrained charging processes in presence of limited resources. The power profile planning concerns the strategy with which the right amount of resources are assigned (i.e., the service offered to each EV).

5.1 Scheduling strategies

The scheduling problem is a typical 'job scheduling' with a priority mechanisms. The 'job scheduling' theory has a strong application in computer science, where the processes executed by a CPU must be managed. The main scheduling algorithms work with a priority mechanism, the most prioritized processes are executed and the others wait in idle state. The main scheduling policies are [251]:

- FCFS ('First Come First Served'): The priority is fixed and it is given to the process with earlier arrival time. The processes increase their priority when the first process is complete (the second process become the most prioritized and so on).
- EDF ('Earliest Deadline First'): the priority is given to the process that is closer to its deadline. When a new process arrives, if its deadline may be closer than the deadlines of other processes, its priority is set at an intermediate value and the priority of the processes with farther deadlines decrease. In this way, an executing process may be interrupted to execute a new process with a closer deadline; algorithms, that allow the interruption of an executing processes, are called preemptive algorithms.
- RR ('Round Robin'): it is a particular preemptive algorithm that executes the charging processes in order of arrival, like the FCFS, but preempts the running process, placing it at the end of the queue of pending processes, if execution takes longer than the set "amount of time", and allowing the execution to continue to the next pending process.

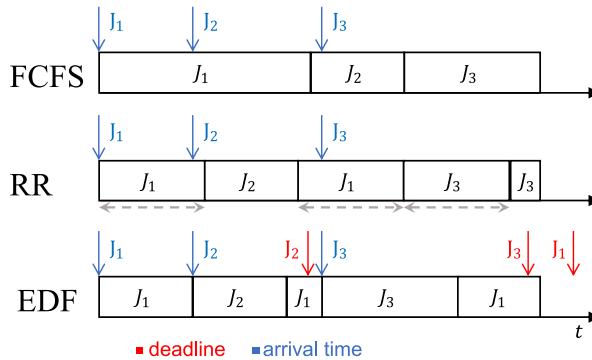


Figure 5.1: Schemes representative of priority algorithms

Fig. 5.1 provides an example of how the above-mentioned algorithms work, in particular it highlights the differences in terms of priority management.

The problem of management of EVs' charge is a scheduling problem in which the charging power requests are the processes, while the number of UFCS charging slots, the amount of energy and power (supplied by the BESS and grid) are the common resources. The most prioritized process is the EV charging process that benefits of the most resources under operating constraints. The other EV charging processes are characterized by lower feature. Therefore, since unlike the Fig. 5.1, the vehicles would not be loaded one at a time but at the same time up to the slot number of the station and with higher performances according to the higher priority, in the following the FCFS algorithm is called FCBS ('First Come Best Served').

The goal of recharging each vehicle in the shortest possible time is achieved through an appropriate power profile planning and is explained below. Instead, the goal of scheduling is to manage the vehicles' queue and the overall charging time.

In fact, if the goal is to liberate a single slot in the shortest possible time,

then the EDF algorithm may be the most suitable one. This feature can be implemented matching the process deadlines with the time left until the end of the charge. Thus, the vehicle that is closest to the deadline is the first in priority. The problem with this strategy is that it favors the vehicles with lower capacity or the vehicles with a higher starting *SoC*, meaning those that require less energy from the station. At the same time, EDF disadvantages the most discharged vehicles even if they were the first connected to the station.

The FCBS algorithm can be used when the vehicle charging schedule is assigned upon its arrival at the station and it must be fulfilled without significant changes. The real case could be that in which the vehicle's owner pays after the charging planning and before the charging starts; in addition, the price varies according to the charging profile, that means the performance in terms of power, energy and charging time.

In this perspective, the customer, who has already paid for a certain service, cannot be provided with a less performing profile than the one planned. For this reason, the charging profile assigned to the vehicles arrived later, although it minimizes the charging time, cannot alter that one of the vehicle with higher priority. So, the arrival order results in the priority order and the performance is affected by this order.

Among the three proposed algorithms, the RR is the most impartial one. When the priority of the processes changes and the process with most priority becomes the least priority one and so on, the charging time of the vehicles that arrived earlier at the station increases, while the charging time of the vehicles arriving later decreases.

To best choose the scheduling algorithm, the objective function of the scheduling

must be declared. In the real case, the goal of the scheduling is strongly influenced by the pricing policy. If the price is only dependent on the number of the supplied kWh , then the EDF is the one that minimizes the length of queue of non-charging vehicles, decreasing the number of vehicles that give the charge up because of the waiting time.

If the payment is made before the start of the charge and depends on both the energy sold and the charging time, then the FCBS seems to be the most respectful strategy for the customer.

5.2 Optimal charging power planning

The optimization strategy was initially formulated with simplified hypotheses in [17]. The simplified hypotheses are subsequently revised and a second version is formulated. For the sake of completeness, both versions are proposed below.

5.2.1 A simplified closed form strategy

The simplified assumptions of the first version of the optimization strategy are:

- the power charging demand is constant in the range of SoC between 20 – 80% for all vehicles;
- all efficiencies are assumed to be constant;
- this strategy is formulated only for two vehicles and the FCBS scheduling algorithm.

The procedure of charging power planning is presented in detail and the case of two vehicles simultaneously connected is discussed. The time of the initial (end)

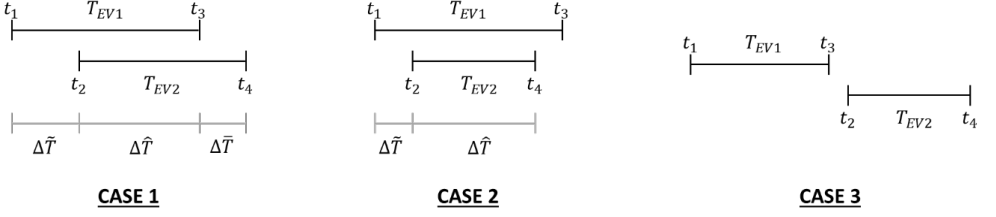


Figure 5.2: Contemporary cases according to the arrival time of second vehicle

of charging of the two vehicles are t_1 (t_3) and t_2 (t_4), respectively 5.2. The vehicle, just arrived at the station, shall notify its battery data to the station through appropriate communication protocol. Among the data provided to the station, the infrastructure control system uses the battery capacity, Q_{EV} , the maximum charging current, $I_{EV,max}$, the maximum charging power, $P_{EV,max}$, and the initial SoC of battery, $SoC_{EV,i}$.

The energy required from the vehicle is calculated on the basis of the battery capacity and the SoC :

$$\Delta E_{EV} = \Delta SoC_{EV} Q_{EV} V_{EV,n} \quad (5.1)$$

where $V_{EV,n}$ is the nominal voltage of the EV battery and $\Delta SoC_{EV} = SoC_{EV,f} - SoC_{EV,i}$. The value of $SoC_{EV,f}$ is conventionally set to 0.8, since a full charged battery is considered at 80% of SoC at high C-rate.

The first vehicle arrived at the station (when no other vehicles are connected) can be charged at maximum available performance. In this first case in which there is one vehicle in charge at the station, the value of ΔSoC_{BESS} can be set as

$$\Delta SoC_{BESS} = SoC_{BESS,i} - SoC_{BESS,min} \quad (5.2)$$

where $SoC_{BESS,i}$ is the value of SoC of the BESS at the beginning of the vehicle charge; $SoC_{BESS,min}$ is set to 0.2. The formulation of the optimization problem changes between the case in which the energy, required from the vehicle, i.e. 5.1, is less than that available from the BESS 5.3 and the case in which the BESS is not sufficiently charged 5.4:

$$\Delta E_{EV_1} \leq \Delta SoC_{BESS} E_{BESS} \eta_{BESS} \eta_{EV} \quad (5.3)$$

$$\Delta E_{EV_1} > \Delta SoC_{BESS} E_{BESS} \eta_{BESS} \eta_{EV} \quad (5.4)$$

If the condition 5.3 is verified, the optimization problem reduces the minimization of the charging time subject to the power limits constrained by the vehicle and the charging station:

$$\left\{ \begin{array}{l} \min_{P_{EV_1}} T_{EV_1} \Rightarrow \min_{P_{EV_1}} \frac{\Delta E_{EV_1}}{P_{EV_1}} \Rightarrow \max_{P_{EV_1}} P_{EV_1} \\ P_{EV_1} \leq P_{EV_1,max} \\ P_{EV_1} \leq P_{grid,max} \eta_{grid} \eta_{EV} + P_{BESS,max} \eta_{BESS} \eta_{EV} \end{array} \right. \quad (5.5)$$

where η_{grid} is the efficiency of the AC/DC active rectifier and the interfacing system with the grid, η_{BESS} is the efficiency of the BESS, η_{EV} is the efficiency of the subsystem including the EV and its DC/DC converter. In 5.5, since the vehicle charging power is constant, the charging time is $T_{EV_1} = \Delta E_{EV_1} / P_{EV_1}$ and the objective function to maximize becomes the vehicle charging power. If the condition 5.4 is verified, the optimization problem must consider also the

energy limits constrained by the BESS:

$$\left\{ \begin{array}{l} \max_{P_{EV1}} P_{EV1} \\ P_{EV1} \leq P_{EV1,\max} \\ P_{EV1} \leq P_{\text{grid}} \eta_{\text{grid}} \eta_{EV} + P_{BESS,\max} \eta_{BESS} \eta_{EV} \\ \Delta E_{EV1} \leq P_{\text{grid}} T_{EV1} \eta_{\text{grid}} \eta_{EV} + \Delta SOC_{BESS} E_{BESS} \eta_{BESS} \eta_{EV} \end{array} \right. \quad (5.6)$$

The problems in 5.5 and 5.6 have respectively these solutions:

$$P_{EV1} = \min \{ P_{EV1,\max}, P_{\text{grid}} \eta_{\text{grid}} \eta_{EV} + P_{BESS,\max} \eta_{BESS} \eta_{EV} \} \quad (5.7)$$

$$P_{EV1} = \min \left\{ P_{EV1,\max}, P_{\text{grid}} \eta_{\text{grid}} \eta_{EV} + P_{BESS,\max} \eta_{BESS} \eta_{EV}, \frac{P_{\text{grid}} \eta_{\text{grid}} \eta_{EV} \Delta E_{EV1}}{\Delta E_{EV1} - \Delta SoC_{BESS} E_{BESS} \eta_{BESS} \eta_{EV}} \right\} \quad (5.8)$$

The distinction between the problems 5.5 and 5.6 is mandatory because, if the solution 5.8 was used in condition 5.3, the charging power reference would be negative, as effect of minimization. In both cases 5.7 and 5.8 the planned charging power is provided from the grid and from the BESS in a certain proportion. If a power constraint saturates, it means that the energy required by the vehicle is available in the BESS, but the power limitations slow down the energy flow. If the energy constraint saturates, it means that the energy required by the vehicle must be supplied from the grid, thus the charging time directly depends on the power grid. The assignment of P_{EV1} and T_{EV1} is enough to start the charge of the first vehicle.

When the second vehicle arrives at the station, the performances of its recharge should adapt to the condition of the station which is already charging the first

vehicle. The power and energy limits must take into account charge power and energy reserved for the first vehicle. According to the arrival time of the second vehicle, three cases can happen, as shown in 5.2.

The case 3 of 5.2 is a degenerate case, the charging power value of the second vehicle can be chosen in the same way of the charging power value of the first vehicle.

When the arrival time of the second vehicle occurs before the end of the charge of the first vehicle ($t_2 < t_3$), case 1 or case 2 can occur depending on the *SoC* of the BESS at time instant t_2 , the energy of the BESS reserved for the first vehicle and the energy required for the second vehicle. It can be noticed that when the second vehicle arrives at the station, it is not clear yet which case happens (case 1 or case 2). To formulate energy conditions of the second vehicle some quantities are defined:

$$\Delta\tilde{E}_{EV1} = \Delta\tilde{T}P_{EV1} \quad (5.9)$$

$$\Delta\hat{E}_{EV1} = \Delta E_{EV1} - \Delta\tilde{E}_{EV1} \quad (5.10)$$

where $\Delta\tilde{T} = t_2 - t_1$ is the time interval between the arrivals of the two vehicles, $\Delta\tilde{E}_{EV1}$ is the energy charged by the first vehicle in the time interval $\Delta\tilde{T}$, ΔE_{EV1} is the energy required from the first vehicle to complete its charge. The formulation of the optimization problem changes according to the conditions 5.11 and 5.12. On the left side of the energy condition, there are the energy ΔE_{EV2} , defined as 5.1, required by the second vehicle, and the energy $\Delta\hat{E}_{EV1}$,

required by the first one. On the right side of the energy condition, there are the energy available from the BESS at time t_1 , reduced by the energy ΔE_{EV_1} provided to the first vehicle in the time interval $\Delta \tilde{T}$, as expressed in 5.13, and the energy of the grid used to charge the first vehicle. The two conditions are:

$$\Delta \hat{E}_{EV_1} + \Delta E_{EV_2} \leq \Delta SoC_{BESS} E_{BESS} \eta_{BESS} \eta_{EV} + P_{grid} \frac{\Delta \hat{E}_{EV_1}}{P_{EV_1}} \eta_{grid} \eta_{EV} \quad (5.11)$$

$$\Delta \hat{E}_{EV_1} + \Delta E_{EV_2} > \Delta SoC_{BESS} E_{BESS} \eta_{BESS} \eta_{EV} + P_{grid} \frac{\Delta \hat{E}_{EV_1}}{P_{EV_1}} \eta_{grid} \eta_{EV} \quad (5.12)$$

where the value of SoC of the BESS is:

$$\Delta SoC_{BESS} = SoC_{BESS,i} - SoC_{BESS,min} - \frac{\Delta \tilde{E}_{EV_1}}{E_{BESS}} \quad (5.13)$$

When the condition 5.11 is verified both case 1 and case 2 of 5.2 can occur, but when the condition 5.12 is verified only the case 1 can happen because there is not enough energy in the BESS to charge the second vehicle before the first one.

If the condition 5.11 is verified, the optimization problem must consider the minimization of the charging time of the second vehicle and the power limits constrained by the vehicle and the charging station:

$$\left\{ \begin{array}{l} \min_{P_{EV_2}} T_{EV_2} \Rightarrow \min_{P_{EV_2}} \frac{\Delta E_{EV_2}}{P_{EV_2}} \Rightarrow \max_{P_{EV_2}} P_{EV_2} \\ P_{EV_2} \leq P_{EV_2,max} \\ P_{EV_1} + P_{EV_2} \leq P_{grid} \eta_{grid} \eta_{EV} + P_{BESS,max} \eta_{BESS} \eta_{EV} \end{array} \right. \quad (5.14)$$

If the condition 5.12 is verified, the optimization problem must also consider the energy limits constrained by the BESS:

$$\left\{ \begin{array}{l} \max_{P_{EV2}} P_{EV2} \\ P_{EV2} \leq P_{EV2,\max} \\ P_{EV1} + P_{EV2} \leq P_{grid}\eta_{grid}\eta_{EV} + P_{BESS,\max}\eta_{BESS}\eta_{EV} \\ \Delta\widehat{E}_{EV1} + P_{EV2}\Delta\widehat{T} \leq P_{grid}\Delta\widehat{T}\eta_{grid}\eta_{EV} + \Delta \text{SoC}_{BESS}E_{BESS}\eta_{BESS}\eta_{EV} \end{array} \right. \quad (5.15)$$

The problems in 5.14 and 5.15 have respectively these solutions:

$$P_{EV2} = \min \{P_{EV2,\max}, P_{grid}\eta_{grid}\eta_{EV} + P_{BESS,\max}\eta_{BESS}\eta_{EV} - P_{EV1}\} \quad (5.16)$$

$$P_{EV2} = \min \left\{ P_{EV2,\max}, P_{grid,\max}\eta_{grid}\eta_{EV} + P_{BESS,\max}\eta_{BESS}\eta_{EV} - P_{EV1} \right. \\ \left. P_{grid}\eta_{grid}\eta_{EV} - P_{EV1} + \frac{\Delta\text{SoC}_{BESS}E_{BESS}}{\Delta\widehat{E}_{EV1}}P_{EV1}\eta_{BESS}\eta_{EV} \right\} \quad (5.17)$$

After the resolution of 5.16 and 5.16, the cases in Fig.2, that can occur, depend on the comparison between T_{EV1} and T_{EV2} : if T_{EV1} is higher than T_{EV2} the solution is given by case 2, otherwise by case 1. In case 2, the assignment of P_{EV2} and T_{EV2} is enough to start the charge of the second vehicle.

In case 1, there is a stage, $\Delta\bar{T}$, in which the second vehicle is the only in charge. In this stage another choice on reference charge power can be done; the charge power of the second vehicle has less constraints than before. The energy to charge in this stage is:

$$\Delta\bar{E}_{EV2} = \Delta\bar{T}P'_{EV2} \quad (5.18)$$

where P'_{EV2} is the second vehicle's charge power in the time interval $\Delta\bar{T}$. In the minimization problems, as in that previously presented, there are two conditions:

$$\Delta\bar{E}_{EV2} \leq \Delta SoC_{BESS} E_{BESS} \eta_{BESS} \eta_{EV} \quad (5.19)$$

$$\Delta\bar{E}_{EV2} > \Delta SoC_{BESS} E_{BESS} \eta_{BESS} \eta_{EV} \quad (5.20)$$

where the value of SoC of the BESS is:

$$\Delta SoC_{BESS} = SoC_{BESS,i} - SoC_{BESS,\min} - \frac{\Delta E_{EV1}}{E_{BESS}} - \frac{\Delta\hat{E}_{EV2}}{E_{BESS}} \quad (5.21)$$

If the condition 5.19 or 5.20 is verified, the optimization problem is the same as 5.5 or 5.6, respectively and the corresponding solutions are 5.22 and 5.23):

$$P'_{EV2} = \min \{ P_{EV2,\max}, P_{\text{grid}} \eta_{\text{grid}} \eta_{EV} + P_{BESS,\max} \eta_{BESS} \eta_{EV} \} \quad (5.22)$$

$$P'_{EV2} = \min \left\{ P_{EV2,\max}, P_{\text{grid}} \eta_{\text{grid}} \eta_{EV} + P_{BESS,\max} \eta_{BESS} \eta_{EV}, \frac{P_{\text{grid}} \eta_{\text{grid}} \eta_{EV} \Delta\bar{E}_{EV2}}{\Delta\bar{E}_{EV2} - \Delta SoC_{BESS} E_{BESS} \eta_{BESS} \eta_{EV}} \right\} \quad (5.23)$$

In the case 2, two different values, P_{EV2} and P'_{EV2} , are evaluated, they are used in different moments of the charge. The charge time is defined as:

$$T_{EV2} = \frac{\Delta\hat{E}_{EV2}}{P_{EV2}} + \frac{\Delta\bar{E}_{EV2}}{P'_{EV2}} \quad (5.24)$$

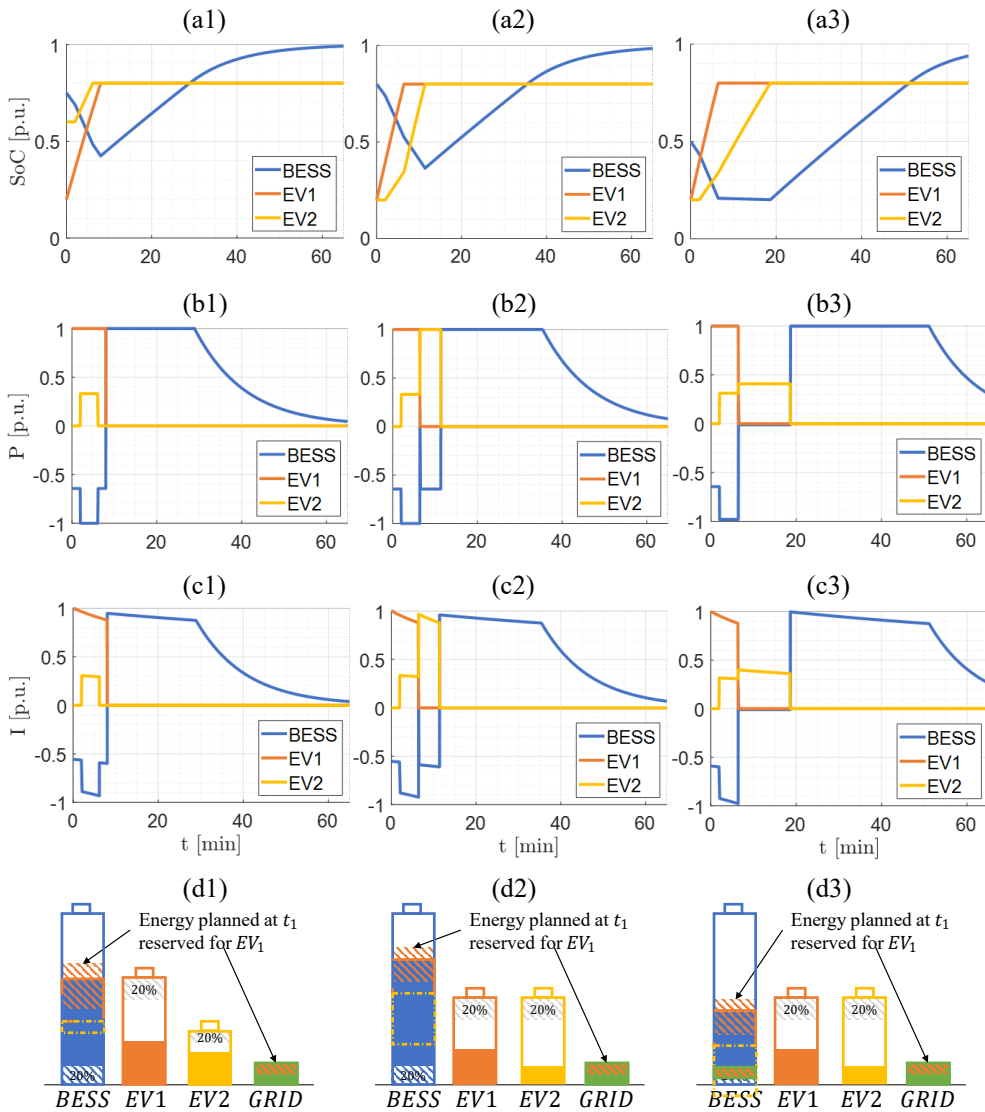


Figure 5.3: Numerical simulations of the simplified charging power planning strategy

This approach allows to set the optimization problem in different use cases and to solve it with closed analytical solutions. The charge planning results in constant or piecewise-constant (max two steps) power charging curves.

The developed charging strategy has been numerically validated. The Fig. 5.3 contain 16 subfigures: on the first (a1, a2, a3), the second (b1, b2, b3) and the third (c1, c2, c3) rows there are the *SoC*, power and current trend of the two vehicles and of the BESS respectively. The fourth row (d1, d2, d3) shows comparisons on energy available and energy required at time t_2 for the second vehicle with the proposed scheduling algorithm (a preliminary planning of charge values of first vehicle is supposed). The values on axis in Fig. 5.3 are expressed in per unit:

- the power and the current of the vehicles are compared to their maximum values, $P_{EV,max}$, and the maximum charge current, $I_{EV,max}$, respectively;
- the power and the current of the BESS are compared to their maximum value of discharge power, $P_{BESS,max}$, and the maximum value of discharge current, $I_{BESS,max}$, during the discharge of the BESS;
- the power and the current of the BESS are compared to the maximum values of charge power and charge current provided by the grid, during the charge of the BESS.

In Fig. 5.3d, the rectangles with only contour indicate empty amount of battery energy, the rectangles colored are full amount of energy, the rectangles with only dashed contour indicate energy comparisons and the rectangles filled with oblique lines are the result of charge planning. In the first column of Fig. 5.3 (a1,

b1, c1, d1), the parameters are: $t_1 = 0min$, $t_2 = 2min$, $E_{EV1} = Q_{EV1}V_{EV1,n} = 50kW$, $E_{EV2} = 25kWh$, $SoC_{EV1,i} = 0.2$, $SoC_{EV2,i} = 0.6$, $SoC_{BESS,i} = 0.75$. This use case is the second of Fig. 5.2. The energy in the BESS is enough to charge both the two vehicles and the power reference is constrained by the maximum charging power of vehicles. The power reference of the first vehicle results from 5.7, since 5.3 is verified. The second vehicle, although it arrived at the station after, is recharged first because has less capability of battery and a higher initial SoC . The power reference of the second vehicle results from 5.16, since condition 5.11 is verified.

In the second column of Fig. 5.3 (a2, b2, c2, d2), the parameters are: $t_1 = 0$, $t_2 = 2min$, $E_{EV1} = 40kWh$, $E_{EV2} = 40kWh$, $SoC_{EV1,i} = 0.2$, $SoC_{EV2,i} = 0.2$, $SoC_{BESS,i} = 0.8$. This use case is the first of Fig. 5.2, the conditions 5.11 and 5.19 are verified. The energy in the BESS is enough to charge both vehicles, but the first vehicle that arrives is the first to leave. The power reference of the second vehicle results from 5.16 for a part of charge and from 5.22 for the remaining part. In particular, the trend curves of SoC of the first vehicle and of the second vehicle - when the first vehicle has left the station - have the same angle. In fact, the power P_{EV1} is constrained with $P_{EV1,max}$ and the power P'_{EV2} , that refers to the time interval $\Delta\bar{T}$ is constrained with $P_{EV2,max}$.

In the third column of Fig. 5.3 (a3, b3, c3, d3), the parameters are: $t_1 = 0$, $t_2 = 2min$, $E_{EV1} = 40kWh$, $E_{EV2} = 40kWh$, $SoC_{EV1,i} = 0.2$, $SoC_{EV2,i} = 0.2$, $SoC_{BESS,i} = 0.5$. This use case is the first of Fig. 5.2, the conditions 5.12 and 5.19 are verified. The energy in the BESS is not enough to charge both vehicles, the saturated constraints are the energy constraints. The power reference of the second vehicle results from 5.17 for part of the charge and from 5.23 for

the remaining part. The time to charge of the second vehicle is very large, so that the *SoC* of the BESS never drops below 20%. The major drawbacks of this approach are:

- it neglects the power losses of the station and may plan values of power which the station cannot supply;
- it neglects the variable demand curve of the vehicles and may plan values of power which the vehicle cannot receive.

The approach proposed in the next paragraph takes into account the power losses of the UFCS and the real current demand curves of the EVs.

5.2.2 An advanced strategy

This charging power planning strategy removes the simplified assumptions of the previous strategy:

- the power charging demand is driven by the vehicle's requests;
- the efficiencies depends on the input/output current and voltage values of converters, as a consequence they also depends on the *SoC* of EVs and BESS;
- this strategy is formulated for a number n of vehicles and it is suitable for both the RR and the FCBS.

The introduction of the time-variation of converters' efficiency and EV current demand imposes the non-linearity and the time-variance of the power and energy constraints during the charging phases. As a consequence, a closed

analytical solution cannot be carried out. Thus, the solution can be found by means of a time discretization of the optimization problem. Parameters and constraints are assumed piecewise-constant for each step, so the charge power profile results piecewise-constant, too. Although the quantities are variable and the relationships are non-linear, the optimization procedure presents an iterative nature and the planning algorithm is still carried out offline, using models to simulate the behavior over time of the EV and the BESS as in [17]. The RR algorithm will be applied providing a cyclical exchange of priorities among EVs, in terms of step of increase of SoC: every time the SoC of the vehicle with the highest priority increases of a fixed ΔSoC , the EV loses its priority and becomes the vehicle with the lowest priority. The FCBS will be applied assigning the priority on the arrival time and maintaining it until the EV charge is completed.

The estimation of UFCS efficiency is based on the computation of power losses of each subsystem. The following power losses are considered:

- AFE: IGBT and Diode conductive losses; IGBT commutation losses [252], [253];
- SAB: IGBT and Diode conductive losses; IGBT commutation losses; transformer conductive and iron losses [253], [254];
- BESS: joule losses.

The calculated UFCS efficiency waveforms as a function of EV charging power, BESS and EV voltage values (i.e., V_{BESS} , SoC_{EV} , respectively) are highlighted in Fig. 5.4. Two groups of curves are represented according to SoC_{EV} equal to

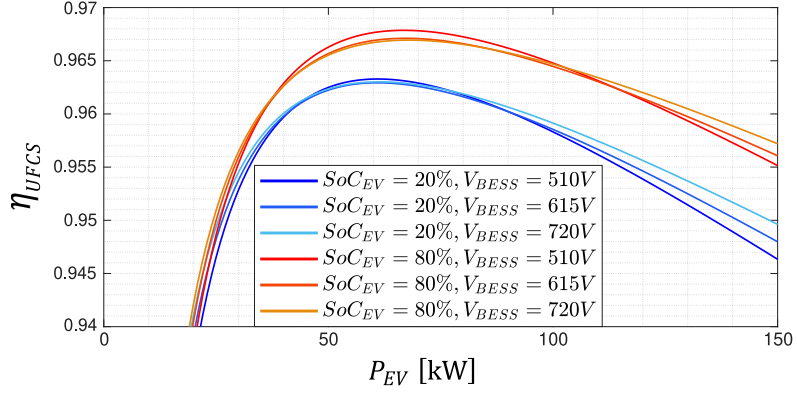


Figure 5.4: UFCS efficiency vs. EV power for different values of SoC_{EV} and V_{BESS} , and with vehicle rated voltage 400 V

20 and 80%. Each group of curves highlights UFCS efficiency as a function of the EV charging power for minimum, intermediate and maximum BESS voltage value. The two groups of curves represent the lower and upper boundaries of operating working area during a fast charge of an EV with 400 V rated voltage. The curves show, clearly, that the efficiency depends strongly on EV power and voltage, whereas less is the dependence on the BESS voltage. The goal of this strategy is the minimization of the EV charging time (i.e., power maximization) taking into account the constraints on power (i.e., supplying and charging limits) and energy, in terms of minimum SoC_{BESS} (i.e., 20% of SoC). In the case of charging more EVs simultaneously, the optimization problem needs to establish a priority mechanism among the EVs. The fundamentals of the strategy are:

1. In the presence of a single EV, it has the highest priority, so the planning of its charging profile is based on the status of the infrastructure, in terms of available grid power and BESS's SoC.

2. In the presence of multiple EVs, a priority algorithm has to be considered. The charging profile of the EV with the highest priority is determined as in the case of a single EV. The planning of the charging profile of EVs with lower priority has to consider power and energy values already assigned to the priority EV. EVs with lower priorities are subject to more restrictive constraints than EVs with higher priorities.

The problem of optimizing the charging profile for the i -th EV arriving at the UFCS can be modelled according to the following minimization problem:

$$\min_{P_{EV}} t_{EV_i, ch} \quad \text{such that} \quad \begin{cases} P_{EV_i}(t) \leq P_{EV_i, max}(t) \\ P_{EV_i}(t) \leq P_{SAB, max}(t) \\ P_{EV_i}(t) \leq P_{EN}(t) \end{cases} \quad (5.25)$$

The objective function seeks to minimize the EVs charging time ($t_{EV_i, ch}$) to release the charging slot as soon as possible, thus, reducing the waiting time for subsequent EVs. The goal is pursued by maximizing the charging power, taking into account the constraints on maximum power values of EV ($P_{EV_i, max}(t)$) and slot ($P_{SAB, max}(t)$), whereas $P_{EN}(t)$ is a power constraint depending on managing the energy flow between grid, BESS and EV. It is to underline, the constraints are time variant due to their dependance on SoC_{EV} and SoC_{BESS} . The following system represents the discrete representation of the optimization model:

$$\max_{P_{EV_i}^{(k)}} t_{EV_i, ch} \quad \text{such that} \quad \begin{cases} P_{EV_i}^{(k)} \leq P_{EV_i, max}^{(k)} \\ P_{EV_i}^{(k)} \leq P_{SAB, max}^{(k)} \\ P_{EV_i}^{(k)} \leq P_{EN_i}^{(k)}. \end{cases} \quad (5.26)$$

Eq.(5.26) is obtained by the discretization of eq.(5.25) through the *forward Euler method*, in which the sample time, ΔT , can be chosen according to the desired levels of accuracy and k is the integer index of the discrete time, such that $t_{k+1} = t_k + \Delta T$.

Hence, the optimization problem can be stated as follows:

$$\max \{P_{EV_i, \max}^{(k)}, P_{SAB, \max}^{(k)}, P_{EN_i}^{(k)}\}, \quad (5.27)$$

according to the imposed constraints, which can be defined as follows:

- **Maximum EV power demand** ($P_{EV_i, \max}^{(k)}$): The EV on-board Battery Management System (BMS) communicates to the charging infrastructure the maximum value of current that the vehicle can draw, which depends on the on-board battery's technology, sizing and SoC_{EV} . It is remarkable that in order to preserve the battery State of Health (SoH), the BMS could define values quite lower than the rated one. Thus, the constraint $P_{EV_i, \max}^{(k)}$ at the k -th time interval can be formulated as follows:

$$P_{EV_i, \max}^{(k)} = I_{EV_i, \max}^{(k)} \cdot V_{EV_i}^{(k)} \quad (5.28)$$

where $V_{EV_i}^{(k)}$ is the terminal battery voltage at maximum battery current value. In order to calculate the voltage, the zero order battery mathematical model can be used:

$$V_{EV_i}^{(k)} = OC_{EV_i}(SoC_{EV_i}^{(k)}) - R_{EV_i} \cdot I_{EV_i}^{(k)} \quad (5.29)$$

$$SoC_{EV_i}^{(k)} = SoC_{EV_i}^{(k-1)} + \frac{V_{EV_i}^{(k-1)} I_{EV_i}^{(k-1)} \cdot \Delta T}{E_{EV_i}} \quad (5.30)$$

where for the current the passive sign convention was adopted.

- **Maximum power constraint of UFCS** ($P_{SAB,max}^{(k)}$): it represents the maximum deliverable power of the SAB converter (it depends on the infrastructure rate). The value of this power constraint is:

$$P_{SAB_i}^{(k)} = I_{SAB,max} \cdot V_{BESS}^{(k)} \eta_{SAB_i}^{(k)}, \quad (5.31)$$

where the product between the maximum deliverable current and the input voltage ($V_{BESS}^{(k)}$) is the theoretical maximum input power of the SAB at the time interval considered.

- **Energy constraint of UFCS** ($P_{EN_i}^{(k)}$): it takes into account the amount of energy available within the BESS. It must be imposed to ensure that: i) the BESS contains energy enough to supply the energy demanded by the i -th EV at the k -th interval; ii) the energy demanded by EV_i does not limit the power already scheduled for the EVs with higher priority. Indeed, the power supplied to the i -th EV could fully discharge the BESS ahead of schedule and, as a consequence, it won't be able to feed the charging profiles already assigned to other EVs.

The residual energy within the BESS at the k -th time interval ($E_{BESS}^{(k)}$) can be calculated according to the following expression:

$$E_{BESS}^{(k)} = E_{BESS}^{(0)} - \sum_{h=0}^{k-1} \frac{P_{BESS,dis}^{(h)}}{\eta_{BESS}^{(h)}} \Delta T, \quad (5.32)$$

in which the sum represents the gross energy supplied by the BESS and the quantity $P_{\text{BESS,dis}}^{(h)}$ is given by the difference between the total input power to all the operating SAB converters at the h -th step, and the power supplied by the grid:

$$P_{\text{BESS,dis}}^{(h)} = \sum_{q \in n(h)} \frac{P_{\text{EV}_q}^{(h)}}{\eta_{\text{SAB}_q}^{(h)}} - P_{\text{grid}} \eta_{\text{AFE}}^{(h)}. \quad (5.33)$$

It should be noted that $n(h)$ in (5.33) is the subset of EVs with higher priority than EV_i at the h -th step, therefore the number of elements of $n(h)$ represents the number of operating SAB converters at each step. Furthermore, when there is no vehicle in charge, the power supplied by the grid is used to charge the BESS, therefore, according to (5.33) $P_{\text{BESS,dis}}$ becomes negative.

The energy constraint consists of the amount of energy that the UFCS makes available to the i -th EV according to the priority mechanism. Indeed, if at the k -th step EV_i has the highest priority, the available energy of the BESS would be the entire $E_{\text{BESS}}^{(k)}$. More in general, for each vehicle, the amount of available energy from the station ($\hat{E}_i^{(k)}$) is defined as follows:

$$\begin{cases} \hat{E}_i^{(k)} = E_{\text{BESS}}^{(k)} - \sum_{h=k}^{k_{\text{end}}-1} \frac{P_{\text{BESS,dis}}^{(h)}}{\eta_{\text{BESS}}^{(h)}} \Delta T \\ k_{\text{end}} = \max \{k_{\text{end},j}\} \quad \forall j \in n(k) \end{cases} \quad (5.34)$$

where $k_{\text{end},j}$ is the steps in which the j -th EV will complete its recharge or its priority will change. In other words, $\hat{E}_i^{(k)}$ consists in the total energy $E_{\text{BESS}}^{(k)}$ decreased of the amount of BESS energy already assigned

to the EVs with higher priority. The energy constraint can be formulated more conveniently in terms of power as follows:

$$P_{\text{EN}_i}^{(k)} = \frac{\hat{E}_i^{(k)}}{\Delta T} \eta_{\text{BESS}} \eta_{\text{SAB}_i} \quad (5.35)$$

$P_{\text{EN}_i}^{(k)}$ represents the EV charging power that would consume the whole $\hat{E}_i^{(k)}$ in a single time interval. The quantity $\frac{\hat{E}_i^{(k)}}{\Delta T} \eta_{\text{BESS}}$ is the power that the BESS would supply to run out the energy available for the i -th EV.

The numerical assessment of the constraints is mandatory for formulating the proposed strategy.

The first constraint $P_{\text{EV}_i, \text{max}}$ can be easily calculated by replacing (5.29) in (5.28), where $I_{\text{EV}_i, \text{max}}$ and $\text{SoC}_{\text{EV}_i}^{(k)}$ are known. Hence:

$$P_{\text{EV}_i, \text{max}}^{(k)} = I_{\text{EV}_i, \text{max}}^{(k)} \cdot \text{OCV}_{\text{EV}_i}^{(k)} \left(\text{SoC}_{\text{EV}_i}^{(k)} \right) - R_{\text{EV}_i} \cdot \left[I_{\text{EV}_i, \text{max}}^{(k)} \right]^2 \quad (5.36)$$

The second constraint $P_{\text{SAB}_i, \text{max}}^{(k)}$, as highlighted by (5.31) depends on the quantity $V_{\text{BESS}}^{(k)}$. It can be calculated according to the battery model by expressing the current $I_{\text{BESS}}^{(k)}$, whose formulation is reported below:

$$I_{\text{SAB}_q}^{(k)} = \frac{P_{\text{EV}_q}^{(k)}}{\eta_{\text{EV}_q}^{(k)} V_{\text{BESS}}^{(k)}} \quad (5.37)$$

$$I_{\text{BESS}}^{(k)} = I_{\text{SAB}, \text{max}} + \sum_{q \in n(h)} I_{\text{SAB}_q}^{(k)} - \frac{P_{\text{grid}} \cdot \eta_{\text{AFE}}^{(k)} (V_{\text{BESS}}^{(k)})}{V_{\text{BESS}}^{(k)}}. \quad (5.38)$$

$$V_{\text{BESS}}^{(k)} = \text{OCV} \left(\text{SoC}_{\text{BESS}}^{(k)} \right) - R_{\text{BESS}} \cdot I_{\text{BESS}}^{(k)} \left(V_{\text{BESS}}^{(k)} \right). \quad (5.39)$$

It worth noting that the cross dependence of $I_{\text{BESS}}^{(k)}$ and $V_{\text{BESS}}^{(k)}$ makes (5.38) and (5.39) non-linear. Furthermore, calculated the BESS voltage, the maximum power of the UFCS can be defined according to the following non-linear system:

$$\begin{cases} P_{\text{SAB}_i, \text{max}}^{(k)} = I_{\text{SAB}, \text{max}} \cdot V_{\text{BESS}}^{(k)} \cdot \eta_{\text{SAB}_i}^{(k)} \left(\frac{P_{\text{SAB}_i, \text{max}}^{(k)}}{V_{\text{EV}_i}^{(k)}} \right) \\ V_{\text{EV}_i}^{(k)} = \text{OCV}^{(k)} \left(\text{SoC}_{\text{EV}_i}^{(k)} \right) - R_{\text{EV}_i} \cdot \frac{P_{\text{SAB}_i, \text{max}}^{(k)}}{V_{\text{EV}_i}^{(k)}}. \end{cases} \quad (5.40)$$

Eq.s (5.39) and (5.40) need to be solved using a numerical method. In this work, the *fixed point iteration* has been chosen.

Also the constraint $P_{\text{EN}_i}^{(k)}$ reported in eq. (5.35) depends on $V_{\text{BESS}}^{(k)}$. It can be calculated by solving, once again with the *fixed point iteration*, the non-linear system:

$$\begin{cases} V_{\text{BESS}}^{(k)} = \text{OCV} \left(\text{SoC}_{\text{BESS}}^{(k)} \right) - R_{\text{BESS}} \cdot I_{\text{BESS}}^{(k)} \\ I_{\text{BESS}}^{(k)} = \frac{\Delta E_{\text{BESS}, \text{pr}}^{(k)}}{\Delta T \cdot V_{\text{BESS}}^{(k)}} \cdot \eta_{\text{BESS}}^{(k)} \left(V_{\text{BESS}}^{(k)} \right), \end{cases} \quad (5.41)$$

where the current supplied by the BESS can be obtained from (5.35), taking into account the grid contribution.

The emulation of the proposed strategy was carried out on the DIETI UFCS. The results highlighted the behaviour of the infrastructure when the two alternative priority algorithms (i.e., FCBS and Round Robin), are used. The case studies aim to show how initial conditions on SoC_{EV_1} , SoC_{EV_2} , SoC_{BESS} , and the management of the priority between the two vehicles can affect the resultant charging power profiles. The optimization strategy has been implemented in Matlab[®] 2019b. A sample time of 1 min was assigned. It is a good compromise

between calculation effort and accuracy.

The numerical validation of the strategy was carried out using the experimental results of charging two different real commercial EVs. The relevant data of the EVs are reported in the following Table 5.1.

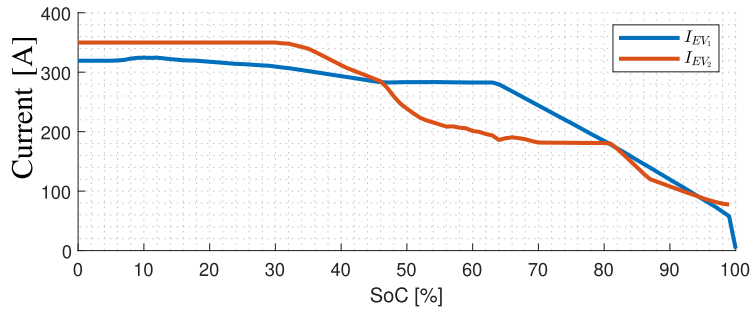
Table 5.1: EVs Data

Parameters	Unit	EV1	EV2
Rated Power	[kW]	230	150
Specific Energy Consumption	[kWh/100 km]	21.7	21.7
Autonomy (WLTO)	[km]	340	520
Energy Battery Stack	[kWh]	71	77
Rated Voltage	[V]	396	450
Max Charge Power up to 0.8 SoC	[kW]	120	120
Full Charge Time	[min]	30	30
Propulsion Type	-	IM	BR

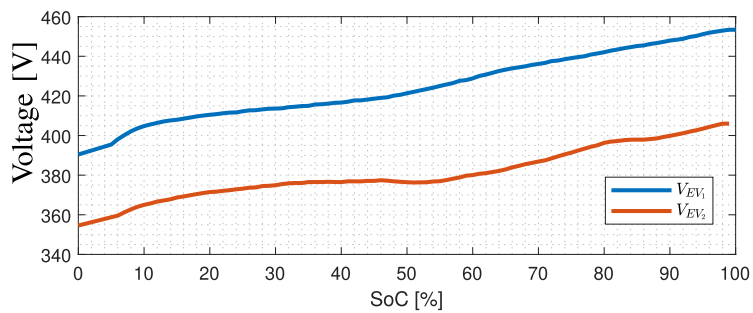
EV charging current profiles In order to validate the optimization strategy in a real scenario, the maximum power demand profile (i.e., $P_{EV,max}$) and the $SoC - I$ characteristic of the two EVs were evaluated in a preventive experimental measurement campaign. As already discussed, the measured power profiles are controlled by the EVs' on-board BMS.

The two vehicles have been charged separately, with the BESS full charged. These measurements are highlighted in Figs. 5.5. It can be noted that the two charging modes as a function of SoC_{EV} are different. The maximum power requirements of EV_2 begins to decrease for values of SoC_{EV} around 40%, whereas EV_1 keeps a constant power (i.e., 120 kW) up to 65% of SoC_{EV} . These behaviours depend on the strategies imposed by the two car makers in order to

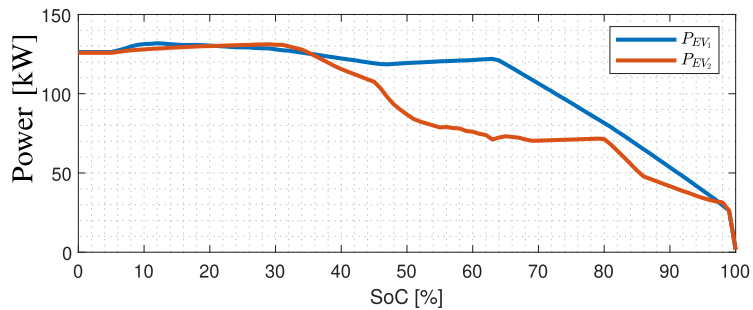
manage the on-board battery temperature (i.e., to preserve battery lifetime).



(a)



(b)



(c)

Figure 5.5: Experimental values of current (a), voltage (b) and power (c) referring to the charge of two different vehicles

FCBS Vs Round Robin Table 5.2 shows the operating conditions used for the two case studies A and B (they differ only for the BESS initial SoC.);

Table 5.2: Case studies

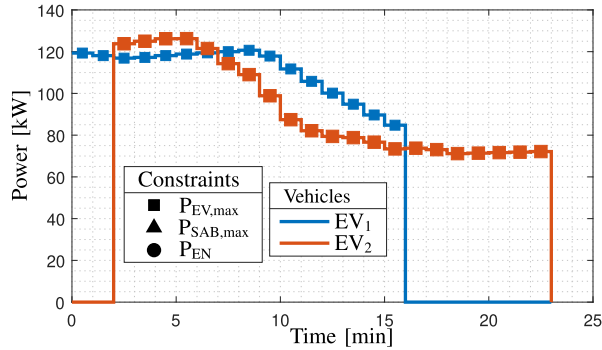
Quantity	Unity	Case A	Case B
Arrival time EV_1	[min]		0
Arrival time EV_2	[min]		2
$SoC_{EV_{10}}$	[pu]		0.4
$SoC_{EV_{20}}$	[pu]		0.2
$SoC_{EV,max}$	[pu]		0.8
SoC_{BESS_0}	[pu]	0.8	0.5

the arrival time of the EVs, their initial and final SoC ($SoC_{EV_{10}}$, $SoC_{EV_{20}}$, $SoC_{EV,max}$), and the BESS initial SoC (SoC_{BESS_0}) are reported.

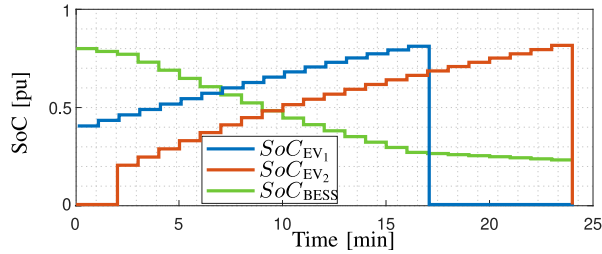
Figs. 5.6 and 5.7 show the results of the optimal power scheduling strategy for the two alternative priority algorithms in terms of power profiles. In particular, the power profiles are marked with:

- square-shaped marker, when the curve is limited by the EV maximum power constraint ($P_{EV,max}$);
- triangle-shaped marker, when the curve is limited by the SAB maximum power constraint ($P_{EV,max}$);
- circle-shaped marker, when the curve is limited by the energy constraint (P_{EN}).

In Case A, when the BESS initial SoC is 0.8, the UFCS charge simultaneously the two EVs. The FCBS and RR algorithms give the same results. Indeed, Fig. 5.6a shows that the active constraint over the entire charging phase is $P_{EV,max}$, moreover Fig. 5.6b highlights that the BESS is not fully discharged at the end of the recharge of both vehicles. As a consequence, the charging profiles of Fig. 5.6a are equivalent to the power profiles of Fig. 5.5 in the SoC



(a) Power



(b) SoC

Figure 5.6: FCBS Vs RR - Case A

range $[0, 0.8]$. UFCS maximum power constraint (i.e., $P_{SAB,max}$) does not act, being higher than the two $P_{EV,max}$.

More relevant is Case B. As a consequence of the lower BESS initial SoC, the priority algorithms give different results. The results are highlighted in Figs. 5.7, in which Figs. 5.7a, 5.7c and 5.7e focus on the results of the FCBS algorithm, whereas Figs. 5.7b, 5.7d and 5.7f relate on the RR algorithm. Figs. 5.7a and 5.7b point out the charging power profile of the two EVs. Figs. 5.7c and 5.7d show the value of the energy constraint, whereas Figs. 5.7e and 5.7f highlight the behaviour of SoC_{EV_1} , SoC_{EV_2} and SoC_{BESS} .

The analysis of the results highlight the differences between the adoption of the two alternative strategies. In Case B, more constraints are active over the entire

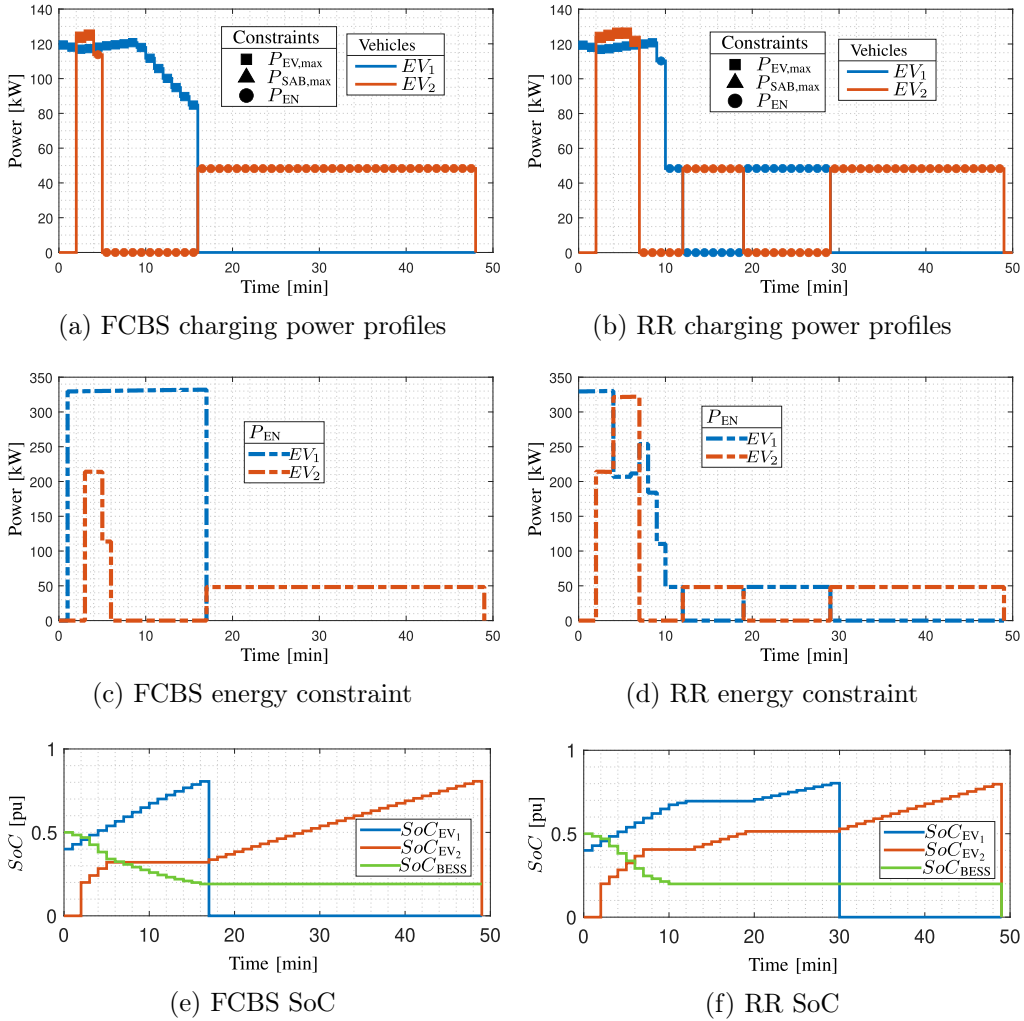


Figure 5.7

charging phase. In case of FCBS, the EV₁ (solid blue line) has the highest priority over its entire charging phase. Therefore, the UFCS makes available to EV₁ the full BESS energy and the grid power. The charge of EV₁ is the fastest as it is possible. The parameters for charging EV₁ are calculated at its arrival at the station. As a consequence, the charging power profile available for the

EV₂ can be calculated by using only the residual BESS energy. This means that the charging profile assigned to EV₁ is a constraint for charging EV₂. In case of FCBS algorithm, the residual BESS energy allows to charge EV₂ at its maximum power only for the first two minutes (Fig. 5.7a). Later, the charge process stops and resumes only when EV₁ is fully charged. So, being SoC_{BESS} empty, the slots charges EV₂ by the grid power (i.e., 50 kW).

RR algorithm varies cyclically EV priority during the charging phase. In detail, each EV holds the priority for a time interval related at increasing its SoC of 20%. The solution provided by the RR algorithm highlights the following charging modes:

- $0 \text{ min} \leq t \leq 4 \text{ min}$: the charging power profiles and the values of P_{EN} are equivalent to those of the FCBS, where EV₁ has the priority. At the time ($t = 4 \text{ min}$) EV₁'s SoC is increased by +20% and, hence, the algorithm assign the priority to EV₂.
- $4 \text{ min} < t \leq 7 \text{ min}$: all the UFCS energy is available for EV₂. Thus, EV₂ can be charged at its maximum power value. This estimated time horizon of priority uses a limited amount of SoC_{BESS} , therefore also EV₁ can be charging at its maximum power value.
- $7 \text{ min} < t \leq 12 \text{ min}$: EV₁ get the highest priority again; the amount of BESS energy is not enough for charging both the vehicles at their maximum powers. Initially, EV₁ charges at its maximum power, whereas EV₂ is not charged; three minutes later, the energy constraint limits the charging power. At $t = 10 \text{ min}$ the BESS is fully discharged, therefore the charging continues using only the grid power.

- $12 \text{ min} < t \leq 49 \text{ min}$: EV_1 and EV_2 are charged alternatively, according to the assigned priority.

Table 5.3: Priority algorithms comparison

	Case A		Case B	
	FCBS	RR	FCBS	RR
T_{EV_1} [min]	16		29	16
T_{EV_2} [min]	21		47	46
$P_{EV_1,avg}$ [kW]	110.84		60.67	110.84
$P_{EV_2,avg}$ [kW]	91.80		40.98	41.46

Table 5.3 shows the comparison between the two proposed priority algorithms, in terms of charging time and average supplied power. If the SoC_{BESS_0} is high, the two priority algorithms produce no differences. If the BESS is only partially charged, the FCBS algorithm favours unequivocally the first arrived vehicle. It is relevant to note that both the algorithms are able to provide the full charge of the two EVs in less than 50 min.

Real case study: UFCS prototype of DIETI

In this chapter, the experimental setup of the UFCS prototype of DIETI is reported. To summarize, all the considerations made in the previous chapters about the design choices, sizing and control strategies are now presented as a finished product. The tests conducted on the prototype highlight the complied requirements. The Fig.6.1 is a picture of the prototype, the main arrangements are the conversion power box and the dispenser; the cooling system is composed of more parts and it is not shown in Fig.6.1.



Figure 6.1: A picture of FCS prototype of DIETI

The PV system has been realized in the real prototype; it is not explicitly shown in Fig.3.4, because it is not a functional subsystem of the station. The PV panels are clustered in modules, a module is a string of panels in series, connected to the DC side of a single-phase inverter. The modules are clustered in three Cascaded H-Bridge (CHB) phase legs, they can be delta -connected or star-connected to the grid. The paper [255], of the author, deals with the power control of a delta connected CHB converter equipped with PV modules. A hierarchical architecture of energy management is proposed: a “Module level” controller performs a Maximum Power Point Tracking (MPPT) algorithm to achieve the optimal utilization of each PV module; a “Leg level” controller manages the power flow control within the modules of a single CHB phase leg, and a “System” level controller manages the active power flow between the three CHB phases and the reactive power generation towards the grid. The active power control is aimed at the compensation of the mismatches between the different PV-powered modules, which may come from partial shadowing phenomena. A power unbalance compensation between cascaded modules is implemented through the Pulse Width Modulation (PWM) algorithm, while the unbalance compensation between the phases is implemented through the phase currents control. To compensate the active power unbalance due to PV module mismatches, the obtained effect is equivalent to the injection of a zero sequence current. A reactive power control has been implemented to perform a power factor (PF) correction, too. A set of numerical simulations validate the effectiveness of the algorithm, which can simultaneously achieve the desired active power generation from all the PV panels and the desired PF control towards the grid.

6.1 Experimental setup

As presented in the chapters 3 and 4, the structure consist of:

- AC/DC converter: It is a bidirectional AFE converter interfaced to the LV grid through an isolation transformer.
- BESS: it is interfaced directly to the common DC bus, without any converters. It is not controlled directly, and it supplies the power required by the DC/DC converter reduced of the power furnished by the AC/DC converter.
- DC/DC converter: it is a current or voltage controlled SAB converter on its primary side. The high side is connected to the common DC bus, the low side is interfaced to the charging dispencer through an LC filter.

AC/DC converter The AFE converter draws power from the utility grid to charge the internal battery of the UFCS prototype. Further information about the input transformer and input clean power filter are:

- Clean Power Filter capacitors: 2SM1000269491B “Three – phase capacitor bank for sinusoidal filter, grid side for AFE”;
- Input transformer and filter reactor: 2SM1000269323B “Insulation transformer with integrated reactor for sinus filter 400V/300V, 50/60Hz, 60kVA”

The technical data of the AFE are:

- AC input voltage: 300V

- DC voltage: 510 – 720V (BESS voltage)
- Rated input power: 50kW
- Load cycle: permanently working at 50kW
- Switching components: 1200V IGBT
- Switching frequency: 4kHz
- DC bus capacitor: 7 x 2.5mF DUCATI DCH 85 C SERIES, Type 059; 2SM1000267616B “METALLIZED POLYPROPYLENE D.C. LINK CAPACITOR”
- Current flowing into DC bus capacitors: 230Arms
- Sensors: 3 current LEMs and 1 DC voltage LEM
- Cooling: water cooled

Due to the necessary compactness of the system, the requirement is to integrate the AFE in the same frame, together with the H-Bridges.

DC/DC converter The two SAB converters of the two charging slots consist of an H-Bridge converter, an HF transformer and a diode rectifier.

The main data of each H-Bridge unit are:

- Input side : 510~720V (BESS voltage)
- Output side: AC square wave @ 2.6kHz with variable duty cycle (input of HF transformer)

- Maximum duty cycle = 0.5
- Switching frequency: $2.6kHz$
- Maximum continuous current: $420A$ for each unit.
- Current flowing into DC bus capacitors: $230A_{rms}$ @ $5.2kHz$
- Switching components: $1200V$ IGBT
- Sensors: 1 current LEM at the output for each H-Bridge
- Cooling: water cooled

The most important characteristics of the HF transformer are listed below:

- Input voltage: AC square wave @ $2.6kHz$ with variable duty cycle (output of H-Bridge converter)
- Maximum input voltage: $600V_{rms}$
- Current: $400A$ at secondary side
- Cooling: water cooled

The diode rectifier converts the AC voltage at the output of HF transformer in a DC voltage waveform. Its main technical data are:

- Input voltage: $720V$ peak
- Input frequency: $2.6kHz$
- Average current: $200A$
- RMS current: $280A$

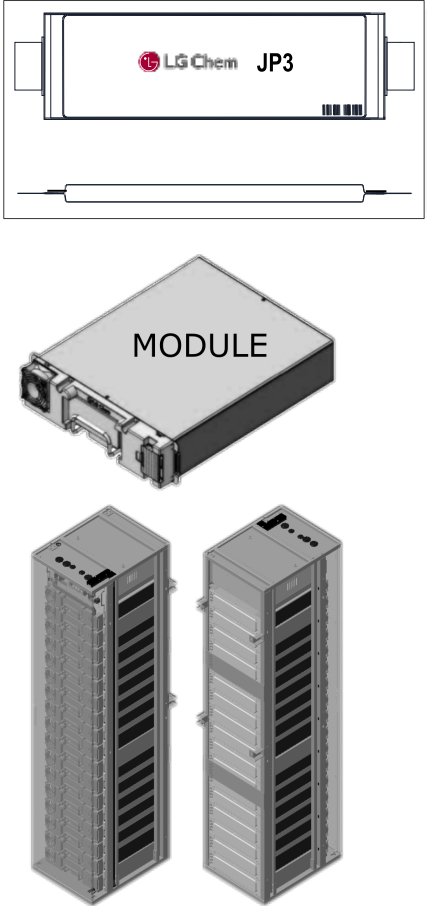
- DC Current: 400A
- Components: Due to the required voltage, current and input frequency, the diode rectifiers will be built using the freewheeling diodes of an IGBT power module, in which the IGBT will be permanently kept in off-state.
- Cooling: water cooled

The diode bridges will be integrated inside the converter frame, together with the AFE and the 2 H-Bridges, cooled by the same heat sink. The output LC filter is designed to reduce the ripple of the current flowing into the EV batteries. The standards require a ripple lower than 6A peak-peak with a frequency lower than 5kHz, and a ripple higher than 12A peak-peak with a frequency higher than 5kHz. Main data of each LC filter are:

- Resistor: 1mH, $I_{\max} = 400A$, 2SM1000269324 B “Iron-core reactor, water cooled
- Capacitor: 1mF, $V_{DC,\max} > 950V$ in configuration ISOP
- Current ripple: $< 7A$ peak-peak @ 5.2kHz
- Resistor + contactor to allow a fast discharge of the capacitor
 - with $R = 1k\Omega$, $\tau = R \cdot C = 1s$: safe discharge in 5 seconds;
 - initial current peak = $950V/1k\Omega < 1A$.

BESS The BESS is placed in a separate cabinet, but it is an integral part of the station. The topology of the BESS is well documented in Fig.6.2. The cells JP3 by LG Chem[®] are clustered in modules, there are 14 cells in

Cell JP3		Unit	JP3
Nominal Capacity	Ah		64.0
Nominal Energy	Wh		235.5
Nominal Voltage	V		3.68
Voltage Range	V		3.0 ~ 4.2
Chemistry	(+)		NMC
	(-)		Graphite
Module	Configuration	14S1P (cells)	
BESS	Configuration	12S2P (modules)	
Nominal Energy	kWh		79.2
Voltage Range	V		510 - 720
Dimension (W x D x H)	mm		520 x 850 x 220
Energy Density	Wh/L		198
Max Current (FR pattern)	A		380 (3 C)
BMS Communication			CAN
Cooling			Air Cooling



The figure includes three visual components: 1) A top-down view of a rectangular LG Chem JP3 battery cell with terminals on both ends. 2) A perspective view of a grey rectangular module with a connector on the left side. 3) Two vertical racks of the BESS system, each containing multiple modules stacked vertically.

Figure 6.2: BESS general information

series in each module. The modules are equipped with proper electrical and thermal management system; there is a set of cooling fans in each module. The BESS is composed by 2 racks in parallel and each rack contains 12 modules in series. Thus, the overall voltage varies in a range of 510 – 720V, the current cannot exceed 3 C-rate, that means about 380A. The BESS doesn't use the same water cooling system of the other subsystems of the station, it is because the right working temperature is quite higher than room temperature.

Communication protocols The main PLC communicates via TCP/IP with the control boards of each subsystem, they are the BMS of the BESS, the dedicated gate drivers of converters, the data acquisition boards, the back-end central system and a Safety PLC. The dedicated gate drivers of converters communicate together with the data acquisition boards via Modbus RTU.

The external PLC will manage: the grid LV circuit breaker, the contactors of the BESS, the contactor for the pre-charge of the DC-Bus capacitors, the main contactor for the energization of the transformer. The star up phase follows these steps:

- the PLC sends the start command to the AFE and it sets the CV control mode at the BESS actual voltage;
- the AFE controller regulates the DC-Bus at the reference value sent by the PLC;
- the BESS is connected to the DC-Bus;
- the PLC sets the CP control mode and it starts to send the P and Q references;
- the AFE controller derive the current references i_d, i_q from the P and Q references;
- the PLC sends the start command to the one SAB or both, it depends on their configuration (independent outputs or ISOP), and it sets the CV control mode at the EV actual voltage;

- when the output voltage of system is balanced with that of the vehicle the converter receives the regulation request in CV, CC or CP from the PLC:
 - (a) In CV, the burden resistors are set in parallel with the load. The PLC sends a ramp-shape voltage reference, then the DAB controller defines the current limits;
 - (b) In CC, burden resistors are disconnected. The PLC sends a ramp-shape current reference, then the DAB controller defines the voltage limits.

6.2 Experimental results

6.2.1 Acceptance testing

The first relevant tests on the functioning of the charging infrastructure concern compliance with the standards.

In Fig.6.3 a routine of the BESS early charging through the AFE converter is proposed. The start-up phase consists of a CV control in the time interval between 4 and 12 seconds and a CP control from 12 second onwards. In Fig.6.3, at the beginning, the voltage of the DC side of the AFE converter is set to 500V as a default value of the DC capacitor pre-charging value. Then, the voltage reference reaches the actual BESS voltage and the control drives the voltage on common bus at the BESS voltage value in a 3s shorter time interval. When the DC side voltage reaches the reference value, the contactors close and the power reference of CP control is assigned. The slew rate of power is about $8kW/s$.

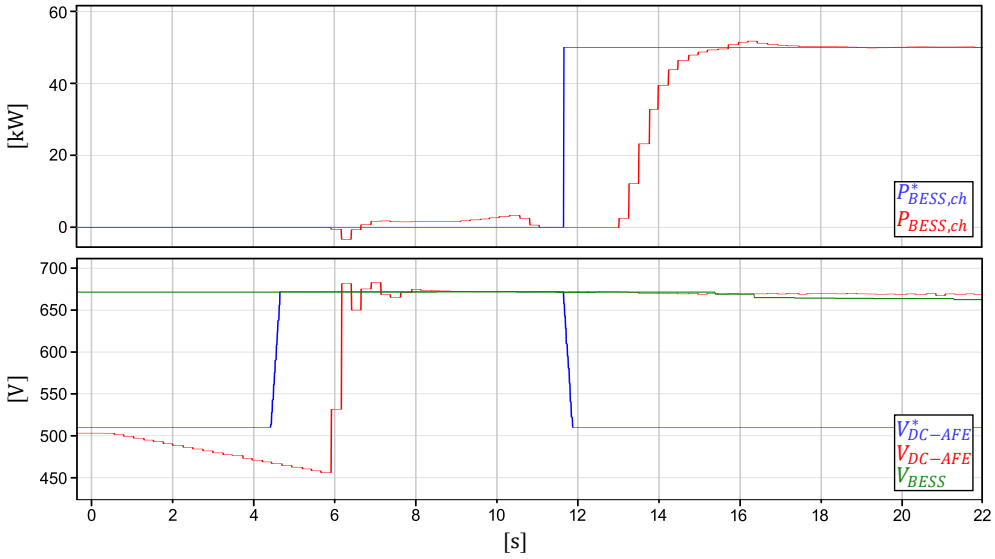


Figure 6.3: AC/DC converter start-up control routine

After the AFE converter and BESS coupling, the charging request from the vehicle drives the SAB converter control. In Fig.6.4, the reference voltage is placed to the maximum available value of 450V while the isolation test is running. At the time 7s, the isolation test results in a successful outcome and the CV control can start to balance the EV battery voltage and the output voltage of the SAB converter. At the time 10s, the contactors close and the CC control is carried out on the vehicle.

To evaluate the compliance of those voltage and current dynamics, in Fig.6.5, the standard prescriptions are reported. Thus, the control routines of Fig.6.4 are compliant with the standards. The same tests are conducted for several working points, and they result in the voltage slew rate that is never more than $0.5V/ms$ and the current ramp slope that is always higher than $80A/s$ (the control works also with a ramp slope until $450A/s$). The same evaluation

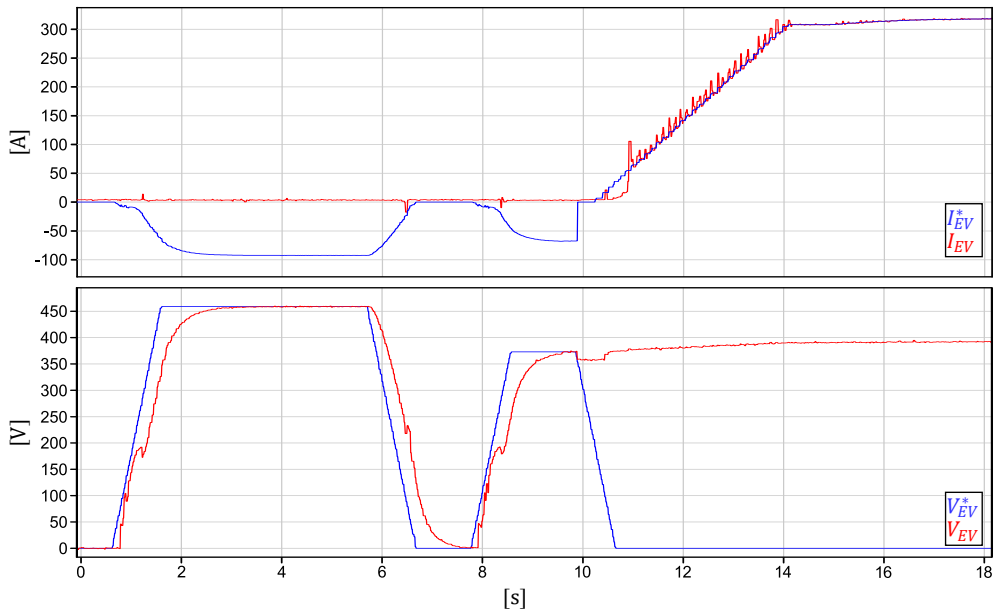


Figure 6.4: DC/DC converter start-up control routine

conducted for the start-up phase are conducted at the controlled end of charge and in emergency shutdown.

The various tests carried out on the infrastructure made it possible to estimate the system's efficiencies. The efficiencies relating to the charging and discharging of the BESS are reported in Fig.6.7.

Fig.6.7 shows that the efficiency slightly decreases while the SoC_{BESS} increases both in the charging and discharging phases; this behavior is due to the fact that the efficiency of the AFE converter increases when the conversion ratio is closer to the unit. Additionally, the efficiency has its maximum values for the highest grid power (closer to the nominal power of sizing) both in the discharging and in the charging phase. When the BESS supplies energy to the grid, the efficiency is quite higher than when the grid charges the BESS.

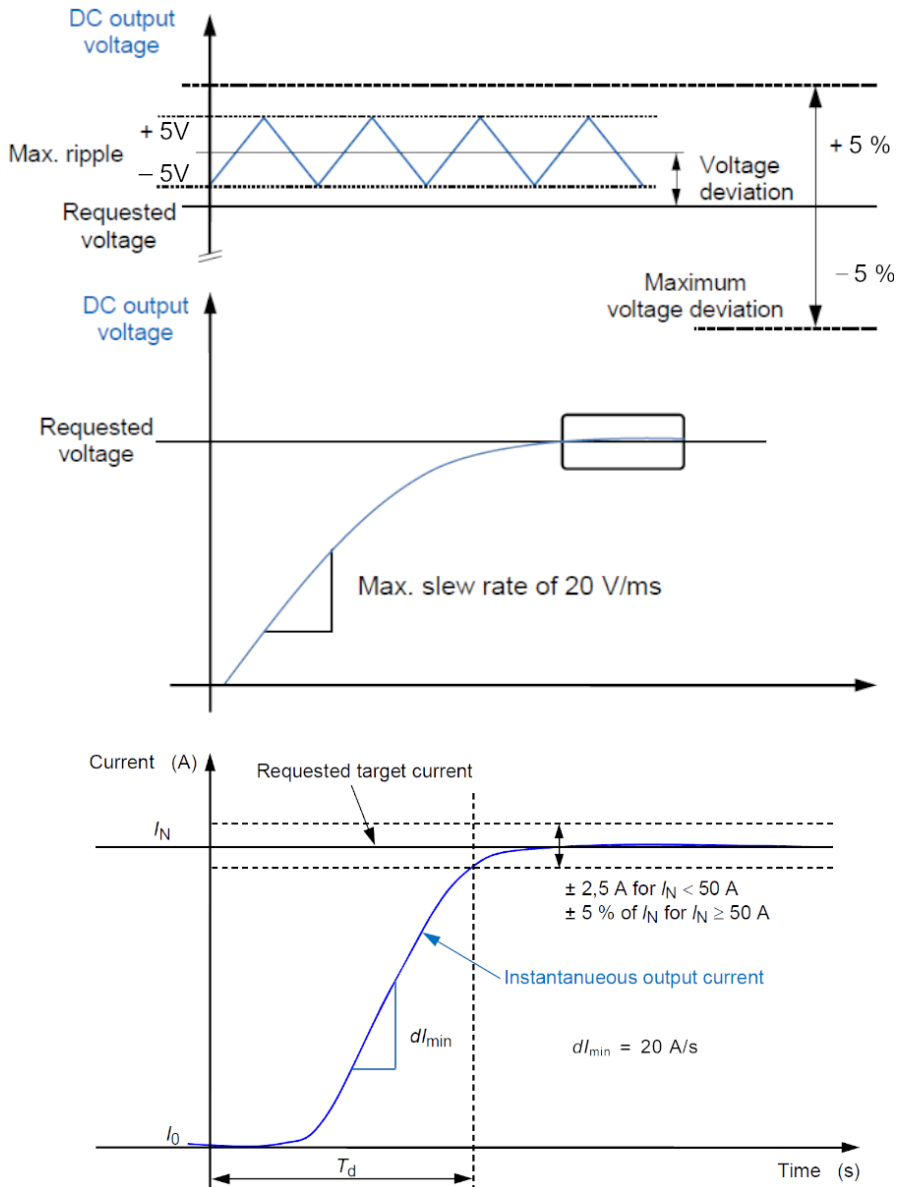


Figure 6.5: Standard step response for CV and CC control of EV

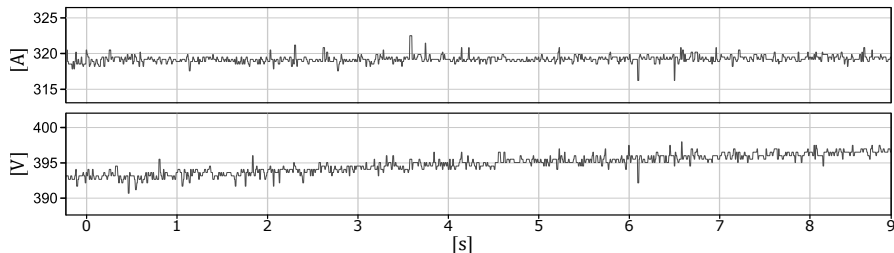


Figure 6.6: Detail of the EV voltage and current ripple in steady-state

6.2.2 Vehicles charging profiles

The goal of the Ultra-Fast charging mode is to minimize the charging times, so among the most interesting obtained results, there are the charging trend tests of real vehicles. The vehicles used in the tests are those in Tab.6.1. The vehicles

Table 6.1: EVs Data

Parameters	Unit	Audi 50quattro E-tron	Volkswagen ID.4	Porsche Taycan 4s
Rated Power	[kW]	230	150	390
Specific Energy Consumption	[kWh/100 km]	22.3	17.2	21.1
Autonomy (WLTO)	[km]	330	520	470
Energy Battery Stack	[kWh]	71	77	79.2
Rated Voltage	[V]	450	400	680
Max Charge Power	[kW]	130	130	230

Audi[®] 50quattro E-tron and Volkswagen[®] ID.4 have a battery voltage less than 450V, so they can also be charged at the same time; in Sec.5.2.2 they were taken as a reference for the validation of charging power planning. The Porsche[®] Taycan 4s has a mean voltage level such that it needs to be recharged by itself using SAB converters in ISOP configuration. The tests were carried out on vehicles with an initial *SoC* of approximately 5% to a full charge. The

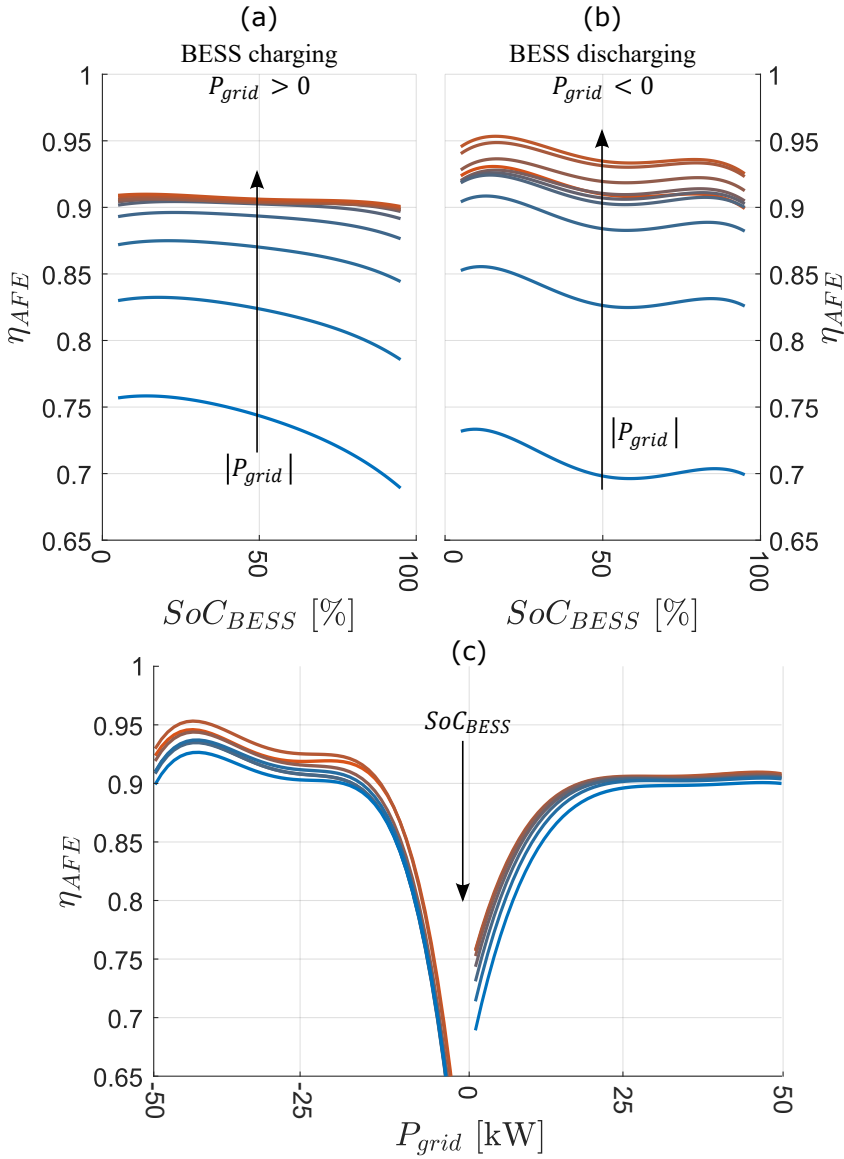


Figure 6.7: The efficiencies of AFE converter in the charging and discharging of the BESS

charging times are therefore to be evaluated in the two zones of fast charge and slow charge. In Fig.6.8, the charge profiles of the vehicles are shown. Each

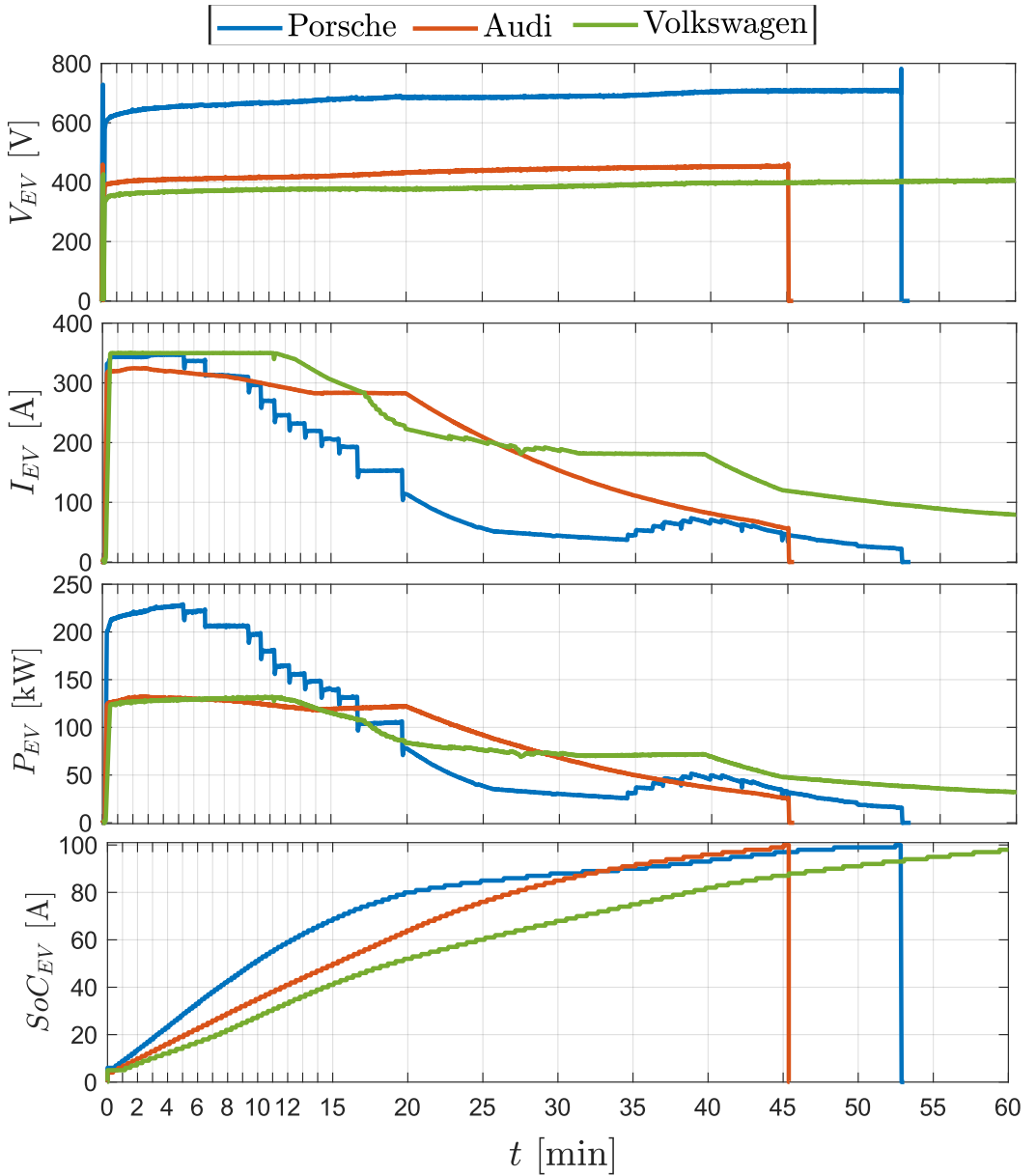


Figure 6.8: EV charging profiles

charge took place with a single vehicle connected to the station at a time, the BESS initially fully charged and with the network supplying $50kW$.

In Fig.6.8a, the voltages do not increase a lot, they are almost linearly dependant on the time. In Fig.6.8b, the current profiles of the three vehicles are very different. Typically, they depend on the geometrical arrangement of the cells in the battery, the position of the battery in the vehicle and the energy and thermal management chosen by the EV's BMS. In Fig.6.8d, the charging time can be analyzed. The Porsche can be charged in $20min$ up to a *SoC* of 80%, the Audi follows with $27min$, and the Volkswagen with $40min$. Out of the three vehicles, the charging times are higher than the $15min$ chosen as project requirements. The missing of the requirements are due to the power limits of the vehicles; in fact, none of the vehicles has required the maximum power.

Conclusions

This thesis is a unified report of the industrial research and development for the installation of the UFCS prototype built at the DIETI (Department of Information Technologies and Electrical Engineering) of University of Naples - Federico II. In this thesis the criteria to a proper sizing, designing and controlling of a UFCS are shown. The main differences between the MV and the LV connection grid and the analysis of the impact of chargers on the grid lead the reader to the evaluation of the design choices. An overview on electrical topologies of the conversion system is presented and the control schemes of the chosen converters are explained. The main contributions are the energy management strategy and the real implementation of the multi-slot Ultra-Fast charging station. A lot of issues met along the way are not reported. They regard: electromagnetic compatibility, communication protocol, types of ground, efficiency estimation, tests carried out on real vehicles, safety critical firmware coding.

Either way, the tests have highlighted the features of this infrastructure, but also its limits due to the vehicles' low charging requests and the limitation size

of the BESS. Nevertheless, this technology is perfectly in line with the needs of the growing market of the Evs and the charging stations on the highway. Some next researches on the topic will be:

- the evaluation of the scheduling strategies in relation to the real time pricing;
- the studying of the thermal and aging effects of Li-ion cells and the BMS corrective measures to increase their life-cycle.

Bibliography

- [1] R. Gilbert, B. Fleet, and J. Li, “Situation analysis for the current state of electric vehicle technology,” *Natural Resources Canada, Canadian Electric Vehicle Research Committee*, 2008.
- [2] M. Kebriaei, A. H. Niasar, and B. Asaei, “Hybrid electric vehicles: An overview,” in *2015 International Conference on Connected Vehicles and Expo (ICCVE)*. IEEE, 2015, pp. 299–305.
- [3] M. C. Falvo, D. Sbordone, I. S. Bayram, and M. Devetsikiotis, “Ev charging stations and modes: International standards,” in *2014 International Symposium on Power Electronics, Electrical Drives, Automation and Motion*, 2014, pp. 1134–1139.
- [4] N. Trivedi, N. S. Gujar, S. Sarkar, and S. Pundir, “Different fast charging methods and topologies for ev charging,” in *2018 IEEMA Engineer Infinite Conference (eTechNxT)*, 2018, pp. 1–5.
- [5] D. J. Berger and A. D. Jorgensen, “A comparison of carbon dioxide emissions from electric vehicles to emissions from internal combustion vehicles,” *Journal of Chemical Education*, vol. 92, no. 7, pp. 1204–1208, 2015.

- [6] J. McLaren, J. Miller, E. O’Shaughnessy, E. Wood, and E. Shapiro, “Emissions associated with electric vehicle charging: Impact of electricity generation mix, charging infrastructure availability, and vehicle type,” National Renewable Energy Lab.(NREL), Golden, CO (United States), Tech. Rep., 2016.
- [7] D. Hall and N. Lutseyen, “Effects of battery manufacturing on electric vehicle life-cycle greenhouse gas emissions,” The international council on clean transportation, Tech. Rep., 2018.
- [8] L. A.-W. Ellingsen, B. Singh, and A. H. Strømman, “The size and range effect: lifecycle greenhouse gas emissions of electric vehicles,” *Environmental Research Letters*, vol. 11, no. 5, p. 054010, 2016.
- [9] R. Nealer, D. Reichmuth, and D. Anair, “Cleaner cars from cradle to grave - how electric cars beat gasoline cars on lifetime global warming emissions,” Union of Concerned Scientists, Tech. Rep., 2015.
- [10] M. Spöttle, K. Jörling, M. Schimmel, M. Staats, L. Grizzel, L. Jerram, W. Drier, J. Gartner, M. Thomas, and C. Ratcliff, “Research for tran committee - charging infrastructure for electric road vehicles,” 2018, [Online; accessed 07-September-2021]. [Online]. Available: [www.europarl.europa.eu/RegData/etudes/STUD/2018/617470/IPOL_STU\(2018\)617470_EN.pdf](http://www.europarl.europa.eu/RegData/etudes/STUD/2018/617470/IPOL_STU(2018)617470_EN.pdf)
- [11] IEA, “Global ev outlook 2021, accelerating ambitions despite the pandemic,” IEA - International Energy Agency, Global Outlook, 4 2021.
- [12] ACEA, “Overview of CO_2 -based motor vehicle taxes in the eu,” European Automobile Manufacturers Association (ACEA),

-
- Tech. Rep., 6 2017. [Online]. Available: www.acea.auto/fact/overview-co2-based-motor-vehicle-taxes-in-the-european-union
- [13] H. Engel, R. Hensley, S. Knupfer, and S. Sahdev, “Charging ahead: Electric-vehicle infrastructure demand,” McKinsey & Company, Tech. Rep., 8 2018. [Online]. Available: www.mckinsey.com/industries/automotive-and-assembly/our-insights/charging-ahead-electric-vehicle-infrastructure-demand
- [14] EAFO, “European union infrastructure electricity,” EAFO (European Alternative Fuels Observatory), Tech. Rep., 2018. [Online]. Available: www.eafo.eu/countries/european-union/23640/infrastructure/electricity
- [15] P. Jochem, E. Szimba, and M. Reuter-Oppermann, “How many fast-charging stations do we need along european highways?” *Transportation Research Part D: Transport and Environment*, vol. 73, pp. 120–129, 2019. [Online]. Available: <https://www.sciencedirect.com/science/article/pii/S1361920919300215>
- [16] P. Franzese and D. Iannuzzi, “Ultrafast charging station for electrical vehicles: Dynamic modelling, design and control strategy,” *Mathematics and Computers in Simulation*, vol. 184, pp. 225–243, 2021, eLECTRIMACS 2019 ENGINEERING - Modelling and computational simulation for analysis and optimisation in electrical power engineering. [Online]. Available: <https://www.sciencedirect.com/science/article/pii/S037847542030149X>
- [17] P. Franzese, D. Iannuzzi, F. Mottola, D. Proto, and M. Pagano, “Charging strategies for ultra-fast stations with multiple plug-in electric vehicle parking

- slots,” in *2020 AEIT International Annual Conference (AEIT)*, 2020, pp. 1–6.
- [18] M. Christel and K. Kang, “Issues in requirements elicitation,” Software Engineering Institute, Carnegie Mellon University, Pittsburgh, PA, Tech. Rep. CMU/SEI-92-TR-012, 1992.
- [19] H.-l. Li, X.-m. Bai, and W. Tan, “Impacts of plug-in hybrid electric vehicles charging on distribution grid and smart charging,” in *2012 IEEE International Conference on Power System Technology (POWERCON)*, 2012, pp. 1–5.
- [20] J. Taylor, A. Maitra, M. Alexander, D. Brooks, and M. Duvall, “Evaluation of the impact of plug-in electric vehicle loading on distribution system operations,” in *2009 IEEE Power Energy Society General Meeting*, 2009, pp. 1–6.
- [21] S. J. Gunter, K. K. Afridi, and D. J. Perreault, “Optimal design of grid-connected pev charging systems with integrated distributed resources,” *IEEE Transactions on Smart Grid*, vol. 4, no. 2, pp. 956–967, 2013.
- [22] M. J. E. Alam, K. M. Muttaqi, and D. Sutanto, “A controllable local peak-shaving strategy for effective utilization of pev battery capacity for distribution network support,” *IEEE Transactions on Industry Applications*, vol. 51, no. 3, pp. 2030–2037, 2015.
- [23] A. N. Brooks, “Vehicle-to-grid demonstration project : grid regulation ancillary service with a battery electric vehicle,” AC Propulsion, Inc. California. Air Resources Board. Research Division, Tech. Rep., 2002.

- [24] N. Erdogan, F. Erden, and M. Kisacikoglu, “A fast and efficient coordinated vehicle-to-grid discharging control scheme for peak shaving in power distribution system,” *Journal of Modern Power Systems and Clean Energy*, vol. 6, no. 3, pp. 555–566, 2018.
- [25] Z. Wang and S. Wang, “Grid power peak shaving and valley filling using vehicle-to-grid systems,” *IEEE Transactions on Power Delivery*, vol. 28, no. 3, pp. 1822–1829, 2013.
- [26] A. Ouammi, “Peak loads shaving in a team of cooperating smart buildings powered solar pv-based microgrids,” *IEEE Access*, vol. 9, pp. 24 629–24 636, 2021.
- [27] J. Engels, B. Claessens, and G. Deconinck, “Optimal combination of frequency control and peak shaving with battery storage systems,” *IEEE Transactions on Smart Grid*, vol. 11, no. 4, pp. 3270–3279, 2020.
- [28] Y. Guo, Q. Zhang, and Z. Wang, “Cooperative peak shaving and voltage regulation in unbalanced distribution feeders,” *IEEE Transactions on Power Systems*, vol. 36, no. 6, pp. 5235–5244, 2021.
- [29] Y. Yu, O. S. Nduka, and B. C. Pal, “Smart control of an electric vehicle for ancillary service in dc microgrid,” *IEEE Access*, vol. 8, pp. 197 222–197 235, 2020.
- [30] T. T. Ku and C. Li, “Implementation of battery energy storage system for an island microgrid with high pv penetration,” in *2020 IEEE/IAS 56th Industrial and Commercial Power Systems Technical Conference (I CPS)*, 2020, pp. 1–8.

- [31] G. Bao, C. Lu, Z. Yuan, and Z. Lu, “Battery energy storage system load shifting control based on real time load forecast and dynamic programming,” in *2012 IEEE International Conference on Automation Science and Engineering (CASE)*, 2012, pp. 815–820.
- [32] M. Bahadornejad, X. Gao, and N.-K. C. Nair, “Iec 61850 based smart load-shifting through on-load tap changer control,” in *2011 IEEE PES Innovative Smart Grid Technologies*, 2011, pp. 1–7.
- [33] J. Merrick, Y. Ye, and R. Entriken, “Assessing the system value of optimal load shifting,” *IEEE Transactions on Smart Grid*, vol. 9, no. 6, pp. 5943–5952, 2018.
- [34] C. Li, X. Yu, W. Yu, G. Chen, and J. Wang, “Efficient computation for sparse load shifting in demand side management,” *IEEE Transactions on Smart Grid*, vol. 8, no. 1, pp. 250–261, 2017.
- [35] C.-C. Lin, D.-J. Deng, W.-Y. Liu, and L. Chen, “Peak load shifting in the internet of energy with energy trading among end-users,” *IEEE Access*, vol. 5, pp. 1967–1976, 2017.
- [36] M. C. Vlot, J. D. Knigge, and J. G. Slootweg, “Economical regulation power through load shifting with smart energy appliances,” *IEEE Transactions on Smart Grid*, vol. 4, no. 3, pp. 1705–1712, 2013.
- [37] Y. Wang, W. Saad, N. B. Mandayam, and H. V. Poor, “Load shifting in the smart grid: To participate or not?” *IEEE Transactions on Smart Grid*, vol. 7, no. 6, pp. 2604–2614, 2016.

- [38] B. Zhou, D. Yang, S. Bu, G. Du, and T. Littler, “The impact of electric vehicle uncertainties on load levelling in the uk,” in *2017 IEEE Power Energy Society General Meeting*, 2017, pp. 1–5.
- [39] B. Zhou, T. Littler, and A. Foley, “Electric vehicle capacity forecasting model with application to load levelling,” in *2015 IEEE Power Energy Society General Meeting*, 2015, pp. 1–5.
- [40] G. Shrinidhi, D. S. M, G. Rajesh, and S. Kochuvila, “Enhancement of electrical distribution system-load levelling,” in *2019 International Conference on Intelligent Computing and Control Systems (ICCS)*, 2019, pp. 435–439.
- [41] P. J. Ramírez, D. Papadaskalopoulos, and G. Strbac, “Co-optimization of generation expansion planning and electric vehicles flexibility,” *IEEE Transactions on Smart Grid*, vol. 7, no. 3, pp. 1609–1619, 2016.
- [42] P.-Y. Kong and G. K. Karagiannidis, “Charging schemes for plug-in hybrid electric vehicles in smart grid: A survey,” *IEEE Access*, vol. 4, pp. 6846–6875, 2016.
- [43] J.-M. Clairand, J. Rodríguez-García, and C. Álvarez Bel, “Smart charging for electric vehicle aggregators considering users’ preferences,” *IEEE Access*, vol. 6, pp. 54 624–54 635, 2018.
- [44] M. Dabbaghjamanesh, A. Kavousi-Fard, and J. Zhang, “Stochastic modeling and integration of plug-in hybrid electric vehicles in reconfigurable microgrids with deep learning-based forecasting,” *IEEE Transactions on Intelligent Transportation Systems*, vol. 22, no. 7, pp. 4394–4403, 2021.

- [45] S. J. Gunter, K. K. Afridi, and D. J. Perreault, “Optimal design of grid-interfaced ev chargers with integrated generation,” in *2012 IEEE PES Innovative Smart Grid Technologies (ISGT)*, 2012, pp. 1–8.
- [46] “Production electric cars,” https://en.wikipedia.org/wiki/Category:Production_electric_cars, accessed: 2021-12-05.
- [47] “Idaho national laboratory: public archive,” <https://avt.inl.gov/content/pubs-az>, accessed: 2021-12-05.
- [48] “The e-station guide to charging your electric or plug-in hybrid car,” <https://www.e-station.store/auto-elettriche>, accessed: 2021-12-05.
- [49] D. Kececioglu, *Reliability Engineering Handbook*. DEStech Publ, 2002, vol. 1.
- [50] H. Tu, H. Feng, S. Srdic, and S. Lukic, “Extreme fast charging of electric vehicles: A technology overview,” *IEEE Transactions on Transportation Electrification*, vol. 5, no. 4, pp. 861–878, 2019.
- [51] S. Bai and S. M. Lukic, “Unified active filter and energy storage system for an mw electric vehicle charging station,” *IEEE Transactions on Power Electronics*, vol. 28, no. 12, pp. 5793–5803, 2013.
- [52] M. S. Agamy, M. Harfman-Todorovic, A. Elasser, S. Chi, R. L. Steigerwald, J. A. Sabate, A. J. McCann, L. Zhang, and F. J. Mueller, “An efficient partial power processing dc/dc converter for distributed pv architectures,” *IEEE Transactions on Power Electronics*, vol. 29, no. 2, pp. 674–686, 2014.

- [53] J. Rojas, H. Renaudineau, S. Kouro, and S. Rivera, "Partial power dc-dc converter for electric vehicle fast charging stations," in *IECON 2017 - 43rd Annual Conference of the IEEE Industrial Electronics Society*, 2017, pp. 5274–5279.
- [54] V. M. Iyer, S. Guler, G. Gohil, and S. Bhattacharya, "An approach towards extreme fast charging station power delivery for electric vehicles with partial power processing," *IEEE Transactions on Industrial Electronics*, vol. 67, no. 10, pp. 8076–8087, 2020.
- [55] S. Augustine, J. E. Quiroz, M. J. Reno, and S. Brahma, "Dc microgrid protection: Review and challenges." U.S. Department of Energy Office of Scientific and Technical Information, Tech. Rep., 8 2018. [Online]. Available: <https://www.osti.gov/biblio/1465634>
- [56] D. Salomonsson, L. Soder, and A. Sannino, "Protection of low-voltage dc microgrids," *IEEE Transactions on Power Delivery*, vol. 24, no. 3, pp. 1045–1053, 2009.
- [57] B. Perea-Mena, J. A. Valencia-Velasquez, J. M. López-Lezama, J. B. Cano-Quintero, and N. Muñoz-Galeano, "Circuit breakers in low- and medium-voltage dc microgrids for protection against short-circuit electrical faults: Evolution and future challenges," *Applied Sciences*, vol. 12, no. 1, 2022. [Online]. Available: <https://www.mdpi.com/2076-3417/12/1/15>
- [58] J.-D. Park and J. Candelaria, "Fault detection and isolation in low-voltage dc-bus microgrid system," *IEEE Transactions on Power Delivery*, vol. 28, no. 2, pp. 779–787, 2013.

- [59] B. Singh, B. Singh, A. Chandra, K. Al-Haddad, A. Pandey, and D. Kothari, “A review of three-phase improved power quality ac-dc converters,” *IEEE Transactions on Industrial Electronics*, vol. 51, no. 3, pp. 641–660, 2004.
- [60] J. W. Kolar and T. Friedli, *The essence of three-phase PFC rectifier systems—Part I*. IEEE Transaction Power Electronic, 2013, vol. 28, no. 1.
- [61] D. Aggeler, F. Canales, H. Zelaya-De La Parra, A. Coccia, N. Butcher, and O. Apeldoorn, “Ultra-fast dc-charge infrastructures for ev-mobility and future smart grids,” in *2010 IEEE PES Innovative Smart Grid Technologies Conference Europe (ISGT Europe)*, 2010, pp. 1–8.
- [62] T. Kang, C. Kim, Y. Suh, H. Park, B.-K. Kang, and D. Kim, “A design and control of bi-directional non-isolated dc-dc converter for rapid electric vehicle charging system,” *2012 Twenty-Seventh Annual IEEE Applied Power Electronics Conference and Exposition (APEC)*, pp. 14–21, 2012.
- [63] N. Celanovic and D. Boroyevich, “A comprehensive study of neutral-point voltage balancing problem in three-level neutral-point-clamped voltage source pwm inverters,” *IEEE Transactions on Power Electronics*, vol. 15, no. 2, pp. 242–249, 2000.
- [64] S. Rivera, B. Wu, J. Wang, H. Athab, and S. Kouro, “Electric vehicle charging station using a neutral point clamped converter with bipolar dc bus and voltage balancing circuit,” in *IECON 2013 - 39th Annual Conference of the IEEE Industrial Electronics Society*, 2013, pp. 6219–6226.
- [65] L. Tan, B. Wu, V. Yaramasu, S. Rivera, and X. Guo, “Effective voltage balance control for bipolar-dc-bus-fed ev charging station with three-level

- dc–dc fast charger,” *IEEE Transactions on Industrial Electronics*, vol. 63, no. 7, pp. 4031–4041, 2016.
- [66] G. Waltrich, J. L. Duarte, and M. A. M. Hendrix, “Multiport converter for fast charging of electrical vehicle battery,” *IEEE Transactions on Industry Applications*, vol. 48, no. 6, pp. 2129–2139, 2012.
- [67] E. I. Pool-Mazun, J. J. Sandoval, P. N. Enjeti, and I. J. Pitel, “An integrated solid-state transformer with high-frequency isolation for ev fast-charging applications,” *IEEE Journal of Emerging and Selected Topics in Industrial Electronics*, vol. 1, no. 1, pp. 46–56, 2020.
- [68] A. Moeini and S. Wang, “Design of fast charging technique for electrical vehicle charging stations with grid-tied cascaded h-bridge multilevel converters,” in *2018 IEEE Applied Power Electronics Conference and Exposition (APEC)*, 2018, pp. 3583–3590.
- [69] J.-M. Kim, J. Lee, T.-H. Eom, K.-H. Bae, M.-H. Shin, and C.-Y. Won, “Design and control method of 25kw high efficient ev fast charger,” in *2018 21st International Conference on Electrical Machines and Systems (ICEMS)*, 2018, pp. 2603–2607.
- [70] S. Chen, W. Yu, and D. Meyer, “Design and implementation of forced air-cooled, 140khz, 20kw sic mosfet based vienna pfc,” in *2019 IEEE Applied Power Electronics Conference and Exposition (APEC)*, 2019, pp. 1196–1203.
- [71] J. A. Anderson, M. Haider, D. Bortis, J. W. Kolar, M. Kasper, and G. Deboy, “New synergetic control of a 20kw isolated vienna rectifier front-

- end ev battery charger,” in *2019 20th Workshop on Control and Modeling for Power Electronics (COMPEL)*, 2019, pp. 1–8.
- [72] A. Mohammadpour, M. R. Zolghadri, and M. Ferdowsi, “Constant input power control of a three phase isolated buck+boost rectifier,” in *Intelec 2010*, 2010, pp. 1–6.
- [73] A. Stupar, T. Friedli, J. Minibock, and J. W. Kolar, “Towards a 99three-phase buck-type pfc rectifier for 400-v dc distribution systems,” *IEEE Transactions on Power Electronics*, vol. 27, no. 4, pp. 1732–1744, 2012.
- [74] B. Guo, F. Wang, and E. Aeloiza, “A novel three-phase current source rectifier with delta-type input connection to reduce the device conduction loss,” *IEEE Transactions on Power Electronics*, vol. 31, no. 2, pp. 1074–1084, 2016.
- [75] J. Lei, S. Feng, J. Zhao, W. Chen, P. Wheeler, and M. Shi, “An improved three-phase buck rectifier topology with reduced voltage stress on transistors,” *IEEE Transactions on Power Electronics*, vol. 35, no. 3, pp. 2458–2466, 2020.
- [76] Y. Du, S. M. Lukic, B. S. Jacobson, and A. Q. Huang, “Review of high power isolated bi-directional dc-dc converters for phev/ev dc charging infrastructure,” *2011 IEEE Energy Conversion Congress and Exposition*, pp. 553–560, 2011.
- [77] P. He and A. Khaligh, “Comprehensive analyses and comparison of 1 kw isolated dc–dc converters for bidirectional ev charging systems,” *IEEE Transactions on Transportation Electrification*, vol. 3, pp. 147–156, 2017.

- [78] J. A. Sabate, V. Vlatkovic, R. B. Ridley, and F. C. Lee, "High-voltage, high-power, zvs, full-bridge pwm converter employing an active snubber," *[Proceedings] APEC '91: Sixth Annual Applied Power Electronics Conference and Exhibition*, pp. 158–163, 1991.
- [79] J.-G. Cho, J. Baek, C.-Y. Jeong, and G. H. Rim, "Novel zero-voltage and zero-current-switching full-bridge pwm converter using a simple auxiliary circuit," *IEEE Transactions on Industry Applications*, vol. 35, pp. 15–20, 1999.
- [80] D. S. Gautam, F. Musavi, W. Eberle, and W. G. Dunford, "A zero-voltage switching full-bridge dc–dc converter with capacitive output filter for plug-in hybrid electric vehicle battery charging," *IEEE Transactions on Power Electronics*, vol. 28, no. 12, pp. 5728–5735, 2013.
- [81] M. Pahlevaninezhad, P. Das, J. Drobnik, P. K. Jain, and A. Bakhshai, "A novel zvzcs full-bridge dc/dc converter used for electric vehicles," *IEEE Transactions on Power Electronics*, vol. 27, no. 6, pp. 2752–2769, 2012.
- [82] M. Pahlevaninezhad, J. Drobnik, P. K. Jain, and A. Bakhshai, "A load adaptive control approach for a zero-voltage-switching dc/dc converter used for electric vehicles," *IEEE Transactions on Industrial Electronics*, vol. 59, no. 2, pp. 920–933, 2012.
- [83] B. Yang, F. C. Lee, A. J. Zhang, and G. Huang, "Llc resonant converter for front end dc/dc conversion," *APEC. Seventeenth Annual IEEE Applied Power Electronics Conference and Exposition (Cat. No.02CH37335)*, vol. 2, pp. 1108–1112 vol.2, 2002.

- [84] J. E. Huber, J. Miniböck, and J. W. Kolar, “Generic derivation of dynamic model for half-cycle dcm series resonant converters,” *IEEE Transactions on Power Electronics*, vol. 33, no. 1, pp. 4–7, 2018.
- [85] I.-O. Lee, “Hybrid dc–dc converter with phase-shift or frequency modulation for nev battery charger,” *IEEE Transactions on Industrial Electronics*, vol. 63, no. 2, pp. 884–893, 2016.
- [86] M. Pahlevani, S. Pan, and P. K. Jain, “A hybrid phase-shift modulation technique for dc/dc converters with a wide range of operating conditions,” *IEEE Transactions on Industrial Electronics*, vol. 63, pp. 7498–7510, 2016.
- [87] H. Wang, S. Dusmez, and A. Khaligh, “Maximum efficiency point tracking technique for llc based pev chargers through variable dc link control,” *IEEE Transactions on Industrial Electronics*, vol. 61, no. 11, pp. 6041–6049, 2014.
- [88] H. Hu, X. Fang, F. Chen, Z. J. Shen, and I. Batarseh, “A modified high-efficiency llc converter with two transformers for wide input-voltage range applications,” *IEEE Transactions on Power Electronics*, vol. 28, no. 4, pp. 1946–1960, 2013.
- [89] H. Wu, X. Zhan, and Y. Xing, “Interleaved llc resonant converter with hybrid rectifier and variable-frequency plus phase-shift control for wide output voltage range applications,” *IEEE Transactions on Power Electronics*, vol. 32, no. 6, pp. 4246–4257, 2017.
- [90] Z. Hu, Y. jie Qiu, L. Wang, and Y. Liu, “An interleaved llc resonant converter operating at constant switching frequency,” *IEEE Transactions on Power Electronics*, vol. 29, pp. 2931–2943, 2014.

- [91] A. Coccia, F. Canales, P. Barbosa, and S. Ponnaluri, "Wide input voltage range compensation in dc/dc resonant architectures for on-board traction power supplies," in *2007 European Conference on Power Electronics and Applications*, 2007, pp. 1–10.
- [92] Y. Nakakohara, H. Otake, T. M. Evans, T. Yoshida, M. Tsuruya, and K. Nakahara, "Three-phase *llc* series resonant dc/dc converter using sic mosfets to realize high-voltage and high-frequency operation," *IEEE Transactions on Industrial Electronics*, vol. 63, no. 4, pp. 2103–2110, 2016.
- [93] Y. Hyok-min, K. Jong-hyun, and S. Eui-ho, "Design of a novel 50 kW fast charger for electric vehicles," *Journal of Central South University*, vol. 20, no. 2, pp. 372–377, Feb. 2013. [Online]. Available: <https://doi.org/10.1007/s11771-013-1497-8>
- [94] M. Kheraluwala, R. Gascoigne, D. Divan, and E. Baumann, "Performance characterization of a high-power dual active bridge dc-to-dc converter," *IEEE Transactions on Industry Applications*, vol. 28, no. 6, pp. 1294–1301, 1992.
- [95] R. De Doncker, D. Divan, and M. Kheraluwala, "A three-phase soft-switched high-power-density dc/dc converter for high-power applications," *IEEE Transactions on Industry Applications*, vol. 27, no. 1, pp. 63–73, 1991.
- [96] H. Akagi, T. Yamagishi, N. M. L. Tan, S.-i. Kinouchi, Y. Miyazaki, and M. Koyama, "Power-loss breakdown of a 750-v, 100-kw, 20-khz bidirectional isolated dc-dc converter using sic-mosfet/sbd dual modules," in *2014 In-*

- ternational Power Electronics Conference (IPEC-Hiroshima 2014 - ECCE ASIA)*, 2014, pp. 750–757.
- [97] J. E. Huber and J. W. Kolar, “Applicability of solid-state transformers in today’s and future distribution grids,” *IEEE Transactions on Smart Grid*, vol. 10, no. 1, pp. 317–326, 2019.
- [98] N. M. L. Tan, T. Abe, and H. Akagi, “Design and performance of a bidirectional isolated dc–dc converter for a battery energy storage system,” *IEEE Transactions on Power Electronics*, vol. 27, no. 3, pp. 1237–1248, 2012.
- [99] H. Wen, W. Xiao, and B. Su, “Nonactive power loss minimization in a bidirectional isolated dc–dc converter for distributed power systems,” *IEEE Transactions on Industrial Electronics*, vol. 61, no. 12, pp. 6822–6831, 2014.
- [100] A. Rodríguez, A. Vázquez, D. G. Lamar, M. M. Hernando, and J. Sebastián, “Different purpose design strategies and techniques to improve the performance of a dual active bridge with phase-shift control,” in *2014 IEEE 15th Workshop on Control and Modeling for Power Electronics (COMPEL)*, 2014, pp. 1–10.
- [101] B. Zhao, Q. Song, W. Liu, and W. Sun, “Current-stress-optimized switching strategy of isolated bidirectional dc–dc converter with dual-phase-shift control,” *IEEE Transactions on Industrial Electronics*, vol. 60, no. 10, pp. 4458–4467, 2013.
- [102] G. Oggier, G. O. García, and A. R. Oliva, “Modulation strategy to operate the dual active bridge dc-dc converter under soft switching in the whole

- operating range,” *IEEE Transactions on Power Electronics*, vol. 26, no. 4, pp. 1228–1236, 2011.
- [103] F. Krismer and J. W. Kolar, “Efficiency-optimized high-current dual active bridge converter for automotive applications,” *IEEE Transactions on Industrial Electronics*, vol. 59, no. 7, pp. 2745–2760, 2012.
- [104] J. Huang, Y. Wang, Z. Li, and W. Lei, “Unified triple-phase-shift control to minimize current stress and achieve full soft-switching of isolated bidirectional dc–dc converter,” *IEEE Transactions on Industrial Electronics*, vol. 63, no. 7, pp. 4169–4179, 2016.
- [105] J. Hiltunen, V. Väisänen, R. Juntunen, and P. Silventoinen, “Variable-frequency phase shift modulation of a dual active bridge converter,” *IEEE Transactions on Power Electronics*, vol. 30, no. 12, pp. 7138–7148, 2015.
- [106] G. G. Oggier and M. Ordonez, “High-efficiency dab converter using switching sequences and burst mode,” *IEEE Transactions on Power Electronics*, vol. 31, no. 3, pp. 2069–2082, 2016.
- [107] A. Taylor, G. Liu, H. Bai, A. Brown, P. M. Johnson, and M. McAmmond, “Multiple-phase-shift control for a dual active bridge to secure zero-voltage switching and enhance light-load performance,” *IEEE Transactions on Power Electronics*, vol. 33, no. 6, pp. 4584–4588, 2018.
- [108] W. Chen, P. Rong, and Z. Lu, “Snubberless bidirectional dc–dc converter with new clc resonant tank featuring minimized switching loss,” *IEEE Transactions on Industrial Electronics*, vol. 57, no. 9, pp. 3075–3086, 2010.

- [109] Z. U. Zahid, Z. M. Dalala, R. Chen, B. Chen, and J.-S. Lai, "Design of bidirectional dc–dc resonant converter for vehicle-to-grid (v2g) applications," *IEEE Transactions on Transportation Electrification*, vol. 1, no. 3, pp. 232–244, 2015.
- [110] J.-H. Jung, H.-S. Kim, M.-H. Ryu, and J.-W. Baek, "Design methodology of bidirectional clc resonant converter for high-frequency isolation of dc distribution systems," *IEEE Transactions on Power Electronics*, vol. 28, no. 4, pp. 1741–1755, 2013.
- [111] S. Zhao, Q. Li, F. C. Lee, and B. Li, "High-frequency transformer design for modular power conversion from medium-voltage ac to 400 vdc," *IEEE Transactions on Power Electronics*, vol. 33, no. 9, pp. 7545–7557, 2018.
- [112] C.-S. Wang, S.-h. Zhang, Y.-f. Wang, B. Chen, and J.-h. Liu, "A 5-kw isolated high voltage conversion ratio bidirectional cltc resonant dc–dc converter with wide gain range and high efficiency," *IEEE Transactions on Power Electronics*, vol. 34, no. 1, pp. 340–355, 2019.
- [113] J. Huang, X. Zhang, Z. Shuai, X. Zhang, P. Wang, L. H. Koh, J. Xiao, and X. Tong, "Robust circuit parameters design for the clc-type dc transformer in the hybrid ac–dc microgrid," *IEEE Transactions on Industrial Electronics*, vol. 66, no. 3, pp. 1906–1918, 2019.
- [114] B. Li, Q. Li, F. C. Lee, Z. Liu, and Y. Yang, "A high-efficiency high-density wide-bandgap device-based bidirectional on-board charger," *IEEE Journal of Emerging and Selected Topics in Power Electronics*, vol. 6, no. 3, pp. 1627–1636, 2018.

- [115] P. He and A. Khaligh, “Design of 1 kw bidirectional half-bridge clc converter for electric vehicle charging systems,” in *2016 IEEE International Conference on Power Electronics, Drives and Energy Systems (PEDES)*, 2016, pp. 1–6.
- [116] C. Zhang, P. Li, Z. Kan, X. Chai, and X. Guo, “Integrated half-bridge clc bidirectional converter for energy storage systems,” *IEEE Transactions on Industrial Electronics*, vol. 65, no. 5, pp. 3879–3889, 2018.
- [117] F. Peng, H. Li, G.-J. Su, and J. Lawler, “A new zvs bidirectional dc-dc converter for fuel cell and battery application,” *IEEE Transactions on Power Electronics*, vol. 19, no. 1, pp. 54–65, 2004.
- [118] H. Li, D. Liu, F. Peng, and G.-J. Su, “Small signal analysis of a dual half bridge isolated zvs bi-directional dc-dc converter for electrical vehicle applications,” in *2005 IEEE 36th Power Electronics Specialists Conference*, 2005, pp. 2777–2782.
- [119] D. Liu and H. Li, “Design and implementation of a dsp based digital controller for a dual half bridge isolated bi-directional dc-dc converter,” in *Twenty-First Annual IEEE Applied Power Electronics Conference and Exposition, 2006. APEC '06.*, 2006, pp. 5 pp.–.
- [120] M. Coleman, W. G. Hurley, and C. K. Lee, “An improved battery characterization method using a two-pulse load test,” *IEEE Transactions on Energy Conversion*, vol. 23, no. 2, pp. 708–713, 2008.
- [121] N. Meddings, M. Heinrich, F. Overney, J.-S. Lee, V. Ruiz, E. Napolitano, S. Seitz, G. Hinds, R. Raccichini, M. Gaberšček, and J. Park, “Application of

electrochemical impedance spectroscopy to commercial li-ion cells: A review,” *Journal of Power Sources*, vol. 480, p. 228742, 2020. [Online]. Available: <https://www.sciencedirect.com/science/article/pii/S0378775320310466>

- [122] N. Hargreaves, *Extension of IEC 61970 for Electrical Energy Storage Modelling*, 1st ed., ser. Electrical Engineering Developments. Nova Sciences Publishers Inc, 2014, vol. 1, pp. 439–462.
- [123] M. Asghari, S. M. J. M. Al-e *et al.*, “Green vehicle routing problem: A state-of-the-art review,” *International Journal of Production Economics*, vol. 231, p. 107899, 2021.
- [124] M. S. Alam Chowdhury, K. A. A. Mamun, and A. M. Rahman, “Modelling and simulation of power system of battery, solar and fuel cell powered hybrid electric vehicle,” in *2016 3rd International Conference on Electrical Engineering and Information Communication Technology (ICEEICT)*, 2016, pp. 1–6.
- [125] M. Hannan, F. Azidin, and A. Mohamed, “Hybrid electric vehicles and their challenges: A review,” *Renewable and Sustainable Energy Reviews*, vol. 29, pp. 135–150, 2014. [Online]. Available: <https://www.sciencedirect.com/science/article/pii/S1364032113006370>
- [126] S. M. Lukic, J. Cao, R. C. Bansal, F. Rodriguez, and A. Emadi, “Energy storage systems for automotive applications,” *IEEE Transactions on Industrial Electronics*, vol. 55, no. 6, pp. 2258–2267, 2008.

- [127] F. A. Azidin, M. A. Hannan, and A. Mohamed, “Renewable energy technologies and hybrid electric vehicle challenges,” *Przegmd Elektrotechniczny*, pp. 150–156, 2013.
- [128] V. Madanipour, M. Montazeri-Gh, and M. Mahmoodi-k, “Multi-objective component sizing of plug-in hybrid electric vehicle for optimal energy management,” *Clean Technologies and Environmental Policy*, vol. 18, pp. 1189–1202, 2016.
- [129] F. Nemry, G. Leduc, and A. Muñoz, “Plug-in hybrid and battery-electric vehicles: State of the research and development and comparative analysis of energy and cost efficiency,” IPTS, Tech. Rep., 01 2009.
- [130] S. Dhameja, *Electric Vehicle Battery Systems*. Newnes, 01 2002.
- [131] S. Vazquez, S. M. Lukic, E. Galvan, L. G. Franquelo, and J. M. Carrasco, “Energy storage systems for transport and grid applications,” *IEEE Transactions on Industrial Electronics*, vol. 57, no. 12, pp. 3881–3895, 2010.
- [132] M. Hannan, M. Hoque, A. Mohamed, and A. Ayob, “Review of energy storage systems for electric vehicle applications: Issues and challenges,” *Renewable and Sustainable Energy Reviews*, vol. 69, pp. 771–789, 2017. [Online]. Available: <https://www.sciencedirect.com/science/article/pii/S1364032116309182>
- [133] T. Fujihara, H. Imano, and K. Oshima, “Development of pump turbine for seawater pumped-storage power plant,” *Hitachi Review*, vol. 47, no. 5, pp. 199–202, 1998.

- [134] S. Lemofouet and A. Rufer, “A hybrid energy storage system based on compressed air and supercapacitors with maximum efficiency point tracking (mept),” *IEEE Transactions on Industrial Electronics*, vol. 53, no. 4, pp. 1105–1115, 2006.
- [135] H. Liu and J. Jiang, “Flywheel energy storage—an upswing technology for energy sustainability,” *Energy and Buildings*, vol. 39, no. 5, pp. 599–604, 2007. [Online]. Available: <https://www.sciencedirect.com/science/article/pii/S0378778806002350>
- [136] B. Bolund, H. Bernhoff, and M. Leijon, “Flywheel energy and power storage systems,” *Renewable and Sustainable Energy Reviews*, vol. 11, no. 2, pp. 235–258, 2007. [Online]. Available: <https://www.sciencedirect.com/science/article/pii/S1364032105000146>
- [137] K. Bhagat and S. K. Saha, “Numerical analysis of latent heat thermal energy storage using encapsulated phase change material for solar thermal power plant,” *Renewable Energy*, vol. 95, pp. 323–336, 2016. [Online]. Available: <https://www.sciencedirect.com/science/article/pii/S096014811630310X>
- [138] D. P. Dubal, O. Ayyad, V. Ruiz, and P. Gómez-Romero, “Hybrid energy storage: the merging of battery and supercapacitor chemistries,” *Chem. Soc. Rev.*, vol. 44, pp. 1777–1790, 2015. [Online]. Available: <http://dx.doi.org/10.1039/C4CS00266K>
- [139] M. Rashid, *Power electronics handbook : devices, circuits, and applications*. Butterworth-Heinemann, 01 2011.

- [140] K. W. Beard, *Linden's handbook of batteries, fifth edition; 5th ed.* McGraw-Hill Education, May 2019. [Online]. Available: <https://cds.cern.ch/record/2669980>
- [141] H. Fayaz, R. Saidur, N. Razali, F. Anuar, A. Saleman, and M. Islam, "An overview of hydrogen as a vehicle fuel," *Renewable and Sustainable Energy Reviews*, vol. 16, no. 8, pp. 5511–5528, 2012. [Online]. Available: <https://www.sciencedirect.com/science/article/pii/S1364032112003929>
- [142] F. A. Silva, "Power electronics handbook, third edition (rashid, m.h.; 2011) [book news]," *IEEE Industrial Electronics Magazine*, vol. 5, no. 2, pp. 54–55, 2011.
- [143] S. F. Tie and C. W. Tan, "A review of energy sources and energy management system in electric vehicles," *Renewable and Sustainable Energy Reviews*, vol. 20, pp. 82–102, 2013. [Online]. Available: <https://www.sciencedirect.com/science/article/pii/S1364032112006910>
- [144] A. Z. AL Shaqsi, K. Sopian, and A. Al-Hinai, "Review of energy storage services, applications, limitations, and benefits," *Energy Reports*, vol. 6, pp. 288–306, 2020, sI:Energy Storage - driving towards a clean energy future. [Online]. Available: <https://www.sciencedirect.com/science/article/pii/S2352484720312464>
- [145] H. Chen, T. N. Cong, W. Yang, C. Tan, Y. Li, and Y. Ding, "Progress in electrical energy storage system: A critical review," *Progress in Natural Science*, vol. 19, no. 3, pp. 291–312, 2009. [Online]. Available: <https://www.sciencedirect.com/science/article/pii/S100200710800381X>

- [146] O. Crowther and M. Salomon, “Oxygen selective membranes for li-air (o₂) batteries,” *Membranes*, vol. 2, no. 2, pp. 216–227, 2012. [Online]. Available: <https://www.mdpi.com/2077-0375/2/2/216>
- [147] M. Sun, L.-F. Zhai, W.-W. Li, and H.-Q. Yu, “Harvest and utilization of chemical energy in wastes by microbial fuel cells,” *Chem. Soc. Rev.*, vol. 45, pp. 2847–2870, 2016. [Online]. Available: <http://dx.doi.org/10.1039/C5CS00903K>
- [148] E. S. Heidrich, S. R. Edwards, J. Dolfing, S. E. Cotterill, and T. P. Curtis, “Performance of a pilot scale microbial electrolysis cell fed on domestic wastewater at ambient temperatures for a 12month period,” *Bioresource Technology*, vol. 173, pp. 87–95, 2014. [Online]. Available: <https://www.sciencedirect.com/science/article/pii/S096085241401342X>
- [149] B. Xu, Z. Ge, and Z. He, “Sediment microbial fuel cells for wastewater treatment: challenges and opportunities,” *Environ. Sci.: Water Res. Technol.*, vol. 1, pp. 279–284, 2015. [Online]. Available: <http://dx.doi.org/10.1039/C5EW00020C>
- [150] A. C. Forse, C. Merlet, J. M. Griffin, and C. P. Grey, “New perspectives on the charging mechanisms of supercapacitors,” *Journal of the American Chemical Society*, vol. 138, no. 18, pp. 5731–5744, 2016, pMID: 27031622. [Online]. Available: <https://doi.org/10.1021/jacs.6b02115>
- [151] Y. Zhang and S. Jin, “Recent advancements in the synthesis of covalent triazine frameworks for energy and environmental applications,” *Polymers*,

-
- vol. 11, no. 1, 2019. [Online]. Available: <https://www.mdpi.com/2073-4360/11/1/31>
- [152] E. Lim, C. Jo, H. Kim, M.-H. Kim, Y. Mun, J. Chun, Y. Ye, J. Hwang, K.-S. Ha, K. C. Roh, K. Kang, S. Yoon, and J. Lee, “Facile synthesis of nb₂o₅@carbon core–shell nanocrystals with controlled crystalline structure for high-power anodes in hybrid supercapacitors,” *ACS Nano*, vol. 9, no. 7, pp. 7497–7505, 2015, pMID: 26095456. [Online]. Available: <https://doi.org/10.1021/acsnano.5b02601>
- [153] M. Semadeni, “Energy storage as an essential part of sustainable energy systems,” *CEPE Center for Energy Policy and Economics, ETH Zurich, CEPE Working paper series*, 01 2003.
- [154] Z. Zhou, M. Benbouzid, J. Frédéric Charpentier, F. Scullier, and T. Tang, “A Review of Energy Storage Technologies for Marine Current Energy Systems,” *Renewable and Sustainable Energy Reviews*, vol. 18, pp. 390–400, Feb. 2013. [Online]. Available: <https://hal.archives-ouvertes.fr/hal-00757890>
- [155] G. Sun, X. Zhang, R. Lin, J. Yang, H. Zhang, and P. Chen, “Hybrid fibers made of molybdenum disulfide, reduced graphene oxide, and multi-walled carbon nanotubes for solid-state, flexible, asymmetric supercapacitors,” *Angewandte Chemie International Edition*, vol. 54, no. 15, pp. 4651–4656, 2015. [Online]. Available: <https://onlinelibrary.wiley.com/doi/abs/10.1002/anie.201411533>
- [156] I. Hadjipaschalis, A. Poullikkas, and V. Efthimiou, “Overview of current and future energy storage technologies for electric power applications,”

- Renewable and Sustainable Energy Reviews*, vol. 13, no. 6, pp. 1513–1522, 2009. [Online]. Available: <https://www.sciencedirect.com/science/article/pii/S1364032108001664>
- [157] R. Georgious, R. Refaat, J. Garcia, and A. A. Daoud, “Review on energy storage systems in microgrids,” *Electronics*, vol. 10, no. 17, 2021. [Online]. Available: <https://www.mdpi.com/2079-9292/10/17/2134>
- [158] Z. Zhang, Q. Zhang, Y. Chen, J. Bao, X. Zhou, Z. Xie, J. Wei, and Z. Zhou, “The first introduction of graphene to rechargeable li-co₂ batteries,” *Angewandte Chemie International Edition*, vol. 54, no. 22, pp. 6550–6553, 2015. [Online]. Available: <https://onlinelibrary.wiley.com/doi/abs/10.1002/anie.201501214>
- [159] I. N. Jiya, N. Gurusinghe, and R. Gouws, “Electrical circuit modelling of double layer capacitors for power electronics and energy storage applications: A review,” *Electronics*, vol. 7, no. 11, 2018. [Online]. Available: <https://www.mdpi.com/2079-9292/7/11/268>
- [160] Z. Lu, X. Zhong, X. Liu, J. Wang, and X. Diao, “Energy storage electrochromic devices in the era of intelligent automation,” *Phys. Chem. Chem. Phys.*, vol. 23, pp. 14 126–14 145, 2021. [Online]. Available: <http://dx.doi.org/10.1039/D1CP01398J>
- [161] A. V. Pan, L. MacDonald, H. Baiej, and P. Cooper, “Theoretical consideration of superconducting coils for compact superconducting magnetic energy storage systems,” *IEEE Transactions on Applied Superconductivity*, vol. 26, no. 3, pp. 1–5, 2016.

- [162] L. Brandeis, D. Sprake, Y. Vagapov, and H. Tun, “Analysis of electrical energy storage technologies for future electric grids,” in *2016 IEEE NW Russia Young Researchers in Electrical and Electronic Engineering Conference (EIconRusNW)*, 2016, pp. 513–518.
- [163] T. Cotterman, *WISE - Energy Storage Technologies: Transforming America’s Intelligent Electrical Infrastructure*. IEEE, 2013. [Online]. Available: <https://ieeexplore.ieee.org/document/6978820>
- [164] B. Zakeri and S. Syri, “Electrical energy storage systems: A comparative life cycle cost analysis,” *Renewable and Sustainable Energy Reviews*, vol. 42, pp. 569–596, 2015. [Online]. Available: <https://www.sciencedirect.com/science/article/pii/S1364032114008284>
- [165] N. Hiroshima, H. Hatta, M. Koyama, J. Yoshimura, Y. Nagura, K. Goto, and Y. Kogo, “Spin test of three-dimensional composite rotor for flywheel energy storage system,” *Composite Structures*, vol. 136, pp. 626–634, 2016. [Online]. Available: <https://www.sciencedirect.com/science/article/pii/S0263822315009678>
- [166] J. Noack, N. Roznyatovskaya, T. Herr, and P. Fischer, “The chemistry of redox-flow batteries,” *Angewandte Chemie International Edition*, vol. 54, no. 34, pp. 9776–9809, 2015. [Online]. Available: <https://onlinelibrary.wiley.com/doi/abs/10.1002/anie.201410823>
- [167] S. Er, C. Suh, M. P. Marshak, and A. Aspuru-Guzik, “Computational design of molecules for an all-quinone redox flow battery,” *Chem. Sci.*,

vol. 6, pp. 885–893, 2015. [Online]. Available: <http://dx.doi.org/10.1039/C4SC03030C>

- [168] J. Yu, “State-of-health monitoring and prediction of lithium-ion battery using probabilistic indication and state-space model,” *IEEE Transactions on Instrumentation and Measurement*, vol. 64, no. 11, pp. 2937–2949, 2015.
- [169] Y. Zhao, Y. Ding, Y. Li, L. Peng, H. R. Byon, J. B. Goodenough, and G. Yu, “A chemistry and material perspective on lithium redox flow batteries towards high-density electrical energy storage,” *Chem. Soc. Rev.*, vol. 44, pp. 7968–7996, 2015. [Online]. Available: <http://dx.doi.org/10.1039/C5CS00289C>
- [170] K. Gong, Q. Fang, S. Gu, S. F. Y. Li, and Y. Yan, “Nonaqueous redox-flow batteries: organic solvents, supporting electrolytes, and redox pairs,” *Energy Environ. Sci.*, vol. 8, pp. 3515–3530, 2015. [Online]. Available: <http://dx.doi.org/10.1039/C5EE02341F>
- [171] J. Winsberg, T. Hagemann, T. Janoschka, M. D. Hager, and U. S. Schubert, “Redox-flow batteries: From metals to organic redox-active materials,” *Angewandte Chemie (International ed. in English)*, vol. 56, no. 3, p. 686–711, January 2017. [Online]. Available: <https://europepmc.org/articles/PMC5248651>
- [172] Y. Xing, E. W. M. Ma, K. L. Tsui, and M. Pecht, “Battery management systems in electric and hybrid vehicles,” *Energies*, vol. 4, no. 11, pp. 1840–1857, 2011.

- [173] C. Ma, D. Yang, J. Zhou, Z. Feng, and Q. Yuan, “Risk riding behaviors of urban e-bikes: A literature review,” *International Journal of Environmental Research and Public Health*, vol. 16, no. 13, 2019. [Online]. Available: <https://www.mdpi.com/1660-4601/16/13/2308>
- [174] C. Spanos, D. E. Turney, and V. Fthenakis, “Life-cycle analysis of flow-assisted nickel zinc-, manganese dioxide-, and valve-regulated lead-acid batteries designed for demand-charge reduction,” *Renewable and Sustainable Energy Reviews*, vol. 43, pp. 478–494, 2015. [Online]. Available: <https://www.sciencedirect.com/science/article/pii/S1364032114008971>
- [175] G. Li, X. Lu, J. Y. Kim, K. D. Meinhardt, H. J. Chang, N. L. Canfield, and V. L. Sprenkle, “Advanced intermediate temperature sodium-nickel chloride batteries with ultra-high energy density,” *Nature communications*, vol. 7, p. 10683, February 2016. [Online]. Available: <https://europepmc.org/articles/PMC4753253>
- [176] A. Khaligh and Z. Li, “Battery, ultracapacitor, fuel cell, and hybrid energy storage systems for electric, hybrid electric, fuel cell, and plug-in hybrid electric vehicles: State of the art,” *IEEE Transactions on Vehicular Technology*, vol. 59, no. 6, pp. 2806–2814, 2010.
- [177] K. Divya and J. Østergaard, “Battery energy storage technology for power systems—an overview,” *Electric Power Systems Research*, vol. 79, no. 4, pp. 511–520, 2009. [Online]. Available: <https://www.sciencedirect.com/science/article/pii/S0378779608002642>

- [178] M. García-Plaza, D. Serrano-Jiménez, J. Eloy-García Carrasco, and J. Alonso-Martínez, “A ni-cd battery model considering state of charge and hysteresis effects,” *Journal of Power Sources*, vol. 275, pp. 595–604, 2015. [Online]. Available: <https://www.sciencedirect.com/science/article/pii/S0378775314018576>
- [179] M. Anderman, G. Benczur-Urmossy, and F. Haschka, “Prismatic sealed nickel-cadmium batteries utilizing fiber structured electrodes. II - Applications as a maintenance free aircraft battery,” in *34th International Power Sources Symposium*, Jan. 1990, pp. 290–294.
- [180] Y. Zhu, W. Zhu, Z. Davis, and B. Tatarchuk, “Simulation of ni-mh batteries via an equivalent circuit model for energy storage applications,” *Advances in Physical Chemistry*, vol. 2016, pp. 1–11, 01 2016.
- [181] L. Gao, Z. Li, Y. Zou, S. Yin, P. Peng, Y. Shao, and X. Liang, “A high-performance aqueous zinc-bromine static battery,” *iScience*, vol. 23, no. 8, p. 101348, 2020. [Online]. Available: <https://www.sciencedirect.com/science/article/pii/S2589004220305356>
- [182] E. Manla, A. Nasiri, C. H. Rentel, and M. Hughes, “Modeling of zinc bromide energy storage for vehicular applications,” *IEEE Transactions on Industrial Electronics*, vol. 57, no. 2, pp. 624–632, 2010.
- [183] D. Swan, B. Dickinson, M. Arikara, and G. Tomazic, “Demonstration of a zinc bromine battery in an electric vehicle,” in *Proceedings of 9th Annual Battery Conference on Applications and Advances*, 1994, pp. 104–109.

- [184] Z.-L. Wang, D. Xu, J.-J. Xu, and X.-B. Zhang, “Oxygen electrocatalysts in metal–air batteries: from aqueous to nonaqueous electrolytes,” *Chem. Soc. Rev.*, vol. 43, pp. 7746–7786, 2014. [Online]. Available: <http://dx.doi.org/10.1039/C3CS60248F>
- [185] M. Park, Y. Kim Ka, H. Seo, Y. E. Cheon, H. Koh Jae, H. Sun, and J. Kim Tae, “Practical challenges associated with catalyst development for the commercialization of li-air batteries,” *J. Electrochem. Sci. Technol*, vol. 5, no. 1, pp. 1–18, 2014. [Online]. Available: <http://www.jecst.org/journal/view.php?number=8>
- [186] F. Cheng and J. Chen, “Metal–air batteries: from oxygen reduction electrochemistry to cathode catalysts,” *Chem. Soc. Rev.*, vol. 41, pp. 2172–2192, 2012. [Online]. Available: <http://dx.doi.org/10.1039/C1CS15228A>
- [187] Z. Guo, Y. Zhao, Y. Ding, X. Dong, L. Chen, J. Cao, C. Wang, Y. Xia, H. Peng, and Y. Wang, “Multi-functional flexible aqueous sodium-ion batteries with high safety,” *Chem*, vol. 3, no. 2, pp. 348–362, 2017. [Online]. Available: <https://www.sciencedirect.com/science/article/pii/S2451929417302176>
- [188] K. G. Gallagher, S. Goebel, T. Greszler, M. Mathias, W. Oelerich, D. Eroglu, and V. Srinivasan, “Quantifying the promise of lithium–air batteries for electric vehicles,” *Energy Environ. Sci.*, vol. 7, pp. 1555–1563, 2014. [Online]. Available: <http://dx.doi.org/10.1039/C3EE43870H>
- [189] M.-C. Kim, J. H. Song, Y.-W. Lee, and J. I. Sohn, “Redox-mediated polymer catalyst for lithium-air batteries with high round-trip

- efficiency,” *Catalysts*, vol. 10, no. 12, 2020. [Online]. Available: <https://www.mdpi.com/2073-4344/10/12/1479>
- [190] Q. Dong and D. Wang, “Catalysts in metal–air batteries,” *MRS Communications*, vol. 8, no. 2, p. 372–386, 2018.
- [191] J. Xu, C. Chen, Z. Han, Y. Yang, J. Li, and Q. Deng, “Recent advances in oxygen electrocatalysts based on perovskite oxides,” *Nanomaterials*, vol. 9, no. 8, 2019. [Online]. Available: <https://www.mdpi.com/2079-4991/9/8/1161>
- [192] T. B. Reddy and D. Linden., *Linden’s handbook of batteries*. New York: McGraw-Hill, 2011. [Online]. Available: <https://www.accessengineeringlibrary.com/content/book/9780071624213>
- [193] Z. Zhirong and F. Maximilian, “Magnesium–sulfur battery: its beginning and recent progress,” *MRS Communications*, vol. 7, pp. 770–784, 2017.
- [194] J. A. Sanguesa, V. Torres-Sanz, P. Garrido, F. J. Martinez, and J. M. Marquez-Barja, “A review on electric vehicles: Technologies and challenges,” *Smart Cities*, vol. 4, no. 1, pp. 372–404, 2021. [Online]. Available: <https://www.mdpi.com/2624-6511/4/1/22>
- [195] L. Sheng, Z. Hao, J. Feng, W. Du, M. Gong, L. Kang, P. R. Shearing, D. J. Brett, Y. Huang, and F. R. Wang, “Evaluation and realization of safer mg-s battery: The decisive role of the electrolyte,” *Nano Energy*, vol. 83, p. 105832, 2021. [Online]. Available: <https://www.sciencedirect.com/science/article/pii/S2211285521000902>

- [196] A. A. Akhil, G. Huff, A. B. Currier, J. Hernandez, D. A. Bender, B. C. Kaun, D. M. Rastler, S. B. Chen, A. L. Cotter, D. T. Bradshaw, W. D. Gauntlett, J. Eyer, T. Olinsky-Paul, M. Ellison, and S. Schoenung, "Doe/epri electricity storage handbook in collaboration with nreca," Sandia National Lab. (SNL-NM), Albuquerque, NM (United States); Electric Power Research Inst. (EPRI), Palo Alto, CA (United States), Tech. Rep., 9 2016. [Online]. Available: <https://www.osti.gov/biblio/1431469>
- [197] G. Li, X. Lu, J. Y. Kim, V. V. Viswanathan, K. D. Meinhardt, M. H. Engelhard, and V. L. Sprenkle, "Batteries: An advanced na-fecl₂ zebra battery for stationary energy storage application (adv. energy mater. 12/2015)," *Advanced Energy Materials*, vol. 5, no. 12, 2015. [Online]. Available: <https://onlinelibrary.wiley.com/doi/abs/10.1002/aenm.201570069>
- [198] Y. Sun, N. Liu, and Y. Cui, "Promises and challenges of nanomaterials for lithium-based rechargeable batteries," *Nature Energy*, vol. 1, p. 16071, 06 2016.
- [199] M. A. Hannan, M. M. Hoque, P. J. Ker, R. A. Begum, and A. Mohamed, "Charge equalization controller algorithm for series-connected lithium-ion battery storage systems: Modeling and applications," *Energies*, vol. 10, no. 9, 2017. [Online]. Available: <https://www.mdpi.com/1996-1073/10/9/1390>
- [200] J. A. Sanguesa, V. Torres-Sanz, P. Garrido, F. J. Martinez, and J. M. Marquez-Barja, "A review on electric vehicles: Technologies and

- challenges,” *Smart Cities*, vol. 4, no. 1, pp. 372–404, 2021. [Online]. Available: <https://www.mdpi.com/2624-6511/4/1/22>
- [201] A. Masias, J. Marcicki, and W. A. Paxton, “Opportunities and challenges of lithium ion batteries in automotive applications,” *ACS Energy Letters*, vol. 6, no. 2, pp. 621–630, 2021. [Online]. Available: <https://doi.org/10.1021/acsenerylett.0c02584>
- [202] J.-Y. Hwang, S.-T. Myung, and Y.-K. Sun, “Sodium-ion batteries: present and future,” *Chem. Soc. Rev.*, vol. 46, pp. 3529–3614, 2017. [Online]. Available: <http://dx.doi.org/10.1039/C6CS00776G>
- [203] D. Akinyele, J. Belikov, and Y. Levron, “Battery storage technologies for electrical applications: Impact in stand-alone photovoltaic systems,” *Energies*, vol. 10, no. 11, 2017. [Online]. Available: <https://www.mdpi.com/1996-1073/10/11/1760>
- [204] W. Duan, M. Zhao, J. Shen, S. Zhao, and X. Song, “Superior lithium-ion insertion/extraction properties of a novel lifepo4/c/graphene material used as a cathode in aqueous solution,” *Dalton Trans.*, vol. 46, pp. 12 019–12 026, 2017. [Online]. Available: <http://dx.doi.org/10.1039/C7DT02341C>
- [205] L. Lu, X. Han, J. Li, J. Hua, and M. Ouyang, “A review on the key issues for lithium-ion battery management in electric vehicles,” *Journal of Power Sources*, vol. 226, pp. 272–288, 2013. [Online]. Available: <https://www.sciencedirect.com/science/article/pii/S0378775312016163>
- [206] S.-H. Kim, K.-H. Choi, S.-J. Cho, S. Choi, S. Park, and S.-Y. Lee, “Printable solid-state lithium-ion batteries: A new route toward

- shape-conformable power sources with aesthetic versatility for flexible electronics,” *Nano Letters*, vol. 15, no. 8, pp. 5168–5177, 2015, pMID: 26176939. [Online]. Available: <https://doi.org/10.1021/acs.nanolett.5b01394>
- [207] “Types of lithium-ion,” <https://batteryuniversity.com/article/bu-205-types-of-lithium-ion>, accessed: 2022-01-30.
- [208] H. Kim, K.-Y. Park, J. Hong, and K. Kang, “All-graphene-battery: Bridging the gap between supercapacitors and lithium ion batteries,” *Scientific reports*, vol. 4, p. 5278, 06 2014.
- [209] P. Keil, M. Englberger, and A. Jossen, “Hybrid energy storage systems for electric vehicles: An experimental analysis of performance improvements at subzero temperatures,” *IEEE Transactions on Vehicular Technology*, vol. 65, no. 3, pp. 998–1006, 2016.
- [210] E.-L. Molina-Ibáñez, E. Rosales-Asensio, C. Pérez-Molina, F. M. Pérez, and A. Colmenar-Santos, “Analysis on the electric vehicle with a hybrid storage system and the use of superconducting magnetic energy storage (smes),” *Energy Reports*, vol. 7, pp. 854–873, 2021, technologies and Materials for Renewable Energy, Environment and Sustainability. [Online]. Available: <https://www.sciencedirect.com/science/article/pii/S2352484721005205>
- [211] S. Aggarwal and A. K. Singh, “Electric vehicles the future of transportation sector: a review,” *Energy Sources, Part A: Recovery, Utilization, and Environmental Effects*, vol. 0, no. 0, pp. 1–21, 2021. [Online]. Available: <https://doi.org/10.1080/15567036.2021.1976322>

- [212] S. Lu, K. A. Corzine, and M. Ferdowsi, “High efficiency energy storage system design for hybrid electric vehicle with motor drive integration,” in *Conference Record of the 2006 IEEE Industry Applications Conference Forty-First IAS Annual Meeting*, vol. 5, 2006, pp. 2560–2567.
- [213] W. Henson, “Optimal battery/ultracapacitor storage combination,” *Journal of Power Sources*, vol. 179, no. 1, pp. 417–423, 2008. [Online]. Available: <https://www.sciencedirect.com/science/article/pii/S0378775307028479>
- [214] A. Chaban, Z. Lukasik, M. Lis, and A. Szafraniec, “Mathematical modeling of transient processes in magnetic suspension of maglev trains,” *Energies*, vol. 13, no. 24, 2020. [Online]. Available: <https://www.mdpi.com/1996-1073/13/24/6642>
- [215] F. Machado, J. P. F. Trovão, and C. H. Antunes, “Effectiveness of supercapacitors in pure electric vehicles using a hybrid metaheuristic approach,” *IEEE Transactions on Vehicular Technology*, vol. 65, no. 1, pp. 29–36, 2016.
- [216] T. Anno and H. Koizumi, “Double-input bidirectional dc/dc converter using cell-voltage equalizer with flyback transformer,” *IEEE Transactions on Power Electronics*, vol. 30, no. 6, pp. 2923–2934, 2015.
- [217] A. Nahavandi, M. T. Hagh, M. B. B. Sharifian, and S. Danyali, “A nonisolated multiinput multioutput dc–dc boost converter for electric vehicle applications,” *IEEE Transactions on Power Electronics*, vol. 30, pp. 1818–1835, 2015.

- [218] G. Yang, P. Dubus, and D. Sadarnac, “Double-phase high-efficiency, wide load range high- voltage/low-voltage *llc* dc/dc converter for electric/hybrid vehicles,” *IEEE Transactions on Power Electronics*, vol. 30, no. 4, pp. 1876–1886, 2015.
- [219] T. Zhu, R. G. Wills, R. Lot, X. Kong, and X. Yan, “Optimal sizing and sensitivity analysis of a battery-supercapacitor energy storage system for electric vehicles,” *Energy*, vol. 221, p. 119851, 2021. [Online]. Available: <https://www.sciencedirect.com/science/article/pii/S0360544221001006>
- [220] T. F. Fuller, M. Doyle, and J. Newman, “Simulation and optimization of the dual lithium ion insertion cell,” *Journal of The Electrochemical Society*, vol. 141, no. 1, pp. 1–10, jan 1994. [Online]. Available: <https://doi.org/10.1149/1.2054684>
- [221] M. Doyle and J. Newman, “The use of mathematical modeling in the design of lithium/polymer battery systems,” *Electrochimica Acta*, vol. 40, no. 13, pp. 2191–2196, 1995, international symposium on polymer electrolytes. [Online]. Available: <https://www.sciencedirect.com/science/article/pii/0013468695001628>
- [222] I. J. Ong and J. Newman, “Double-layer capacitance in a dual lithium ion insertion cell,” *Journal of The Electrochemical Society*, vol. 146, no. 12, pp. 4360–4365, dec 1999. [Online]. Available: <https://doi.org/10.1149/1.1392643>
- [223] M. Doyle, J. P. Meyers, and J. Newman, “Computer simulations of the impedance response of lithium rechargeable batteries,” *Journal of The*

Electrochemical Society, vol. 147, no. 1, p. 99, 2000. [Online]. Available: <https://doi.org/10.1149/1.1393162>

[224] J. P. Meyers, M. Doyle, R. M. Darling, and J. Newman, “The impedance response of a porous electrode composed of intercalation particles,” *Journal of The Electrochemical Society*, vol. 147, no. 8, p. 2930, 2000. [Online]. Available: <https://doi.org/10.1149/1.1393627>

[225] T. F. Fuller, M. Doyle, and J. Newman, “Relaxation phenomena in lithium-ion-insertion cells,” *Journal of The Electrochemical Society*, vol. 141, no. 4, pp. 982–990, apr 1994. [Online]. Available: <https://doi.org/10.1149/1.2054868>

[226] J. P. Schmidt, *Verfahren zur Charakterisierung und Modellierung von Lithium-Ionen Zellen*. KIT Scientific Publishing, 2013, vol. 25.

[227] M. Petit, E. Calas, and J. Bernard, “A simplified electrochemical model for modelling li-ion batteries comprising blend and bidispersed electrodes for high power applications,” *Journal of Power Sources*, vol. 479, 2020. [Online]. Available: <https://www.sciencedirect.com/science/article/pii/S0378775320310703>

[228] D. N. T. How, M. A. Hannan, M. S. Hossain Lipu, and P. J. Ker, “State of charge estimation for lithium-ion batteries using model-based and data-driven methods: A review,” *IEEE Access*, vol. 7, pp. 136 116–136 136, 2019.

[229] S. N. Motapon, A. Lupien-Bedard, L.-A. Dessaint, H. Fortin-Blanchette, and K. Al-Haddad, “A generic electrothermal li-ion battery model for rapid

- evaluation of cell temperature temporal evolution,” *IEEE Transactions on Industrial Electronics*, vol. 64, no. 2, pp. 998–1008, 2017.
- [230] R. Relan, Y. Firouz, J.-M. Timmermans, and J. Schoukens, “Data-driven nonlinear identification of li-ion battery based on a frequency domain nonparametric analysis,” *IEEE Transactions on Control Systems Technology*, vol. 25, no. 5, pp. 1825–1832, 2017.
- [231] M. Kim and S. Han, “Novel data-efficient mechanism-agnostic capacity fade model for li-ion batteries,” *IEEE Transactions on Industrial Electronics*, vol. 68, no. 7, pp. 6267–6275, 2021.
- [232] W. Liu, Y. Xu, and X. Feng, “A hierarchical and flexible data-driven method for online state-of-health estimation of li-ion battery,” *IEEE Transactions on Vehicular Technology*, vol. 69, no. 12, pp. 14 739–14 748, 2020.
- [233] K. Liu, Y. Shang, Q. Ouyang, and W. D. Widanage, “A data-driven approach with uncertainty quantification for predicting future capacities and remaining useful life of lithium-ion battery,” *IEEE Transactions on Industrial Electronics*, vol. 68, no. 4, pp. 3170–3180, 2021.
- [234] J. Lee, D. Kwon, and M. G. Pecht, “Reduction of li-ion battery qualification time based on prognostics and health management,” *IEEE Transactions on Industrial Electronics*, vol. 66, no. 9, pp. 7310–7315, 2019.
- [235] L. Cai, J. Meng, D.-I. Stroe, J. Peng, G. Luo, and R. Teodorescu, “Multiobjective optimization of data-driven model for lithium-ion battery soh estimation with short-term feature,” *IEEE Transactions on Power Electronics*, vol. 35, no. 11, pp. 11 855–11 864, 2020.

- [236] A. A.-H. Hussein and I. Batarseh, “An overview of generic battery models,” in *2011 IEEE Power and Energy Society General Meeting*, 2011, pp. 1–6.
- [237] C. M. Shepherd, “Design of primary and secondary cells,” *Journal of The Electrochemical Society*, vol. 112, no. 7, p. 657, 1965. [Online]. Available: <https://doi.org/10.1149/1.2423659>
- [238] L. Unnewehr and S. Nasar, *Electric vehicle technology*. England: Bumpus, Haldane and Maxwell Limited, 1982.
- [239] A.-S. Feiner and A. McEvoy, “The nernst equation,” *Journal of chemical education*, vol. 71, no. 6, p. 493, 1994.
- [240] X. Tang, Y. Wang, and Z. Chen, “A method for state-of-charge estimation of lifepo4 batteries based on a dual-circuit state observer,” *Journal of Power Sources*, vol. 296, pp. 23–29, 2015. [Online]. Available: <https://www.sciencedirect.com/science/article/pii/S0378775315300756>
- [241] O. Tremblay, L.-A. Dessaint, and A.-I. Dekkiche, “A generic battery model for the dynamic simulation of hybrid electric vehicles,” in *2007 IEEE Vehicle Power and Propulsion Conference*, 2007, pp. 284–289.
- [242] O. Tremblay and L.-A. Dessaint, “Experimental validation of a battery dynamic model for ev applications,” *World Electric Vehicle Journal*, vol. 3, no. 2, p. 289–298, Jun 2009. [Online]. Available: <http://dx.doi.org/10.3390/wevj3020289>

- [243] H. Fang, X. Zhao, Y. Wang, Z. Sahinoglu, T. Wada, S. Hara, and R. A. de Callafon, “State-of-charge estimation for batteries: A multi-model approach,” in *2014 American Control Conference*, 2014, pp. 2779–2785.
- [244] G. L. Plett, “Extended kalman filtering for battery management systems of lipb-based hev battery packs: Part 3. state and parameter estimation,” *Journal of Power Sources*, vol. 134, no. 2, pp. 277–292, 2004. [Online]. Available: <https://www.sciencedirect.com/science/article/pii/S0378775304003611>
- [245] V. Srinivasan, J. W. Weidner, and J. Newman, “Hysteresis during cycling of nickel hydroxide active material,” *Journal of The Electrochemical Society*, vol. 148, no. 9, p. A969, 2001. [Online]. Available: <https://doi.org/10.1149/1.1385846>
- [246] X. Hu, F. Sun, Y. Zou, and H. Peng, “Online estimation of an electric vehicle lithium-ion battery using recursive least squares with forgetting,” in *Proceedings of the 2011 American Control Conference*, 2011, pp. 935–940.
- [247] M. Greenleaf, H. Li, and J. P. Zheng, “Modeling of $li_x fepo_4$ cathode li-ion batteries using linear electrical circuit model,” *IEEE Transactions on Sustainable Energy*, vol. 4, no. 4, pp. 1065–1070, 2013.
- [248] N. Watrin, R. Roche, H. Ostermann, B. Blunier, and A. Miraoui, “Multiphysical lithium-based battery model for use in state-of-charge determination,” *IEEE Transactions on Vehicular Technology*, vol. 61, no. 8, pp. 3420–3429, 2012.

- [249] N. E. Galushkin, N. N. Yazvinskaya, and D. N. Galushkin, “A critical review of using the peukert equation and its generalizations for lithium-ion cells,” *Journal of The Electrochemical Society*, vol. 167, no. 12, jan 2020. [Online]. Available: <https://doi.org/10.1149/1945-7111/abad69>
- [250] Q.-Q. Yu, R. Xiong, L.-Y. Wang, and C. Lin, “A comparative study on open circuit voltage models for lithium-ion batteries,” *Chinese Journal of Mechanical Engineering*, vol. 31, no. 1, Aug. 2018. [Online]. Available: <https://doi.org/10.1186/s10033-018-0268-8>
- [251] M. Chetto, Ed., *Real-Time Systems Scheduling 1*. John Wiley & Sons, Inc., Aug. 2014. [Online]. Available: <https://doi.org/10.1002/9781118984413>
- [252] J. K. Murali, V. Chandrasekar, S. Mohan *et al.*, “Analysis, estimation and minimization of power loss in ccm operated psfb converter,” in *2016 IEEE International Conference on Power Electronics, Drives and Energy Systems (PEDES)*. IEEE, 2016, pp. 1–5.
- [253] D. Gravoc and M. Purschel, “Igbt power losses calculation using the data-sheet parameters,” *Infineon Tech. AG, Neubiberg, Germany*, p. 17, 2009.
- [254] Z. Emami, M. Nikpendar, N. Shafiei, and S. R. Motahari, “Leading and lagging legs power loss analysis in zvs phase-shift full bridge converter,” in *2011 2nd Power Electronics, Drive Systems and Technologies Conference*. IEEE, 2011, pp. 632–637.
- [255] P. Franzese, A. Cervone, and D. Iannuzzi, “Power control strategy of a delta-connected photovoltaic cascaded h-bridge converter for low voltage

distribution networks in energy community,” in *2021 IEEE 6th International Forum on Research and Technology for Society and Industry (RTSI)*, 2021, pp. 346–351.

Standards

- [S1] *IEC 61851-1:2017*, International Electrotechnical Commission IEC Standard, 2 2017.
- [S2] *IEC 62196-1:2014*, International Electrotechnical Commission IEC Standard, 6 2014.
- [S3] E. Parliament and of the Council, *Directive 2014/94/EU*, European Parliament and of the Council Std., 2014,
<https://eur-lex.europa.eu/legal-content/en/TXT/?uri=CELEX%3A32014L0094>.
- [S4] *IEC 60038:2009*, International Electrotechnical Commission IEC Standard, 6 2009.
- [S5] *IEC 61439:2020*, International Electrotechnical Commission IEC Standard, 5 2020.
- [S6] *IEC 60364:2017*, International Electrotechnical Commission IEC Standard, 2017.

- [S7] *IEC 62196:2015*, International Electrotechnical Commission IEC Standard, 2 2015.
- [S8] *IEC 61558:2017*, International Electrotechnical Commission IEC Standard, 9 2017.
- [S9] *IEC 60664:2020*, International Electrotechnical Commission IEC Standard, 10 2020.
- [S10] *IEC 60947:2021*, International Electrotechnical Commission IEC Standard, 7 2021.
- [S11] *IEC 61180:2016*, International Electrotechnical Commission IEC Standard, 6 2016.
- [S12] *IEC 60309:2021*, International Electrotechnical Commission IEC Standard, 6 2021.
- [S13] *IEC 61810:2015*, International Electrotechnical Commission IEC Standard, 2 2015.
- [S14] *IEC 61508:2010*, International Electrotechnical Commission IEC Standard, 4 2010.
- [S15] *IEC 60950:2004*, International Electrotechnical Commission IEC Standard, 5 2004.
- [S16] *ISO 17409:2020*, International Organization for Standardization ISO Standard, 2 2020.

- [S17] *IEC 61851-23:2015*, International Electrotechnical Commission IEC Standard, 10 2015.
- [S18] *IEC 61851-24:2015*, International Electrotechnical Commission IEC Standard, 10 2015.
- [S19] E. Parliament and of the Council, *Directive 2016/631/EU*, European Parliament and of the Council Std., 2016,
<https://eur-lex.europa.eu/legal-content/EN/TXT/?uri=CELEX%3A32016R0631>.
- [S20] —, *Directive 2016/1388/EU*, European Parliament and of the Council Std., 2016,
https://eur-lex.europa.eu/legal-content/EN/TXT/?uri=uriserv%3AOJ.L_.2016.223.01.0010.01.ENG.
- [S21] —, *Directive 2016/1447/EU*, European Parliament and of the Council Std., 2016,
<https://eur-lex.europa.eu/eli/reg/2016/1447/oj>.
- [S22] C. X. S. aspects of electrical energy supply, *Requirements for micro-generating plants to be connected in parallel with public low-voltage distribution networks*, European Standardisation Organisations Std., 2013,
<https://standards.iteh.ai/catalog/standards/clc/125d70a3-2f51-403d-8df3-3c0abff9a741/en-50438-2013-is1-2015>.
- [S23] C. T. Italiano, *Regola tecnica di riferimento per la connessione di Utenti attivi e passivi alle reti AT ed MT delle imprese distributrici di energia*

elettrica, Comitato Tecnico Italiano Std., 6 2021,

<https://www.ceinorme.it/it/norme-cei-0-16-e-0-21.html>.

[S24] —, *Regola tecnica di riferimento per la connessione di Utenti attivi e passivi alle reti BT delle imprese distributrici di energia elettrica*, Comitato Tecnico Italiano Std., 12 2020,

<https://www.ceinorme.it/it/norme-cei-0-16-e-0-21.html>.